An Empirical Study of Algebraic Reconstruction Techniques

AN EMPIRICAL STUDY OF ALGEBRAIC RECONSTRUCTION TECHNIQUES

BY

EHSAN MOHAMMAD KAZEMI, B.Sc.

A THESIS

SUBMITTED TO THE DEPARTMENT OF COMPUTING AND SOFTWARE

AND THE SCHOOL OF GRADUATE STUDIES

OF MCMASTER UNIVERSITY

IN PARTIAL FULFILMENT OF THE REQUIREMENTS

FOR THE DEGREE OF

MASTER OF SCIENCE

Master of Science (2011) McMaster University

(Computing And Software) Hamilton, Ontario, Canada

TITLE:	An Empirical Study of Algebraic Reconstruction Techniques
AUTHOR:	Ehsan Mohammad Kazemi B.Sc., (Computer Software Engineering) Islamic Azad University, Mashhad, Iran
SUPERVISOR:	Dr. Ned. Nedialkov
NUMBER OF PAGES:	xxi, 170

Dedicated to my parents, my family and my love, Maryam, because of all their steadfast supports, assistance, tolerance, and enthusiasm.

There is no doubt in my mind that without their continued support and encouragement I could not have completed this program.

Abstract

A computerized tomography scan enables the visualization of an object interior without opening it up. This technique is used in many fields e.g. in medical imaging, geology, and industry. To obtain information about an object, exterior measurements by means of X-rays are performed. Then, to reconstruct an image of the objects interior, image-reconstructions methods are applied. The problem of reconstructing images from measurements of X-ray radiation belongs to the class of inverse problems. A class of important methods for inverse problems is Algebraic Reconstruction Techniques (ART). The performance of these methods depends on the choice of a relaxation parameter.

In this thesis, we compare numerically various ART methods, namely Kaczmarz, symmetric Kaczmarz, randomized Kaczmarz and simultaneous ART. We perform an extensive numerical investigation of the behaviour of these methods, and in particular, study how they perform with respect to this relaxation parameter. We propose a simple heuristic for finding a good relaxation parameter for each of these methods. Comparisons of the new proposed strategy with a previously proposed one shows that our strategy has a slightly better performance in terms of relative error, relative residual and image discrepancy of the reconstructed image. Both strategies showed

relatively close numerical results, but interestingly enough, for different values of this parameter.

Acknowledgements

I would like to express the deepest appreciation to my supervisor, Dr. Ned Nedialkov who is the idealest supervisor that every student is ambitious to have. His support of my academic pursuits, sage advice, insightful criticisms, and patient encouragement aided the completion of my Master's study and the writing of this thesis in innumerable ways. I would also like to acknowledge the support and assistance given me by Dr. Kenneth R. Jackson and his Ph.D. student Nargol Rezvani, at University of Toronto, and also Dr. Dhavide Aruliah, at University of Ontario Institute of Technology, for all their ideas, feedback and advice.

Contents

List of Tables

List of Figures

Chapter 1

Introduction

In the first section of this chapter, the problem of image reconstruction is introduced. In the second section, the background of the introduced problem is discussed. Then, the thesis results are summarized, and at the end, the outline of the thesis is provided.

1.1 The Image Reconstruction Problem

The requirement to see the interior of an object is a problem that arises in many areas. A brain surgeon needs to know where a tumor is exactly located without opening the brain before operating, and also a geologist needs to finds out the possible locations for Earth resources without excavating the ground. To solve such problems, it is possible to use tomography, which is a technique being used in a wide range of areas.

Computerized Axial Tomography (CAT or CT) scan enables the formation and visualization of an image of the interior, by measuring data accessible from the exterior. Standard tomography usually uses X-ray as the source for taking projections by

letting X-rays pass through an object. The more amount of X-ray data is collected, the better quality the reconstructed image normally has.

The reconstructed image gives information describing the matter that the rays have passed through. The problem of reconstructing images from measurements of the X-ray radiation around the object, which is being scanned, belongs to the class of inverse problems. These are typically solved using Filtered Back-Projection (FBP) [11], and Iterative Reconstruction Techniques such as Algebraic Reconstruction Techniques (ART) [8].

For different applications on various environments, changing the emitting source or modifying the reconstruction algorithms to achieve the results we want is feasible. On the other hand, tomography is an imaging tool having several mathematical algorithms involved in it. For example, the central slice theorem [3] and algebraic reconstruction algorithm are two of the most important methods for images reconstruction. Hence, several techniques can be used to reconstruct an image from its projections.

1.2 Background

The mathematical basis for tomography was first studied by Radon in 1917 [20], but the first Computerized Tomography (CT) scanner was invented in 1972. To reconstruct images from a series of angular projections, Algebraic Reconstruction Techniques as the first methods were used in CTs' machines while in numerical linear algebra, the original method is known as Kaczmarz's method [16].

Kaczmarz's method, based on the work of the Polish mathematician Stefan Kaczmarz [16], has been found very useful in the area of image reconstruction from different angular projections and has been demonstrated by Herman to be superior, in some biomedical imaging applications, to other methods such as the filtered back projection method [14].

Various versions of the Kaczmarz's method, such as symmetric Kaczmarz's method and randomized Kaczmarz's method, have been already introduced in such a way that each of them consists of an important parameter, which is called *relaxation parameter*. It is already proved that a carefully adjusted relaxation parameter can lead to a high quality reconstructed image [18].

Idealistically, there must exist an adaptive strategy to find a relaxation parameter for each iteration in any of the ART iterative methods, but it is not a straightforward task to find the best relaxation parameter, since there is no unique choice for it. Hence, up to now, some strategies have been proposed for finding just an optimum value of relaxation parameter (λ), since finding an adaptive strategy is not an easy task to do, however none of them are unanimously accepted.

One of the proposed strategies, which is of high importance in this thesis, was proposed by Maria Saxild-Hansen and her supervisor, Dr. Per Christian Hansen, in her Master's thesis at Technical University of Denmark [10]. This strategy proposes a training method by which the optimal value of the relaxation parameter (λ) for

two of the ART methods, Kaczmarz and Symmetric Kaczmarz, can be determined. The optimal value of λ in [10] is defined as the value that gives rise to the fastest convergence to the smallest relative error in the solution.

Now, in Chapter 4 of this thesis, a new training strategy for finding both adaptive and fixed value of λ is proposed. We will compare this method with the previously mentioned training strategy [10].

1.3 Summary of Thesis Results

In this thesis, we will try to give an overview and explanation of two image reconstruction techniques: analytical techniques and algebraic techniques. The analytical techniques, Filtered Back Projection algorithms, are based on a continuous description of the image and the data, and form a continuous solution.

The other image reconstruction techniques, which are mainly discussed in this thesis, are ART algorithms starting from a discretized version of the image formed by a limited set of components, such as pixels. We start with some of the common concepts that are used in both of these algorithms.

In this thesis, a new training strategy for finding an adaptive or fixed relaxation parameter is proposed, which is comparable to the other previously proposed strategies, and can be applied to various ART methods. The numerical results of this training strategy indicate that the selected relaxation parameters for each of the ART iterative methods is different from the other ART methods', and no matter what the test

phantom is, the selected relaxation parameters are close to each other.

Comparing the results obtained from the new proposed strategy with a previously proposed strategy, for finding relaxation parameter, indicates that however our proposed strategy, for finding a fixed relaxation parameter, in two of the ART methods has a better performance in terms of relative error, relative residual and image discrepancy, both strategies represent generally the same numerical results.

The experimental results also show that the ranges of the selected relaxation parameters for various ART methods, depending on the method, can be reduced to different smaller intervals instead of (0,2) which is the convergence interval for all the ART methods.

1.4 Thesis Outline

The rest of this thesis is organized as follows. In Chapter 2, the foundations and underlying concepts of two analytical and iterative reconstruction algorithms which are respectively FBP and ART are explained. In Chapter 3, we overview related work and image reconstruction methods. In Chapter 4, the performance of ART methods is investigated. Chapter 5 investigates the performance of FBP. Finally, in Chapter 6, the results from the previous chapters are summarized, and directions for future research are discussed.

Chapter 2

Preliminaries

In this chapter, we firstly overview the main concepts corresponding to FBP, and then we will have a general survey on the basic notions of ART theory.

2.1 Overview of FBP Theory

In this section, we briefly define the formulas and notions which are basically underlying concepts of FBP.

2.1.1 Radon Transform

The Radon transform ($\Re$), introduced in 1917 and named after the Austrian mathematician Johann Radon [20], is the integral transform consisting of the integral of a function over straight lines. For a function f which may be represented as an attenuation-coefficient function, which is a quantity that characterizes how easily a material or medium can be penetrated by a beam of light, sound, particles and the domain of which is the coordinate plane, the Radon transform of f is a multi-step

process that, for each pair of values of t and θ, integrates f along a different line $\ell_{t,\theta}$ [7]:

$$\Re f(t,\theta) := \int_{\ell_{t,\theta}} f ds = \int_{s=-\infty}^{\infty} f(t\cos(\theta) - s\sin(\theta), t\sin(\theta) + s\cos(\theta)) ds.$$

We have to note that f and $\Re f$ are functions in Cartesian coordinates of x and y and in polar coordinates of t and θ, respectively. The Radon transform is widely applicable to tomography, the creation of an image from the scattering data (X-ray data) associated to cross-sectional scans of an object.

If a function f represents an unknown density such as an attenuation-coefficient function, then the Radon transform represents the scattering data obtained as the output of a tomographic scan. Hence, by knowing the definition of the inverse of the Radon transform, which is called here back projection, we can reconstruct the original attenuation-coefficient function from the scattering data, and thus it forms the mathematical structure for tomographic reconstruction which is also known as image reconstruction. Meanwhile, the projection data collected, which are the Radon transform of the unknown object, is called *sinogram*.

2.1.2 Fourier Transform

For a given function f, the Fourier transform (FT) of the object function f, for each real number ω, can be defined as [21]

$$\mathcal{F}f(\omega) = \int_{-\infty}^{\infty} f(x)e^{-i\omega x}dx,$$

where for each value of ω, the value of the Fourier transform captures the component of f with the periodicity $2\pi/\omega$. The inverse of the Fourier transform (IFT), for each real number x, can also be defined by

$$f(x) = \mathcal{F}^{-1}(\mathcal{F}f(\omega)) = \frac{1}{2\pi}\int_{-\infty}^{\infty} \mathcal{F}f(\omega)e^{i\omega x}d\omega.$$

2.1.3 Central Slice Theorem

This theory was first derived by Bracewell in 1956 [3] and involves the interaction between the Radon transform and the Fourier transform, which is known as either central projection or central slice theorem. Hence, for any suitable function f, say, an X-ray attenuation coefficient function of two dimensional Cartesian coordinates, the central slice theorem for all real numbers S and θ can be defined as

$$\mathcal{F}_2 f(S\cos(\theta), S\sin(\theta)) = \mathcal{F}(\Re f)(S, \theta),$$

where the symbols $\mathcal{F}$ and $\mathcal{F}_2$ denote the one- and two-dimensional Fourier transforms, respectively.

This theorem is used in the analysis of medical CT scans, where a projection is an X-ray image of an internal organ. The Fourier transforms of these images are seen to be slices through the Fourier transform of the density of the internal organ, and these slices can be interpolated to build up a complete Fourier transform of that

density. The inverse Fourier transform is then used to reconstruct the density of the object.

2.1.4 Convolution

The concern, which is all along with the signals analysis, is the noise presence, which is any effect corrupting a signal. To remove the noise effects and form a clearer picture of a signal, filters are used. Hence, using the notion of filters, Convolution [24] can be defined by a mathematical operation on two functions f and g producing a third function that is viewed as a modified version of one of the original functions which is indeed filtered as following.

$$(f * g)(x) = \int_{-\infty}^{\infty} f(t)g(x-t)dt.$$

One of the main properties between the convolution and the Fourier transform that plays a significant role in what is to come in this thesis is that, for suitable functions f and g, the product of their Fourier transforms is equal to the Fourier transform of their convolution as following,

$$(\mathcal{F}\phi \cdot \mathcal{F}g)(s,\theta) = \mathcal{F}(\phi * g)(s,\theta).$$

2.1.5 Discrete Radon Transform

In discrete Radon transform, the X-ray machine does not assess the attenuation along every line $\ell_{t,\theta}$. Instead, the Radon transform is sampled for a finite number of angles θ between 0 and π, and at each of these angles, for some finite number of t's. Both the angles and the t values are typically evenly spaced. If the X-ray machine

takes scan at N different angles, then $\Delta\theta = \pi/N$, and the specific values of θ that occur are $\{k\pi/N : 0 \leq k \leq N-1\}$. The values of t are also $\{j \cdot d : -M \leq j \leq M\}$ as

$$-M \cdot d, (-M+1) \cdot d, ..., 0, ..., M \cdot d$$

Hence, the discrete Radon transform $\Re_D$ values of f are given as input for $-M \leq j \leq M$ and $0 \leq k \leq (N-1)$, where $2M+1$ is the number of beams at each angle, N is the number of angles, and d is the sample spacing between beams. That is,

$$\Re_D f_{j,k} = \Re f(jd, k\pi/N),$$

where a typical value of N is 180, and a typical value of M depends on the design of the X-ray machine, and also on the size of the object that the X-ray machine is designed to scan.

2.1.6 Discrete Fourier Transform

The Discrete Fourier Transform (DFT), denoted by $\mathcal{F}_D$, transforms an N-periodic discrete function f into another N-periodic discrete function $\mathcal{F}_D f$ as follows,

$$(\mathcal{F}_D f)_j = \sum_{k=0}^{N-1} f_k e^{-i2\pi kj/N} \qquad \text{for} \quad j = 0, 1, ..., (N-1).$$

For two discrete functions $f = \{f_k : 0 \leq k \leq N-1\}$ and $g = \{g_k : 0 \leq k \leq N-1\}$ with the same period, we have

$$\mathcal{F}_D(f \bar{*} g) = (\mathcal{F}_D f) \cdot (\mathcal{F}_D g).$$

In words, the discrete Fourier transform of a convolution is the product of the discrete transforms, individually. Also for two discrete N-periodic function f and g, we have

$$\mathcal{F}_D(f \cdot g) = \frac{1}{N}(\mathcal{F}_D f) \bar{*} (\mathcal{F}_D g).$$

The Discrete Inverse Fourier transform (DIFT) of g, which is an N-periodic discrete function, is the N-periodic function defined as following,

$$(\mathcal{F}_D^{-1} g)_m = \frac{1}{N} \sum_{k=0}^{N-1} g_k \; e^{i2\pi km/N}.$$

for a given integer m with $0 \leq m \leq (N-1)$.

2.1.7 Discrete Convolution

In analogy with the integral that defines continuous convolution, the discrete convolution of two discrete functions f and g, denoted by $f \bar{*} g$, is defined by

$$(f \bar{*} g)_m = \sum_{j=-\infty}^{\infty} f_j \cdot g_{(m-j)}.$$

In practice, we typically know the values of a function f only at a finite set of points, say $\{k \cdot d : k = 0, 1, ..., (N-1)\}$, in that f is periodic with period N and zero outside. N is the total number of points at which f has been computed, and d is the sample spacing.

For two N-periodic discrete functions $f = \{f_k : 0 \leq k \leq N-1\}$ and $g = \{g_k :$

$0 \leq k \leq N-1\}$, the discrete convolution, denoted as $f \bar{*} g$, is defined by

$$(f \ \bar{*} \ g)_m = \sum_{j=0}^{N-1} f_j \cdot g_{(m-j)} \quad \text{for each integer m.}$$

The following holds [7]. Let f and g be two-way infinite discrete functions, and suppose there is some natural number K such that $g_k = 0$ whenever $k < 0$ or $k \geq K$. Let M be an integer satisfying $M \geq K-1$, and let $\tilde{f}$ and $\tilde{g}$ be the $(2M+1)$-periodic discrete functions defined by $\tilde{f}(m) = f(m)$ and $\tilde{g}(m) = g(m)$ for $-M \leq m \leq M$. Then for all m which satisfy $0 \leq m \leq K-1$, we have

$$(f \ \bar{*} \ g)_m = \left(\tilde{f} \ \bar{*} \ \tilde{g}\right)(m). \tag{2.1}$$

By means of zero padding, we can take a finite set of values of a function like g and, by padding the sequence of values with a lot of zeros, form a periodic discrete function $\tilde{g}$ in such a way that the periodic discrete convolution gives the same value as the true discrete convolution, at least at the points where the value has been sampled.

Now, we apply equation (2.1) to the discrete convolution of the sampled band-limited function $\mathcal{F}^{-1}A$, where A is a low-pass filter, and the sampled Radon transform $\Re_D f$, where f is the attenuation function we wish to reconstruct. Since the scanned object is finite in size, we can set $\Re_D f(j, \theta) = 0$ whenever j, the beam number, is sufficiently large.

Thus, with enough zero padding, the discrete Radon transform can be extended to be periodic in the radial variable (jd). For discrete functions defined using polar

coordinates, the discrete convolution is carried out in the radial variable only. In particular, for a given filter A, we compute the discrete convolution of the sampled inverse Fourier transform of A with the discrete Radon transform of f as

$$(\mathcal{F}_D^{-1}A \circledast \Re_D f)_{m,\theta} = \sum_{j=0}^{N-1} \mathcal{F}_D^{-1}A_j \cdot \Re_D f_{m-j,\theta}.$$

2.1.8 Discrete Back Projection

In the continuous setting, the back projection is defined by

$$\beta\mathcal{H}(x,y) = \frac{1}{\pi}\int_{\theta=0}^{\pi} \mathcal{H}(x\cos(\theta) + y\sin(\theta), \theta)\ d\theta. \tag{2.2}$$

In the discrete setting, the continuously variable angle θ is replaced by the discrete set of angles $\{k\pi/N : 0 \le k \le N-1\}$. So the value of $d\theta$ becomes π/N and the back-projection integral is replaced by the sum [7],

$$\beta_D\mathcal{H}(x,y) = \Big(\frac{1}{N}\Big)\sum_{k=0}^{N-1} \mathcal{H}(x\cos(k\pi/N) + y\sin(k\pi/N), k\pi/N).$$

This is applied to $\mathcal{H} = (\mathcal{F}_D^{-1}A) \circledast (\Re_D f)$. The obstacle here is that the reconstruction grid, within which the final image is to be presented, is a rectangular array of pixels, located at points $\{(x_m, y_n)\}$, each of which is to be assigned a color or greyscale value. Thus the discrete back projection (DBP) requires the values of $(\mathcal{F}_D^{-1}A) \circledast (\Re_D f)$ at the corresponding points $\{(x_m\cos(k\pi/N) + y_n\sin(k\pi/N), k\pi/N)\}$. However, the Radon transform samples and the values of $(\mathcal{F}_D^{-1}A) \circledast (\Re_D f)$ are known only at the points $\{(jd, k\pi/N)\}$. To overcome this problem, observe that, for a given (x,y) and a given k, the number $(x\cos(k\pi/N) + y\sin(k\pi/N)$ will lie in between two multiples

of d. That is, there is some value n such that [7]

$$nd \leq (x\cos(k\pi/N) + y\sin(k\pi/N) < (n+1)d.$$

Hence, we wish to interpolate a value for $(\mathcal{F}_D^{-1}A) \bar{*} (\Re_D f)$ at the point $(x\cos(k\pi/N) + y\sin(k\pi/N), k\pi/N)$, using the known values at nearby points to create a continuous or piecewise continuous function, which closely fits the known data points. The most common interpolation schemas, which can be used, are Nearest neighbor, Linear, Cubic spline and Lagrange interpolations.

2.1.9 Overall Method of Discrete Image Reconstruction

To reconstruct an image, attenuation coefficient function $f(x, y)$, using Filtered Back Projection when complete continuous X-ray data are available, we have [7]

$$f(x,y) = \frac{1}{2}\beta\Big[\mathcal{F}^{-1}\big[|S|\mathcal{F}\ (\Re f)(t,\theta)\big]\Big](x,y).$$

Replacing $|S|$ with a low-pass filter A, obtained by multiplying the absolute value by a window function that vanishes outside some finite interval, in place of the above formula, we use the approximation

$$f(x,y) \approx \frac{1}{2}\beta(\mathcal{F}^{-1}A * \Re f)(x,y).$$

The starting point in the implementation of the above approximation in the practical reconstruction of images from X-ray data is that only a finite number of values of $\Re f(t,\theta)$ are given and available in a real study. More details, about image reconstruction using FBP, are available in [7].

2.2 Overview of ART Theory

The first CT scanners, designed in the late 1960s by Godfrey Hounsfield, used an approach grounded in linear algebra and matrix theory to generate an image from machine readings. Algorithms that adopt this point of view are known as Algebraic Reconstruction Techniques (ART). In this section, we briefly define the notions regarding to algebraic reconstruction techniques.

2.2.1 Basis Functions

Suppose an image is to be constructed in a K-by-K grid of pixels, and the pixels are numbered (row-wise) from 1 to K^2. The pixel basis functions $b_1, ..., b_{K^2}$ are defined by

$$b_k(x,y) = \begin{cases} 1 & \text{if } (x,y) \text{ lies inside pixel number } k, \\ 0 & \text{if } (x,y) \text{ does not lie inside pixel number } k \end{cases}$$

for $k = 1, 2, ..., K^2$ and points (x, y) in the plane. By assigning a color value x_k to the kth pixel, the resulting image will be presented by the function

$$\widetilde{f}(x,y) = \sum_{k=1}^{K^2} x_k \, b_k(x,y)$$

Applying Radon ($\Re$) transform to both sides of this function and using the linearity of $\Re$, we obtain that for each choice of t and θ,

$$\Re\widetilde{f}(t,\theta) = \sum_{k=1}^{K^2} x_k \, \Re b_k(t,\theta)$$

In practice, an X-ray machine produces values of $\Re f(t,\theta)$ for some finite set of lines $\ell_{t,\theta}$.

A system of equations for some positive integer J can be written as:

$$p_j = \Re\widetilde{f}(t_j,\theta_j) = \sum_{k=1}^{K^2} x_k \, \Re b_k(t_j,\theta_j) \qquad \text{for} \;\; j = 1,...,J.$$

The connection between $\widetilde{f}(x,y)$ and $\Re\tilde{f}(t_j,\theta_j)$ is provided by Radon transform ($\Re$) [20]. Since our ultimate objective is computing the function $\widetilde{f}(x,y)$ given values of $\Re\widetilde{f}(t_j,\theta_j)$, we need to do the inversion of the Radon transform. Since the pixel basis function b_k has the value 1 on its pixel and 0 elsewhere, the value of the integral $\Re b_k(t_j,\theta_j)$ is equal to the length of the intersection of the line ℓ_{t_j,θ_j} with pixel number k, which is denoted by r_{jk}. That is,

$$r_{jk} = \Re b_k(t_j,\theta_j), \qquad \text{for } j = 1,...,J, \;\; k = 1,...,K^2,$$

which can also be stated as a system of J linear equations in K^2 unknowns $(x_1,...,x_{K^2})$:

$$p_j = \sum_{k=1}^{K^2} x_k \, r_{jk} \qquad \text{for } j = 1,...,J.$$

Now we can formally describe the input of the linear system $Ax = p$ as a vector of $p_j = \Re\widetilde{f}(t_j,\theta_j)$ for a sinogram, which is the resulting image after applying Radon transform on it, and a projection matrix $A \in R^{m\times n}$ with components of $r_{jk} = \Re b_k(t_j,\theta_j)$. The output vector of x_k contains the color value of each pixel of the resulting image.

It is good to know that the described physical model is not limited to a certain scanning geometry technique of the CT scanner. It can use different scanning geometry techniques such as parallel beam, fan beam, spiral beam and cone beam geometries. The last two geometries have been developed for use in later generation scanning machines facilitating the collection of data for more than one slice at the same time.

To compute the solution of the linear system $Ax = p$, we intend to use Kaczmarz's method which is an iterative algorithm or procedure for approximating a solution to linear systems that we will specifically talk about it in Chapter 3. If we denote by r_i to ith row of the matrix A, and by p_i to ith coordinate of the vector p, then the system $Ax = p$ is the same as having $r_i x = p_i$ for every value of i.

In fact, this method works by producing a sequence of vectors, each of which satisfies one of the individual equations $r_i x = p_i$. Now before looking at Kaczmarz's method, let's make the following definition which is to be used in Kaczmarz's method. For a fixed n-dimensional vector r and a number p, the affine space $\varphi_{r,p}$ is defined by:

$$\varphi_{r,p} = \{\, x \in R^n : r^T x = p \,\}$$

Note that the affine space $\varphi_{r,p}$ is a subspace of R^n if and only if $p = 0$, and each of the lines $\ell_{t,\theta}$ is an affine space.

2.2.2 Affine Projection

Given a vector u and an affine space $\varphi_{r,p}$ for some vector r and some number p, the affine projection of u in $\varphi_{r,p}$ is the vector u_* in $\varphi_{r,p}$ that is closest to u among all vectors in $\varphi_{r,p}$. To move from u to the closest point in the affine space, it is evident that we should move orthogonally to the affine space [7]. Thus, the vector u_* that we seek should have the following form for some number λ, $u_* = u - \lambda r$. Substituting $u_* = u - \lambda r$ into the equation $r^T u_* = p$ and solving for λ we obtain,

$$\lambda = \frac{r^T u - p}{r^T r}$$

Then, the affine projection u_* of the vector u in the affine space $\varphi_{r,p}$ is given by the equation:

$$u_* = u - \frac{r^T u - p}{r^T r} r$$

Chapter 3

Algorithmic Formulation of FBP and ART

In the first section of this chapter, we will write both the continuous and discrete filtered back projection in algorithmic ways, and subsequently, the number of operations in discrete FBP will be counted. In the last section, we will discuss the properties and complexities of different ART methods, and we will briefly review the previously proposed strategies for finding relaxation parameters and stopping rules.

3.1 Filtered Back Projection

Using the notations defined in the previous chapter, we discuss each of the steps of FBP in an algorithmic way. First, we overview the continuous FBP(3.1.1), then we overview the continuous FBP using convolution(3.1.2), and then we discuss the discrete FBP(3.1.3). Finally, we derive the discrete FBP complexity.

3.1.1 Continuous Filtered Back Projection

For a given function f, the FBP is derived as follows:

1. Assume we are given the Radon transform $\Re$ of f for each (t, θ):

$$\Re f(t,\theta) := \int_{\ell_{t,\theta}} f ds = \int_{s=-\infty}^{\infty} f(t\cos(\theta) - s\sin(\theta), t\sin(\theta) + s\cos(\theta)) ds,$$

   Then we obtain $f(x, y)$ as follows,

2. Compute the Fourier transform $\mathcal{F}$ of $g(t, \theta) = \Re f(t, \theta)$ by

$$\mathcal{F}(g)(t,\theta) := \int_{-\infty}^{\infty} g(t,\theta) e^{-i\omega t} dt,$$

3. Compute an absolute-value function,

$$|S|\mathcal{F}(g)(t,\theta),$$

4. Compute the inverse Fourier transform

$$\mathcal{F}^{-1}\Big[|S|\mathcal{F}(g)(t,\theta)\Big],$$

5. Compute the back projection β as

$$\begin{aligned} f(x,y) &= \frac{1}{2}\beta\Big(\mathcal{F}^{-1}\big[|S|\mathcal{F}(g)(t,\theta)\big]\Big)(x,y) \\ &= \frac{1}{2\pi}\int_0^{\pi} \mathcal{F}^{-1}\big[|S|\mathcal{F}(g)(t,\theta)\big]\big(x\cos(\theta) + y\sin(\theta), \theta\big) d\theta \end{aligned}$$

3.1.2 Filtered Back Projection Using Convolution

Since the Radon transform $\Re$ of f may have a component at a high frequency which may be magnified by the factor $|S|$ leading to noise exaggeration in the data, we do not use the above scheme in which the factor $|S|$ is used.

Indeed, we use a function that is close to the absolute-value function for $|S|$ near 0, and vanishes when the value of $|S|$ is large, which corrupts the reconstructed image. This kind of function is called low-pass filter since it does not affect the lower frequencies, while cuts off the higher frequencies including noise. Hence, for a given function f, whose domain is the plane, instead of steps number 3 to 5 in the above scheme we do:

3. Let $\phi(t)$ be a function for which $\mathcal{F}\phi(S) = |S|$. Then

$$\Big[|S|\mathcal{F}(g)\Big](s,\theta) = [\mathcal{F}\phi \cdot \mathcal{F}g](s,\theta) = \mathcal{F}(\phi * g)(s,\theta),$$

   where $*$ denotes convolution.

4. Compute the IFT of the FT of convolution $\mathcal{F}(\phi * g)(s,\theta)$:

$$\mathcal{F}^{-1}\Big[\mathcal{F}(\phi * g)(s,\theta)\Big] = (\phi * g)(t,\theta),$$

5. The f is recovered by,

$$f(x,y) = \frac{1}{2}\beta(\phi * g)(x,y), \tag{3.1}$$

where β is the back projection (2.2).

The fact is that such a $\phi(t)$ function does not exist that its FT is equal to the absolute-value function $|S|$. Hence, in practice we replace $|S|$ by something else which is a low-pass filter (A) to approximate $\mathcal{F}\phi$ and $f(x, y)$. Since $\mathcal{F}\phi \approx A$, so $\phi \approx \mathcal{F}^{-1}A$ and equation (3.1) can be rewritten as,

$$f(x, y) \approx \frac{1}{2}\beta(\mathcal{F}^{-1}A * g)(x, y),$$

An instant example for a discrete low-pass filter A is the *Shepp–Logan* filter as following:

$$\begin{aligned} A(\omega) &= |\omega| \cdot \Big(\frac{\sin(\pi\omega/(2L))}{\pi\omega/(2L)}\Big) \cdot \sqcap_L(\omega) \\ &= \begin{cases} \frac{2L}{\pi} \cdot |\sin(\pi\omega/(2L))| & \text{if } |\omega| \le L, \\ 0 & \text{if } |\omega| > L, \end{cases} \end{aligned}$$

for some choices of $L > 0$, where $\sqcap_L(\omega)$ is a simple square wave as below:

$$\sqcap_L(\omega) = \begin{cases} 1 & \text{if } |\omega| \le L, \\ 0 & \text{if } |\omega| > L, \end{cases}$$

3.1.3 Discrete Filtered Back Projection

To reconstruct an unknown function f, whose domain is the plane, we have the following algorithm in which the input and output are as:

- Inputs: Discrete Radon transform $\Re_D$ values of f

Low-pass filter

Interpolation method

- Output: Reconstructed unknown function f

1. The discrete Radon transform $\Re_D$ values of f are given as input for $-M \leq j \leq M$ and $0 \leq k \leq (N-1)$, where $2M+1$ is the number of beams at each angle, N is the number of angles, and d is the sample spacing between beams.

$$\Re_D f_{j,k} = \Re f(jd, k\pi/N).$$

A typical value of N is 180, and a typical value of M depends on the design of the X-ray machine, and also on the size of the object that the X-ray machine is designed to scan.

2. The DFT of $g_{j,k} = \Re_D f_{j,k}$ is,

$$\begin{aligned}(\mathcal{F}_D g)_{j,k} &= \sum_{l=-M}^{M} \sum_{m=0}^{N-1} g(ld, m\pi/N) \cdot e^{-i2\pi mk/N} \cdot e^{-i2\pi lj/(2M+1)} \\ &= \sum_{l=-M}^{M} \sum_{m=0}^{N-1} g(ld, m\pi/N) \cdot e^{-i2\pi(mk/N + lj/(2M+1))}\end{aligned}$$

for $-M \leq j \leq M$ and $0 \leq k \leq (N-1)$.

3. As said earlier, since there is not such a function $\phi(t)$, whose Fourier transform satisfies $\mathcal{F}\phi(S) = |S|$, we replace $|S|$ with a function of the form $\mathcal{F}\phi \approx A$, where

A is nonzero on some finite interval and zero outside that interval. Indeed, we approximate $|S|$ by a function A and try to find $\phi \approx \mathcal{F}^{-1}A$. So, we have:

$$|S| \cdot \mathcal{F}_D g = \mathcal{F}_D \phi \cdot \mathcal{F}_D g \approx A \cdot \mathcal{F}_D g,$$

where A is a discrete low-pass filter.

4. Compute the DIFT of $(A \cdot \mathcal{F}_D g)_{l,m}$ for $-M \leq l \leq M$ and $0 \leq m \leq (N-1)$:

$$\begin{aligned} \mathcal{F}_D^{-1}(A \cdot \mathcal{F}_D g)_{l,m} &= (\mathcal{F}_D^{-1}A \bar{*} \mathcal{F}_D^{-1}\mathcal{F}_D g)_{l,m} \\ &= (\mathcal{F}_D^{-1}A \bar{*} g)_{l,m} \\ &= \sum_{j=-M}^{M} \sum_{k=0}^{N-1} (\mathcal{F}_D^{-1}A)_k \cdot (g)_{l-j,m-k} \cdot (\mathcal{F}_D^{-1}A)_j \end{aligned}$$

where $\bar{*}$ denotes discrete convolution.

5. Interpolate the function $(\mathcal{F}_D^{-1}A \bar{*} g)$ by an interpolation method. For simplicity of notation, we denote the interpolated function of $(\mathcal{F}_D^{-1}A \bar{*} g)$ by $\mathcal{I}$. In fact, the value of the interpolated function $\mathcal{I}(t, k\pi/N)$ are computed according to the previously computed values of $(\mathcal{F}_D^{-1}A \bar{*} g)(jd, k\pi/N)$ and also the interpolation method we are going to use which can be Nearest neighbor, Linear, Cubic spline or Lagrange interpolation.

6. Compute the DBP(β_D), where $\mathcal{I}$ is the interpolated function of $(\mathcal{F}_D^{-1}A \bar{*} g)$

$$f(x,y) \approx \frac{1}{2}\beta_D \mathcal{I}(x,y) = \frac{1}{2N} \sum_{k=0}^{N-1} \mathcal{I}\big(x\cos(k\pi/N) + y\sin(k\pi/N), k\pi/N\big)$$

3.1.4 MATLAB Description of Discrete FBP

Given `RI` the Radon transform values of an image `I`, `A` the Low-pass filter, and `intpol` the interpolation method as inputs,

1. We take the Fast Fourier transform of `RI`

   ```
   FFTRI = fft(RI)
   ```

2. We compute a filtered sinogram by applying a low-pass filter `A` to the Fast Fourier transform of `RI`

   ```
   FilteredFFTRI = FFTRI.* A
   ```

3. We compute the Inverse Fast Fourier transform of `FilteredFFTRI`

   ```
   InvFilteredFFTRI = ifft(FilteredFFTRI)
   ```

4. Now we compute the back projection

   ```
   BackProj = iradon(InvFilteredFFTRI, intpol)
   ```

3.1.5 Operations Count for Discrete FBP

To find out the complexity of discrete FBP algorithm, and also to be able to compare the complexity of FBP with the complexities of ART methods, we count the number of operations in each image reconstruction method. In discrete FBP, assume I is an $n \times n$ image, N is the number of angles and there are $2M+1$ beams per angle.

1. Taking the Fast Fourier transform of RI consists of: $O(NM \log M)$ operations since in one angle the FFT complexity for $2M+1$ beams is $O((2M+1)\log(2M+1)))$, so for N angles the FFT complexity is

   $$O(N(2M+1)\log(2M+1))) \approx O(NM \log M)$$

2. Applying a low-pass filter (A) to the Fast Fourier transform of RI has

   $O(N(2M+1)) \approx O(NM)$ operations

3. Computing the Inverse Fast Fourier transform also includes of

   $$O(N(2M+1)\log(2M+1))) \approx O(NM \log M)$$

4. Finally, computing the back projection of interpolation function includes of $O(Nn^2)$ operations since interpolation consists of n^2 operations for each (x, y) and we have N times interpolation. Hence, in this stage we have $O(Nn^2)$ operations.

Summing up all the number of operations, we can claim that the discrete FBP has the complexity of

$$O(NM \log M + Nn^2) = O(N(M \log M + n^2)).$$

3.2 Algebraic Reconstruction Techniques

CT has been extensively studied for years and widely used in modern society. Although FBP algorithm is the method of choice by manufacturers nowadays, efforts are being made to revisit iterative methods due to their unique advantages, such as simplicity and superior performance with incomplete noisy data [15]. To this point, we have summarized how transform-based methods are used in image reconstruction, and how these approaches are used in the algorithms of today's CT scan machines.

To reach our goal, which is reconstructing the attenuation function $\widetilde{f}(x, y)$, we shall use ART to find an approximate solution to the system of linear equations. To implement an ART algorithm, it is necessary to know the values of $\Re\widetilde{f}(t, \theta)$ coming from CT machine for a variety of choices of t for each of the selected angles θ.

To start with physical model, we have to know that ART treats the problem of image reconstruction as a discrete problem from the beginning. Any image we produce will be constructed inside a rectangular grid of picture elements, or pixels such that a specific color value is assigned to each of them. The number of pixels in an image may be large, but it is nonetheless finite.

3.2.1 Kaczmarz's Method

Now we put our knowledge of affine spaces to define Kaczmarz's method [16] which is an iterative algorithm or procedure for finding an approximate solution to a linear system $Ax = p$. Again, denote the ith row of the matrix A by r_i and the ith coordinate of the vector p by p_i. Then each of the equations $r_i x = p_i$ describes an affine

space.

Kaczmarz's method proceeds by starting with an initial guess for x, a vector of prospective color values, and then computes the affine projection of this initial guess onto the first affine space in our list. This projection is then projected onto the next affine space in the list, and so on until we have gone through the entire list of affine spaces. Starting with initial guess $x^{0,0}$, we have,

$$x^{0,1} = x^{0,0} - \frac{r_1^T x^{0,0} - p_1}{r_1^T r_1} r_1 \tag{3.2}$$

Where in $x^{0,1}$, 1 and 0 are the projection and iteration numbers, respectively. If the matrix A has J rows, then the vectors $x^{0,1}$, $x^{0,2}$, ..., $x^{0,J}$ will be computed, and once $x^{0,J}$ has been computed, set $x^{1,0} = x^{0,J}$ and compute the vectors $x^{1,1}$, $x^{1,2}$, ..., $x^{1,J}$ in a similar manner, and we stop the iterations when a stopping criterion is satisfied. If the linear system $Ax = p$ has at least one solution in the least squares sense,

$$\min \|Ax - p\|$$

then Kaczmarz's method converges to a solution of this system [7]. Moreover, if $x^{0,0}$ is in the range of A^T, then Kaczmarz's method converges to the solution of minimum norm [7, p.110].

3.2.2 Kaczmarz's Method with a Relaxation Parameter

The most commonly employed variation of Kaczmarz's method [16] involves the introduction of a relaxation parameter. For each row i and iteration k, let λ_{ik} be

a relaxation parameter, satisfying $0 < \lambda_{ik} < 2$. Instead of computing with formula (3.2), we compute with,

$$x^{k,i} = x^{k,i-1} - \lambda_{ik} \frac{r_i^T x^{k,i-1} - p_i}{r_i^T r_i} r_i \tag{3.3}$$

Where in $x^{k,i}$, i and k are projection and iteration numbers, respectively. The usual requirement is that the value of λ_{ik} should be bounded as $0 \leq \lambda_{ik} \leq 2$. If $\lambda_{ik} = 1$, formula (3.3) is the pure Kaczmarz's method without a relaxation parameter. When $0 < \lambda_{ik} < 1$, the vector $x^{k,i-1}$ is projected only part of the way to the affine space φ_{r_i,p_i}. If $1 < \lambda_{ik} < 2$, the vector $x^{k,i-1}$ is projected on the other side of the affine space, and finally when $\lambda_{ik} = 2$, the vector $x^{k,i}$ is just the reflection of $x^{k,i-1}$ across φ_{r_i,p_i} [7].

3.2.3 Operations Count For Kaczmarz's Method

Assume I is an $n \times n$ image, N is the number of angles and M is the number of beams in each angle. Count of operations including addition, multiplication, division and subtraction for Kaczmarz's method is as following:

for $k = 1 : K$

  for $i = 1 : m$

    $x^{k,i} = x^{k,i-1} - \lambda_{ik}(\frac{r_i^T x^{k,i-1} - p_i}{r_i^T r_i})r_i$

  end

end

where n^2, m and λ are the number of pixels, the number of angles times the number of beams per angle and the relaxation parameter, respectively.

1. $r_i^T x^{k,i-1}$ has: $(n^2)^{Mult} + (n^2-1)^{Add} = (2n^2-1)^{opt}$
2. $r_i^T r_i$ has: $(n^2)^{Mult} + (n^2-1)^{Add} = (2n^2-1)^{opt}$
3. $r_i^T x^{k,i-1} - p_i$ has: 1^{opt}
4. $\dfrac{r_i^T x^{k,i-1} - p_i}{r_i^T r_i}$ has: 1^{opt}
5. $\lambda_{ik}\dfrac{r_i^T x^{k,i-1} - p_i}{r_i^T r_i}$ has: 1^{opt}
6. $\lambda_{ik}\dfrac{r_i^T x^{k,i-1} - p_i}{r_i^T r_i}.r_i$ has: $(n^2)^{opt}$
7. $x^{k,i-1} - \lambda_{ik}(\dfrac{r_i^T x^{k,i-1} - p_i}{r_i^T r_i})r_i$ has: $(n^2)^{Sub}$

The sum of all the above steps number of operations is equal to $6n^2 + 1$ which must be multiplied by K and m, which are respectively the number of iterations and the number of angles times the number of beams in each angle as following:

$$K \times m \times (6n^2 + 1) = K \times M \times N \times (6n^2 + 1)$$

Hence, the complexity of Kaczmarz's method is $O(NMn^2K)$.

3.2.4 Symmetric Kaczmarz's Method

Another variant of Kaczmarz's method is the symmetric Kaczmarz's method [2] in which the equations of the projection matrix are used in reverse order. On the other hand, unlike Kaczmarz's method in which there are m steps (m equations), in symmetric Kaczmarz's method, there are $2m-2$ number of steps, which are actually projections, in each iteration to approximate to a solution. The algorithm for symmetric Kaczmarz's method is as following:

$$x^{k,i} = x^{k,i-1} - \lambda_{ik}\frac{r_i^T x^{k,i-1} - p_i}{r_i^T r_i} r_i$$

where $i = 1, ..., m, m-1, ..., 2$.

3.2.5 Operations Count For Symmetric Kaczmarz's Method

Assuming N is the number of angles and M is the number of beams in each angle, operations count regarding to symmetric Kaczmarz's method is as below:

1. $r_i^T x^{k,i-1}$ has: $(n^2)^{Mult} + (n^2 - 1)^{Add} = (2n^2 - 1)^{opt}$
2. $r_i^T r_i$ has: $(n^2)^{Mult} + (n^2 - 1)^{Add} = (2n^2 - 1)^{opt}$
3. $r_i^T x^{k,i-1} - p_i$ has: 1^{opt}
4. $\frac{r_i^T x^{k,i-1} - p_i}{r_i^T r_i}$ has: 1^{opt}
5. $\lambda_{ik}\frac{r_i^T x^{k,i-1} - p_i}{r_i^T r_i}$ has: 1^{opt}
6. $\lambda_{ik}\frac{r_i^T x^{k,i-1} - p_i}{r_i^T r_i}.r_i$ has: $(n^2)^{opt}$
7. $x^{k,i-1} - \lambda_{ik}(\frac{r_i^T x^{k,i-1} - p_i}{r_i^T r_i})r_i$ has: $(n^2)^{Sub}$

The sum of all the above steps number of operations is equal to $6n^2 + 1$ which must be multiplied by K and $(2m-2)$ which are respectively the number of iterations and $(2M \times N - 2)$ as following:

$$K \times 2m - 2 \times (6n^2 + 1) = K \times (2M \times N - 2) \times (6n^2 + 1)$$

where n^2, m and λ are the number of pixels, the number of angles times the number of beams per angle and the relaxation parameter, respectively. Hence, the Big O notation for symmetric Kaczmarz's method is $O(NMn^2K)$.

3.2.6 Randomized Kaczmarz's Method

The next variant of Kaczmarz's method is randomized Kaczmarz's method [23] and is proved to have exponential expected convergence rate in which the rate is not dependent on the number of projections or equations in the system [23]. In this method, the index i, indicating the projection number, is chosen randomly from the equations set of $\{ 1, ..., m \}$.

$$x^{k,i} = x^{k,i-1} - \lambda_{ik} \frac{r_i^T x^{k,i-1} - p_i}{r_i^T r_i} r_i$$

In randomized Kaczmarz's method, the i^{th} equation is selected with probability proportional to $\|r_i\|^2$. Since in randomized Kaczmarz all the rows are chosen, the operations count for this method is the same as standard Kaczmarz's method which is $O(NMn^2K)$.

3.2.7 Simultaneous Algebraic Reconstruction Techniques

In 1984, Simultaneous Algebraic Reconstruction Techniques (SART) was developed as a major refinement of the ART [1]. The idea behind this method is that SART considers a subset of the ray sums in projection matrix which is related to a specific angle.

The implementation of this method generates a good reconstruction in only one iteration, and have a computational advantage over the traditional implementation of ART [1]. In fact, SART unlike Kaczmarz's method that updates the solution x in each projection, only updates the solution per iteration after computing all the projections of the current solution. In this thesis, we will compare SART with the

other proposed algorithms in terms of resulting image quality (image discrepancy), accuracy and convergence speed in Chapter 4. Modeling the same linear system of eqautions proposed in ART, for SART we also have,

$$A \cdot x = p,$$

where matrix $A \in R^{M \times N}$, $x \in R^N$ and $p \in R^M$ represent the projection matrix, solution and the collected data, respectively. The SART method can be written in the following matrix form [1],

$$x_j^k = x_j^{k-1} - \frac{\lambda}{A_{+,j}} \sum_{i=1}^{M} \frac{A_{i,j}}{A_{i,+}} (A_{i,:} \cdot x^{k-1} - p_i),$$

where k and $\lambda \in (0, 2)$ are the number of iterations and relaxation parameter, respectively. $A_{i,j}$, $A_{i,+}$, and $A_{+,j}$ are,

$$\begin{aligned} A_{+,j} &= \sum_{i=1}^{M} A_{i,j} \quad \text{for } j = 1, ..., N, \\ A_{i,+} &= \sum_{j=1}^{N} A_{i,j} \quad \text{for } i = 1, ..., M, \end{aligned}$$

where $A_{i,j}$, $A_{i,+}$, and $A_{+,j}$ denote the coefficients of the imaging system, the row sums, and the column sums, respectively. Meanwhile, $A_{i,j}$ must be non-negative, and both $A_{i,+}$ and $A_{+,j}$ must be none zero for $i = 1, ..., M$ and $j = 1, ..., N$.

3.2.8 Operations count for SART

Assume I as an $n \times n$ image, N the number of angles, and M the number of beams in each angle, count of operations including addition, multiplication, division and

subtraction for SART method is as following:

1. $A_{i,:} \cdot x^k$ has: $(n^2)^{Mult} + (n^2 - 1)^{Add} = (2n^2 - 1)^{opt}$
2. $\frac{A_{i,j}}{A_{i,+}}$ has: 1^{opt}
3. $A_{i,:} \cdot x^k - p_i$ has: 1^{opt}
4. $\frac{A_{i,j}}{A_{i,+}}(A_{i,:} \cdot x^k - p_i)$ has: 1^{opt}
5. $\sum_{i=1}^{m} \frac{A_{i,j}}{A_{i,+}}(A_{i,:} \cdot x^k - p_i)$ has: $m^{opt} \times (2n^2 + 2)$
6. $\frac{\lambda}{A_{+,j}} \sum_{i=1}^{M} \frac{A_{i,j}}{A_{i,+}}(A_{i,:} \cdot x^k - p_i)$ has: $(2n^2)^{opt}$
7. $x^{k-1} - \frac{\lambda}{A_{+,j}} \sum_{i=1}^{M} \frac{A_{i,j}}{A_{i,+}}(A_{i,:} \cdot x^k - p_i)$ has: $(n^2)^{Sub}$

where n^2, m and λ are the number of pixels, the number of angles times the number of beams per angle and the relaxation parameter, respectively. The sum of all the above steps number of operations is equal to $2mn^2 + 3n^2 + 2m$ which must be multiplied by K, which is the number of iterations as following:

$$K \times (2mn^2 + 3n^2 + 2m) \approx Kmn^2 = KMNn^2$$

Hence, the complexity of SART method is $O(KMNn^2)$, which is the same as the other previously discussed ART methods' complexities. Related operations count to each of the discussed methods in this chapter is shown in table 3.1,

Method	Complexity
FBP	$O(N(M \log M + n^2))$
Kaczmarz	$O(KMNn^2)$
Symmetric Kaczmarz	$O(KMNn^2)$
Randomized Kaczmarz	$O(KMNn^2)$
SART	$O(KMNn^2)$

Table 3.1: Methods complexities

3.2.9 Choice of Relaxation Parameter

As introduced in the variations of Kaczmarz's method, we will need a relaxation parameter λ_k for each iteration of an ART iterative method. It's already claimed that if ART's relaxation parameter is carefully adjusted to the reconstruction procedure, it can produce high-quality images in short computational time [18].

It is known that the choice of the relaxation parameter value is critical to the quality and speed of image reconstruction using ART. However several approaches have been already proposed for finding the optimal value of λ, no specific method is generally accepted.

Nevertheless, some facts are unanimously accepted that the choice of λ depends on the purpose of image reconstruction, and it may vary from one purpose to another. It is good know that greater values of λ in the interval $(0, 2)$ lead to fast convergence in ART, but also to noisy reconstruction images.

On the other hand, low values of λ lead to smooth images but slow convergence [12]. λ can have a constant value which can be also an optimal value over all the

iterative method or it can depend on the iteration number in order to maximize image quality using the least amount of time. This can be done in a way that its value can be chosen by previous evaluation for a certain kind of examination or it can be calculated as a function of some parameters measured from the image obtained in the previous iteration [12, 13]. Hence, the value of λ is chosen to optimize the algorithm convergence speed and also to maximize the image uniformity.

As said before, λ can also be a function of the k^{th} iteration, so we can assume that for every integer k there is a positive real number λ_k. However, it is not an easy task finding the relaxation parameter that best fits the reconstruction process and there is not a unique choice for the best relaxation parameter [12]. Generally speaking, the choice of relaxation parameter depends on [13]:

- Medical purpose of reconstruction
- Method of X-ray data acquisition
- Existence of noise on the measurements
- Number of iterations that we intend to do

Until now, very few methods and strategies have been proposed to find a fixed relaxation parameter for each of the ART methods, but roughly speaking, most of them were not proposing an adaptive strategy, which is the ideal case, for finding the suitable relaxation parameter in each iteration.

3.2.10 Hansen's Strategy For Finding Relaxation Parameters

The most significant strategy, which was extended for ART methods, was proposed by Maria Saxild-Hansen and her supervisor, Dr. Per Christian Hansen in her Master's thesis at Department of Informatics and Mathematical Modeling at Technical University of Denmark [10]. It proposes a training method by use of which the optimal value of the relaxation parameter (λ) for two of the ART methods, Kaczmarz and Symmetric Kaczmarz, can be determined.

The optimal value of λ in Hansen's strategy is defined as the value that gives rise to the fastest convergence to the smallest relative error in the solution. In this thesis, to compare the selected λ values from Hansen's strategy with of ours, we have used Hansen's AIR MATLAB package [10].

Hansen's strategy mainly includes of two parts. The first part is determining the resolution limit and the second one is determining the optimal value of relaxation parameter (λ) which reaches the resolution limit using fewest number of iterations. Resolution limit is basically a bound for how accurate a solution can get and indeed is the minimum relative error using the smallest number of iterations depending on the given problem and the used iterative reconstruction method.

Therefore, in the first part of this strategy, the minimum relative error using a safe choice of relaxation parameter to determine the resolution limit is found. After finding the minimum relative error, the upper bound (ub) of the resolution limit is defined to be the found relative error plus 1%.

In the second part of this training strategy, a modified version of the golden section search to find the value of λ reaching the resolution limit within fewest number of iterations is used [17].

3.2.11 Stopping Rules

All regularization methods make use of a certain regularization parameter that controls the amount of stabilization imposed on the solution. In iterative methods, the number of iterations can be used as regularization parameter. When an iterative method is used, the user can also study on-line adequate visualizations of the iterates as soon as they are computed, and simply halt the iteration when the desired approximations are reached. This may actually be the most appropriate stopping rule in many practical applications, but it requires a good intuitive imagination of what to expect.

In other situations, the user may need computer's help to determine the optimal approximation. The stopping rule strategies are naturally divided into two categories: rules which are based on knowledge of the norm of the errors, and rules which do not require such information [5]. If the error norm is known within reasonable accuracy, perhaps the most well known stopping rule is the Discrepancy Principle (DP) [19] and the other related stopping rule is the Monotone Error (ME) rule [9].

These two stopping rule strategies are based on some kind of knowledge of the noise level δ which is the norm of the errors and also a user-chosen parameter τ. Since

studying these two stopping rules is out of the discussion of this thesis, we skip from them. Through out this thesis, we have simply used a certain number of iterations as our stopping rule.

Chapter 4

Numerical Study of ART Methods

4.1 Introduction

In this chapter, we explain the test phantoms and error measuring being used throughout this thesis. Then, we assess the behavior of different ART methods with various test phantoms and relaxation parameters for different image sizes.

Then, a new adaptive strategy for finding the best relaxation parameter both in each iteration and in all iterations is proposed. At the end, the experimental results obtained using the new proposed strategy are compared to the numerical results obtained using another previously proposed strategy for finding an optimal relaxation parameter.

4.2 Phantoms

The most desirable way to test and compare the accuracy of different image reconstruction methods is to apply each method to data obtained from a human organ. However, a disadvantage of this approach is that, in most of the situations, we do not know precisely what we should expect to see in our reconstructed images. Hence, we try to use exact data from an object, which is called *phantom*.

As a matter of fact, without knowing the exact data, it is difficult to determine the accuracy of a reconstructed image. Hence, we apply different methods to data obtained from a physical object for which the internal structure is known. This way, we know exactly what our resulting images should look like, and we are able to recognize errors or inaccuracies in a given method and compare various methods.

Figure 4.1: Shepp-Logan phantom

In this thesis, to assess different ART techniques, three different phantoms are used. The first phantom is the Shepp-Logan phantom, Figure 4.1, whose structure is completely defined by mathematical formulas[1] [22]. Thus, no errors occur in collecting data for this image. The Shepp-Logan phantom is composed of eleven ellipses of various sizes, eccentricities, and locations. Since we can compute exactly the Radon transform of any ellipse, the Shepp-Logan phantom has proven to be a reliable model, on which to test reconstruction algorithms.

The second phantom is the para-sagittal MRI scan of a head[2], Figure 4.2, with aliasing artifacts (nose and forehead appear at the back of the head). The third phantom is the sagittal MRI scan image of a knee[3], Figure 4.3.

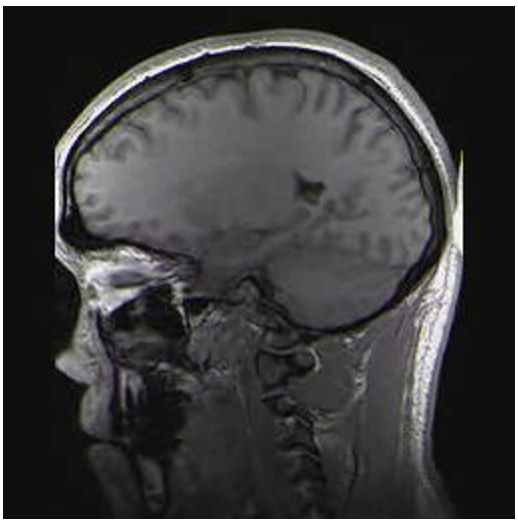

Figure 4.2: Head phantom

[1]http://en.wikipedia.org/wiki/File:Shepplogan.png
[2]http://en.wikipedia.org/wiki/File:StructuralMRIanimation.ogv
[3]http://en.wikipedia.org/wiki/File:MRKnee.jpg

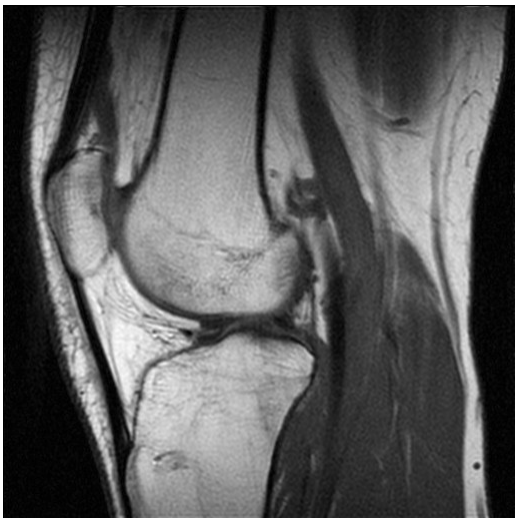

Figure 4.3: Knee phantom

The last two phantoms, unlike Shepp-Logan phantom, are not defined by mathematical formulas and are much closer to real MRI scanned images. Roughly speaking, in this thesis, we have tried to use both mathematically defined and real test phantoms to evaluate different ART techniques.

4.3 Measuring Image Quality

In this thesis to measure the quality of the reconstructed images by means of each of the methods, four kinds of measurements are used.

1. The relative error of the reconstructed image:

$$\text{Relative Error} = \frac{\|X^k - T\|}{\|T\|}, \tag{4.4}$$

where X^k are the pixel values of the reconstructed image at iteration number k,

and T are the pixel values of the original phantom. Both X and T are vectors of size $n \times n$, corresponding to an $n \times n$ image, where the value of the pixels are stored row by row. Throughout this thesis, we use the 2-norm.

2. The relative residual of the reconstructed image:

$$\text{Relative Residual} = \frac{\|b - AX^k\|}{\|b\|},$$

where X^k are the pixel values of the reconstructed image at iteration number k, A is the projection matrix, and b is the right hand side of $AX = b$.

3. The relative solution differences between iteration k and iteration $k + 1$:,

$$\text{Relative Solution Differences} = \frac{\|X^{k+1} - X^k\|}{\|X^k\|},$$

where X^k are the pixel values of the reconstructed image (solution) at iteration number k, and X^{k+1} are the pixel values of the reconstructed image (solution) at iteration number $k + 1$.

4. The discrepancy between the exact image (phantom) and the reconstructed image, which is of high importance in this thesis. It is also called Colsher's discrepancy metric [4].

$$\delta(k) = \sqrt{\frac{\sum_i \left(X_i^k - T_i\right)^2}{\sum_i \left(T_i - \overline{T}\right)^2}}, \tag{4.5}$$

where X^k are the reconstructed pixel values at iteration number k, T are the true pixel values of the original phantom, $\overline{T}$ is the mean value of the original phantom pixel values, and finally i is the index of the image pixel number for $i = 1, ..., n^2$.

In fact, the denominator of Colsher's discrepancy metric formula is the standard deviation of the true image and the numerator is the root mean square error of the reconstructed image. The closer the value of this formula is to zero, the less is the discrepancy between reconstructed image and original phantom [4].

4.4 Numerical Experiments

As said before, to test the previously discussed methods, we use three different phantoms: Shepp-Logan, MRI scan of a head, and MRI scan of a knee, where the two later ones are more practical than the first one, since they are obtained from real MRI scans.

In the linear equation system of $Ax = b$ being used in iterative image reconstruction methods, the projection matrix A is typically underdetermined, meaning the number of unknowns (pixels) is greater than the number of equations (projections).

Otherwise it is an overdetermined system since the number of equations (projections) is more than the number of unknowns which is mostly not the case and as common as underdetermined systems.

size	no. of equations	no. of pixels	system
128×128	18000	16384	overdetermined
256×256	18000	65536	underdetermined
512×512	18000	262144	underdetermined

Table 4.2: Number of equations (projections) and variables (pixels) in three projection matrices for overdetermined and underdetermined systems using 180 angles, $\theta = 1, 2, ..., 179$, and 100 projections per angle.

However to clearly understand the situations and to cover all possible cases in this thesis, we have tested the used phantoms with three different image sizes such as 128×128, 256×256 and 512×512, where the projection matrix in a 128×128 phantom results in an overdetermined system, and consecutively the projection matrices in 256×256 and 512×512 phantoms result in underdetermined systems.

In our numerical results, we have assessed all the methods using simulated X-ray data using 180 angles, $\theta = 1, 2, ..., 179$, and 100 projections per angle[4], Table 4.2. Due to large number of plots and data for each test phantom, in this chapter, we just have data for MRI Head test phantom, and the rest data and plots for Shepp-Logan and MRI Knee test phantoms are in appendix A and B, respectively.

[4]http://www.medwow.com/med/ct-scanner/toshiba/aquilion-64/8953.model-spec

4.4.1 Experimental Results on MRI Head Test Phantom

Experimental results, obtained by applying Kaczmarz's, Symmetric Kaczmarz's, Randomized Kaczmarz's and SART methods to an overdetermined system corresponding to 128×128 image size and two underdetermined system corresponding to 256×256 and 512×512 MRI Head phantom image sizes, are plotted in Figures 4.1–4.4, 4.5–4.8 and 4.9–4.12, respectively. The results in these Figures 4.1–4.12 are computed for relaxation parameters, $\lambda = 0.2, 0.4, .., 1$, for 20 iterations.

Reconstructed images of 128×128, 256×256 and 512×512 MRI Head phantoms using Kaczmarz, Symmetric Kaczmarz, Randomized Kaczmarz and SART for relaxation parameter $\lambda = 0.4$ are given in Figures 4.13, 4.14 and 4.15, respectively for three different iterations.

Consecutively, to compute numerical results for other relaxation parameters, $\lambda = 1, 1.2, .., 1.8$, for 20 iterations, we have applied these methods to overdetermined system corresponding to 128×128 image size and underdetermined systems corresponding to 256×256 and 512×512 MRI Head phantom image sizes. The plots are shown in Figures 4.16–4.19, 4.20–4.23 and 4.24–4.27, respectively. Related Reconstructed images of 128×128, 256×256 and 512×512 MRI Head phantoms using Kaczmarz, Symmetric Kaczmarz, Randomized Kaczmarz and SART for relaxation parameter $\lambda = 1.2$ are shown in Figures 4.28, 4.29 and 4.30, respectively for three different iterations.

Head, Kaczmarz, 128×128 **image,** $\lambda = 0.2, 0.4, .., 1$

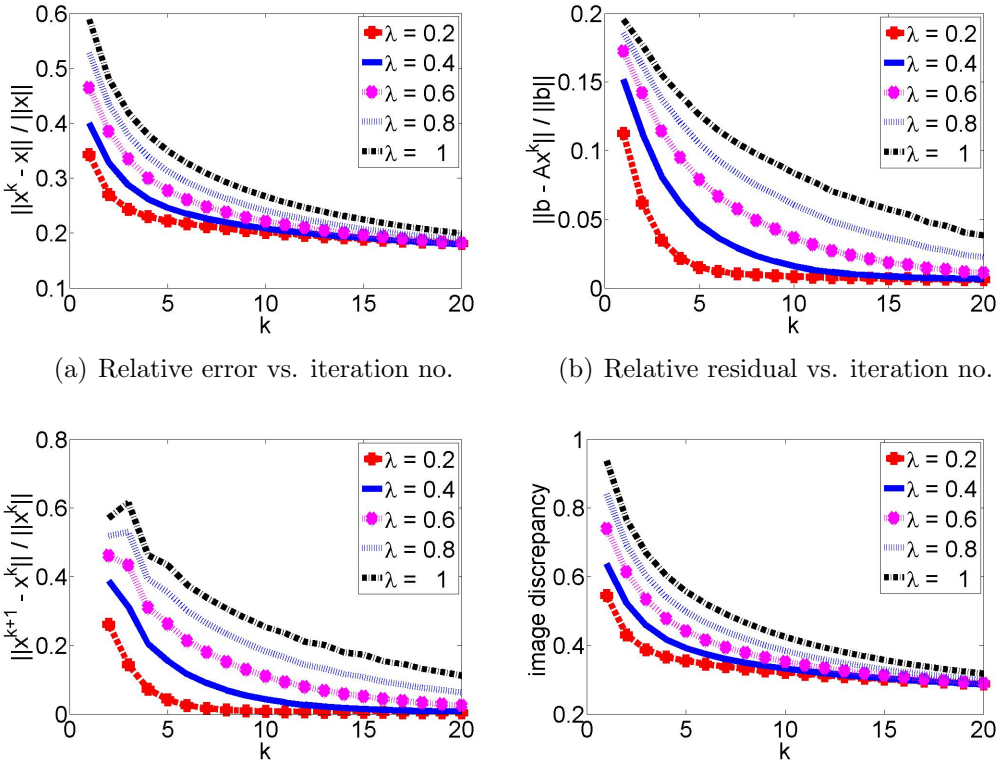

(a) Relative error vs. iteration no.

(b) Relative residual vs. iteration no.

(c) Relative solution difference vs. iteration no.

(d) Image discrepancy vs. iteration no.

Figure 4.1: ART(Kaczmrarz's method) applied to MRI Head Phantom for a 128×128 image and $\lambda = 0.2, 0.4, .., 1$.

In the last iteration,

	min relative error	min relative residual	min relative solution difference	min discrepancy
λ	0.2	0.2	0.2	0.2

Head, Symmetric Kaczmarz, 128×128 **image,** $\lambda = 0.2, 0.4, .., 1$

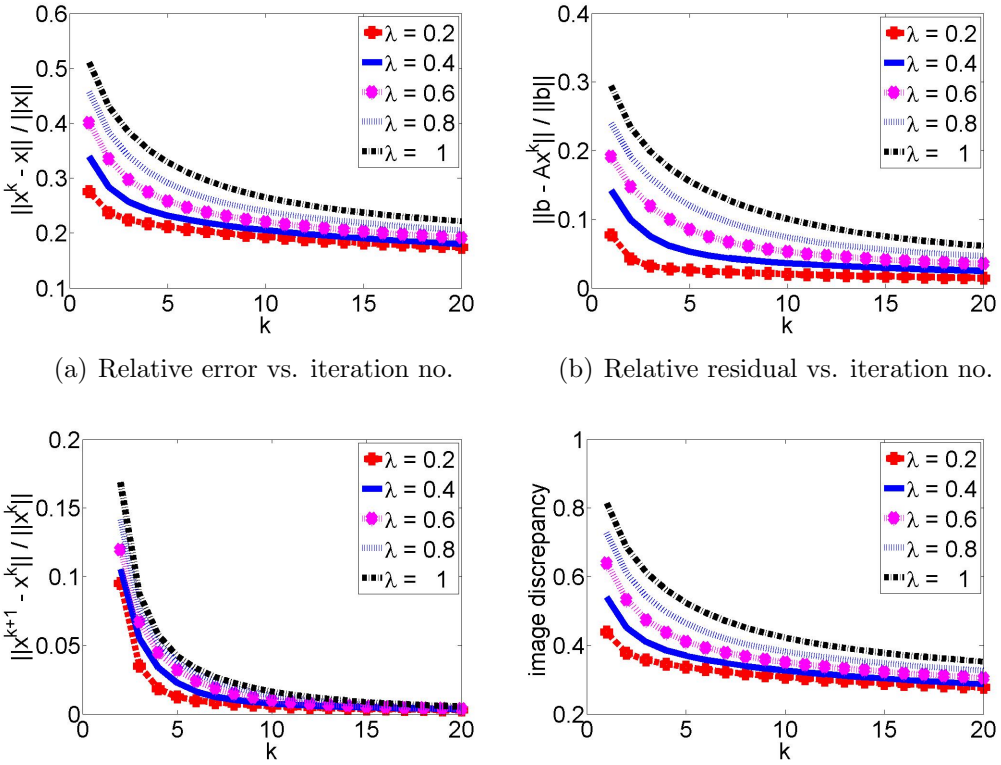

(a) Relative error vs. iteration no.

(b) Relative residual vs. iteration no.

(c) Relative solution difference vs. iteration no.

(d) Image discrepancy vs. iteration no.

Figure 4.2: Symmetric Kaczmarz's method applied to MRI Head Phantom for a 128 $\times$ 128 image and $\lambda = 0.2, 0.4, .., 1$.

In the last iteration,

	min relative error	min relative residual	min relative solution difference	min discrepancy
λ	0.2	0.2	0.2	0.2

Head, Randomized Kaczmarz, 128×128 **image,** $\lambda = 0.2, 0.4, .., 1$

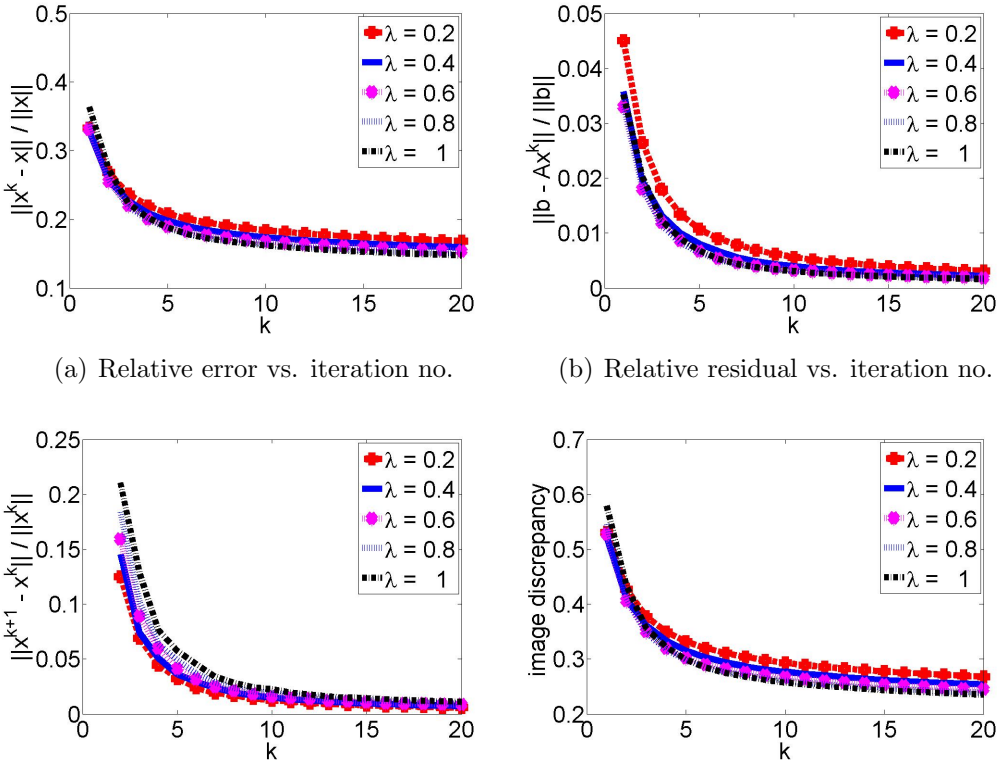

(a) Relative error vs. iteration no.

(b) Relative residual vs. iteration no.

(c) Relative solution difference vs. iteration no.

(d) Image discrepancy vs. iteration no.

Figure 4.3: Randomized Kaczmarz's method applied to MRI Head Phantom for a 128×128 image and $\lambda = 0.2, 0.4, .., 1$.

In the last iteration,

	min relative error	min relative residual	min relative solution difference	min discrepancy
λ	1	1	0.2	1

Head, SART, 128×128 **image,** $\lambda = 0.2, 0.4, .., 1$

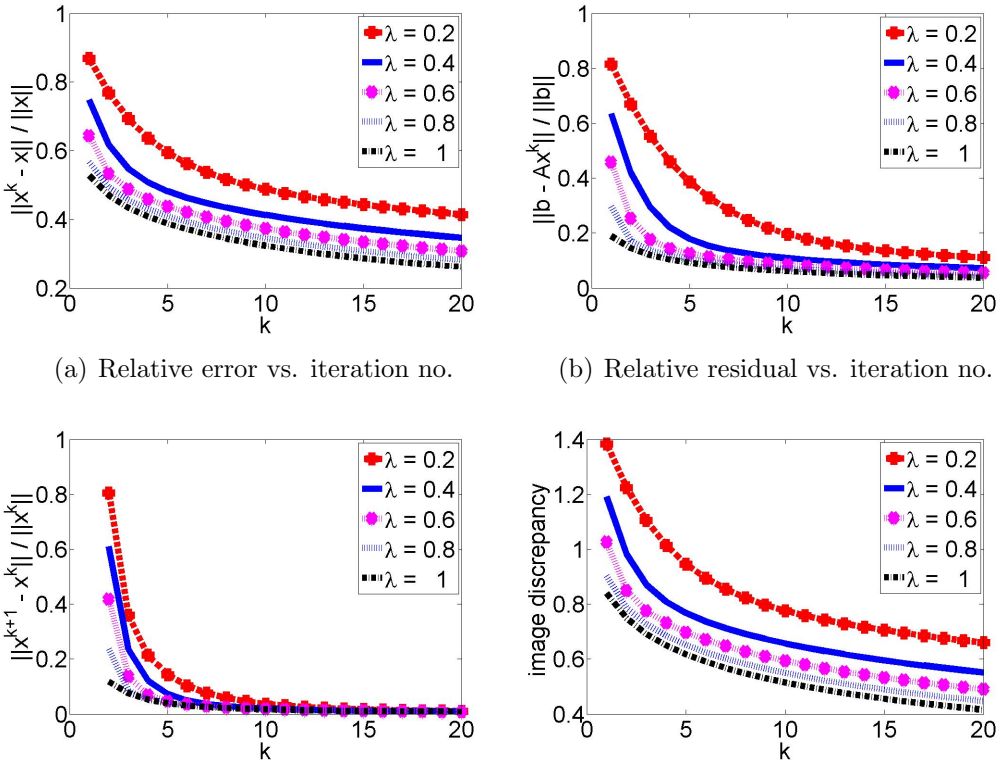

(a) Relative error vs. iteration no.

(b) Relative residual vs. iteration no.

(c) Relative solution difference vs. iteration no.

(d) Image discrepancy vs. iteration no.

Figure 4.4: SART method applied to MRI Head Phantom for a 128×128 image and $\lambda = 0.2, 0.4, .., 1$.

In the last iteration,

	min relative error	min relative residual	min relative solution difference	min discrepancy
λ	1	1	1	1

Head, Kaczmrarz, 256×256 **image,** $\lambda = 0.2, 0.4, .., 1$

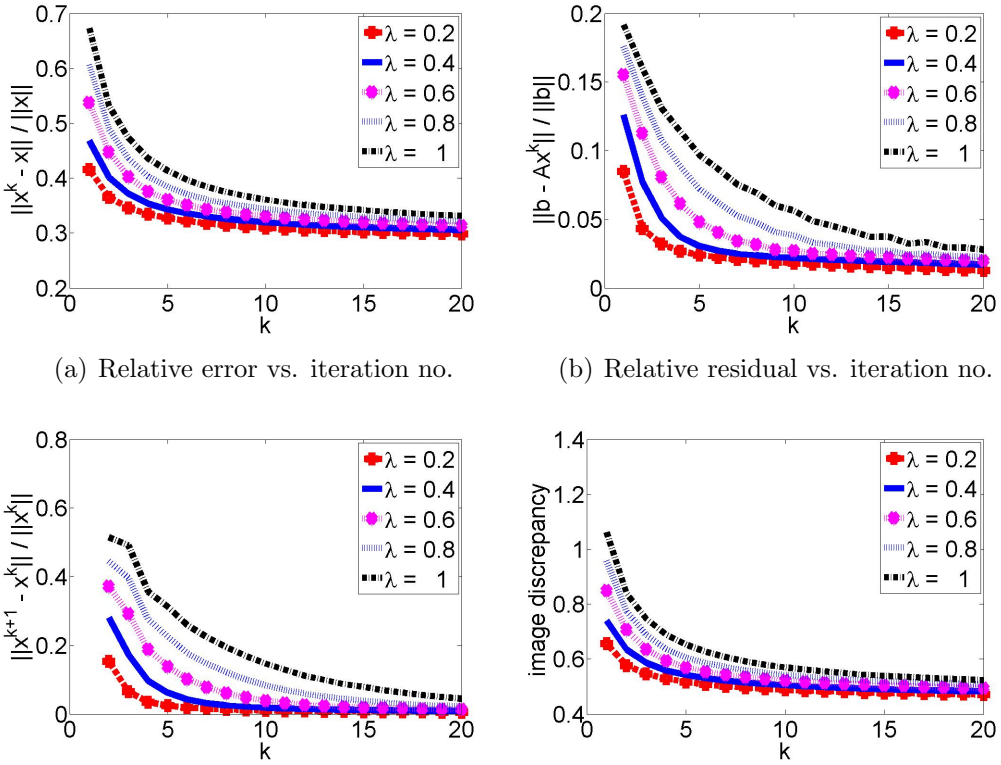

(a) Relative error vs. iteration no.

(b) Relative residual vs. iteration no.

(c) Relative solution difference vs. iteration no.

(d) Image discrepancy vs. iteration no.

Figure 4.5: ART(Kaczmrarz's method) applied to MRI Head Phantom for a 256×256 image and $\lambda = 0.2, 0.4, .., 1$.

In the last iteration,

	min relative error	min relative residual	min relative solution difference	min discrepancy
λ	0.2	0.2	0.2	0.2

Head, Symmetric Kaczmrarz, 256×256 **image,** $\lambda = 0.2, 0.4, .., 1$

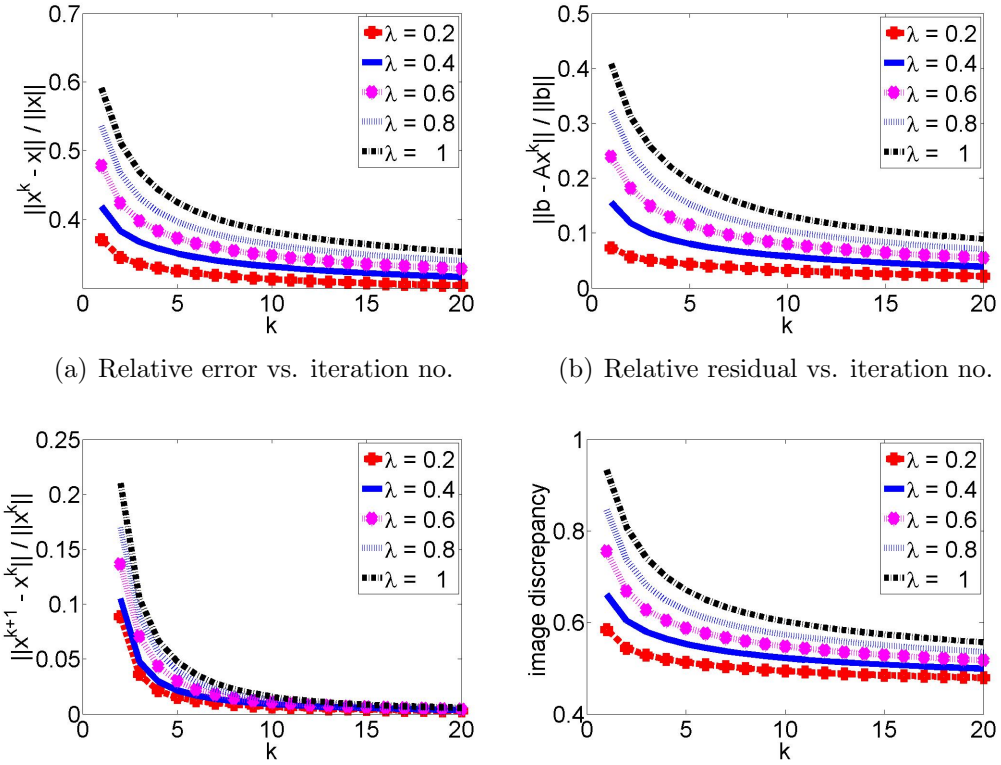

(a) Relative error vs. iteration no.

(b) Relative residual vs. iteration no.

(c) Relative solution difference vs. iteration no.

(d) Image discrepancy vs. iteration no.

Figure 4.6: Symmetric Kaczmarz's method applied to MRI Head Phantom for a 256 $\times$ 256 image and $\lambda = 0.2, 0.4, .., 1$.

In the last iteration,

	min relative error	min relative residual	min relative solution difference	min discrepancy
λ	0.2	0.2	0.2	0.2

Head, Randomized Kaczmrarz, 256×256 **image,** $\lambda = 0.2, 0.4, .., 1$

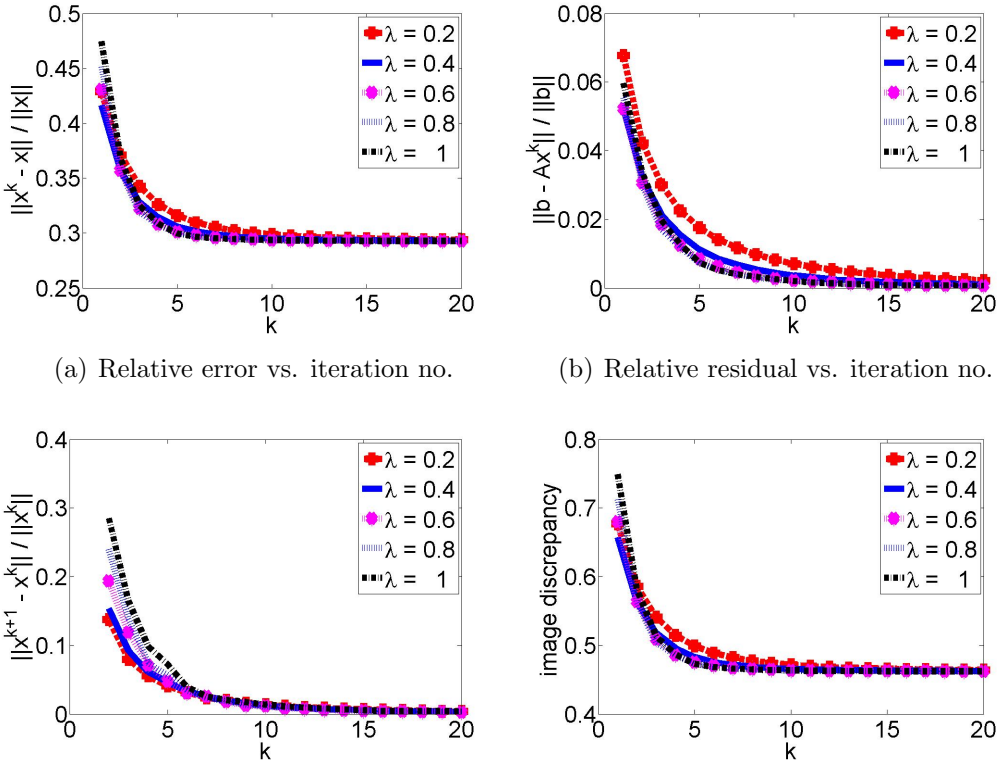

(a) Relative error vs. iteration no.

(b) Relative residual vs. iteration no.

(c) Relative solution difference vs. iteration no.

(d) Image discrepancy vs. iteration no.

Figure 4.7: Randomized Kaczmarz's method applied to MRI Head Phantom for a 256×256 image and $\lambda = 0.2, 0.4, .., 1$.

In the last iteration,

	min relative error	min relative residual	min relative solution difference	min discrepancy
λ	1	1	1	1

Head, SART, 256×256 **image,** $\lambda = 0.2, 0.4, .., 1$

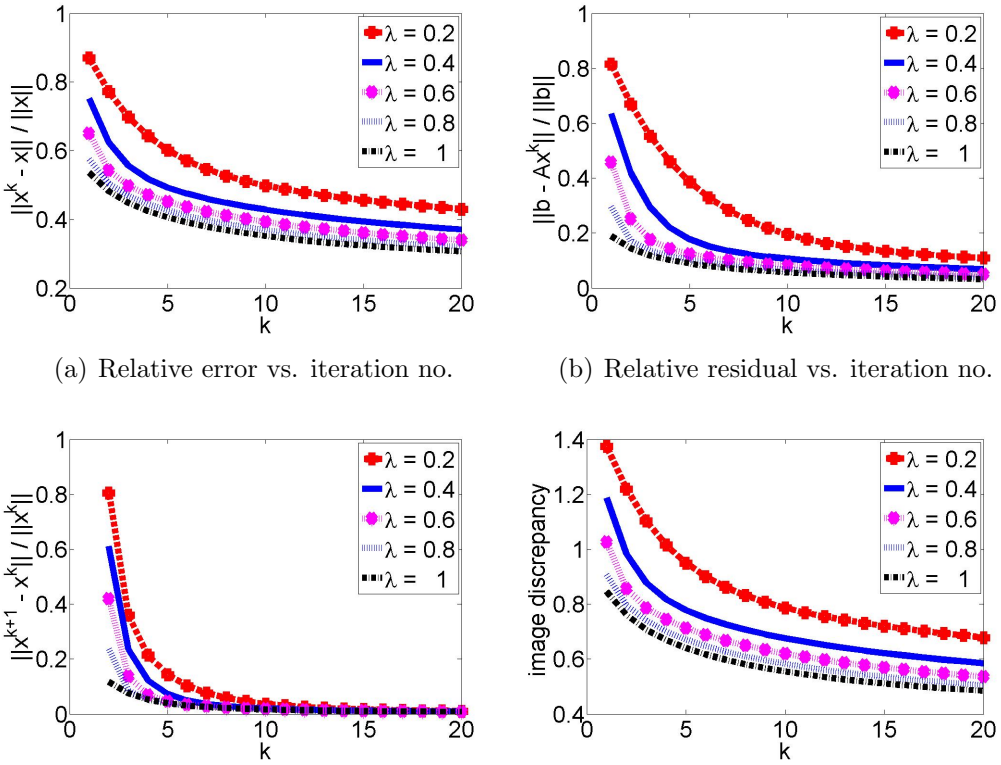

(a) Relative error vs. iteration no.

(b) Relative residual vs. iteration no.

(c) Relative solution difference vs. iteration no.

(d) Image discrepancy vs. iteration no.

Figure 4.8: SART method applied to MRI Head Phantom for a 256×256 image and $\lambda = 0.2, 0.4, .., 1$.

In the last iteration,

	min relative error	min relative residual	min relative solution difference	min discrepancy
λ	1	1	1	1

Head, Kaczmrarz, 512×512 **image,** $\lambda = 0.2, 0.4, .., 1$

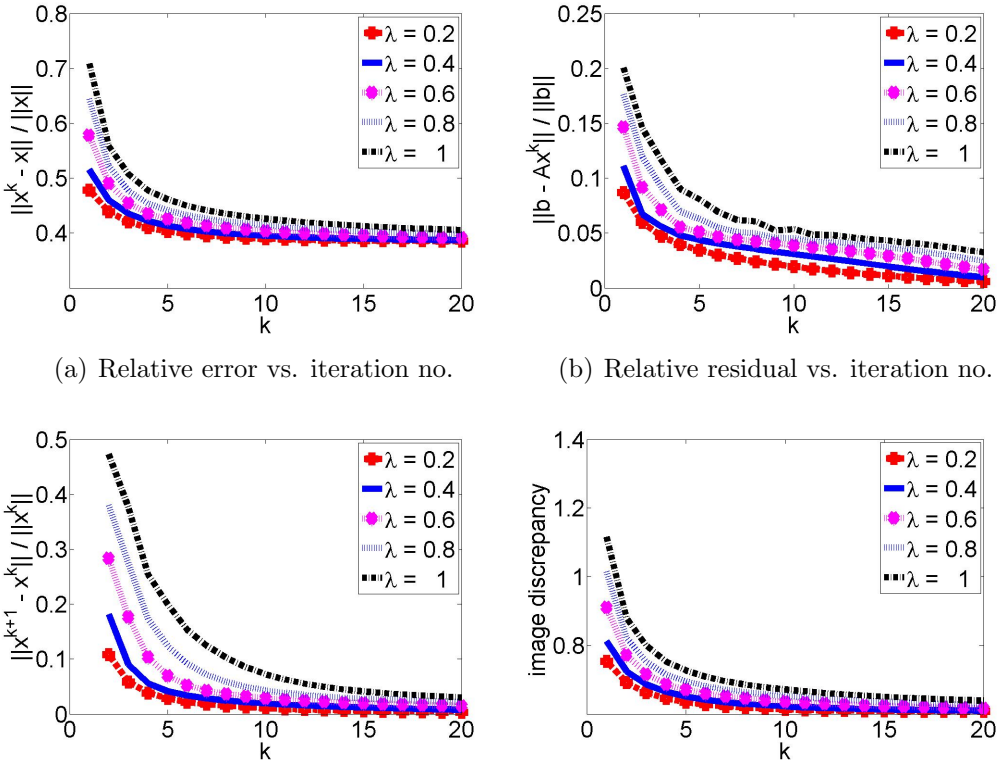

(a) Relative error vs. iteration no.

(b) Relative residual vs. iteration no.

(c) Relative solution difference vs. iteration no.

(d) Image discrepancy vs. iteration no.

Figure 4.9: ART(Kaczmrarz's method) applied to MRI Head Phantom for a 512×512 image and $\lambda = 0.2, 0.4, .., 1$.

In the last iteration,

	min relative error	min relative residual	min relative solution difference	min discrepancy
λ	0.2	0.2	0.2	0.2

Head, Symmetric Kaczmrarz, 512×512 **image,** $\lambda = 0.2, 0.4, .., 1$

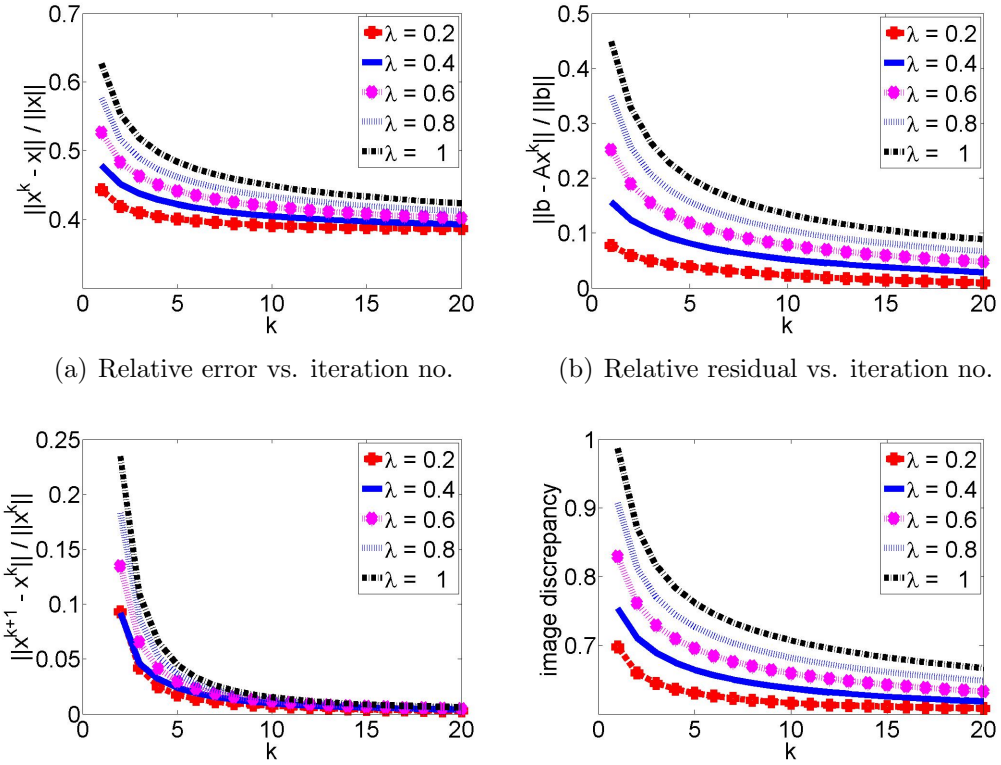

(a) Relative error vs. iteration no.

(b) Relative residual vs. iteration no.

(c) Relative solution difference vs. iteration no.

(d) Image discrepancy vs. iteration no.

Figure 4.10: Symmetric Kaczmarz's method applied to MRI Head Phantom for a 512 $\times$ 512 image and $\lambda = 0.2, 0.4, .., 1$.

In the last iteration,

	min relative error	min relative residual	min relative solution difference	min discrepancy
λ	0.2	0.2	0.2	0.2

Head, Randomized Kaczmrarz, 512×512 **image,** $\lambda = 0.2, 0.4, .., 1$

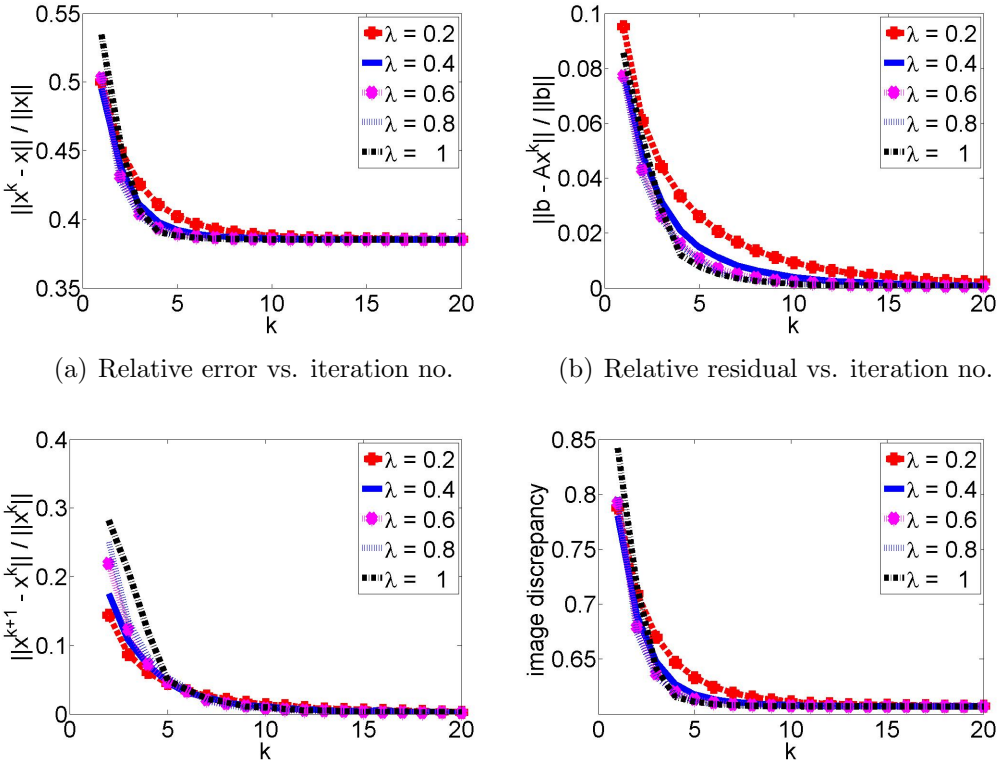

(a) Relative error vs. iteration no.

(b) Relative residual vs. iteration no.

(c) Relative solution difference vs. iteration no.

(d) Image discrepancy vs. iteration no.

Figure 4.11: Randomized Kaczmarz's method applied to MRI Head Phantom for a 512×512 image and $\lambda = 0.2, 0.4, .., 1$.

In the last iteration,

	min relative error	min relative residual	min relative solution difference	min discrepancy
λ	1	1	1	1

Head, SART, 512×512 **image,** $\lambda = 0.2, 0.4, .., 1$

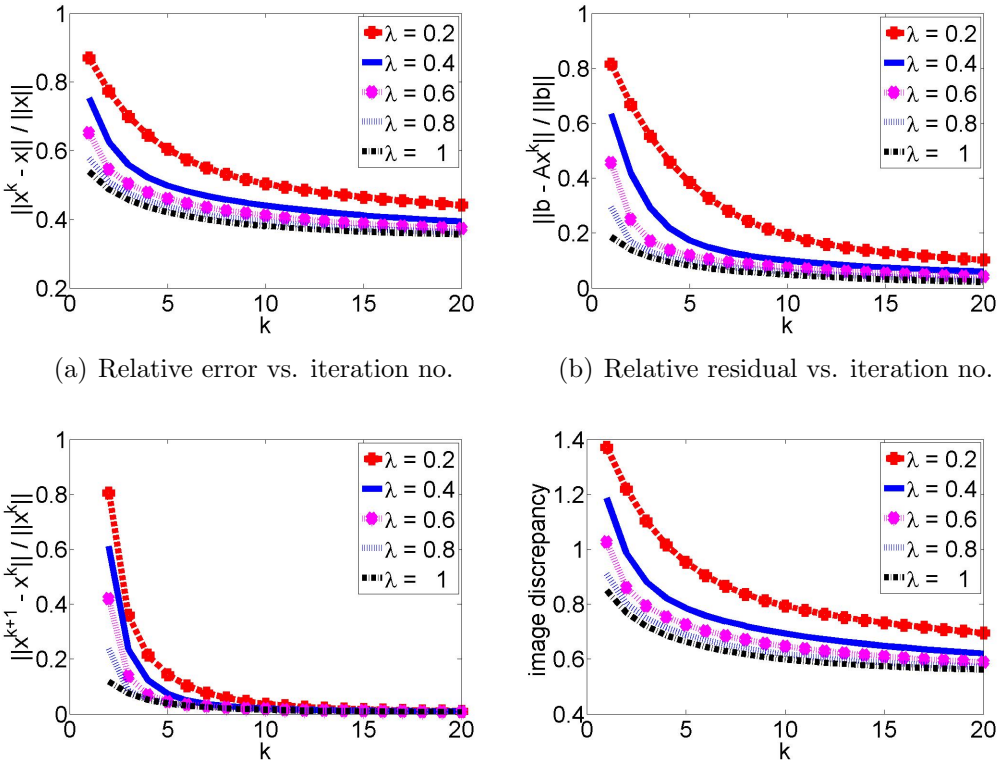

(a) Relative error vs. iteration no.

(b) Relative residual vs. iteration no.

(c) Relative solution difference vs. iteration no.

(d) Image discrepancy vs. iteration no.

Figure 4.12: SART method applied to MRI Head Phantom for a 512×512 image and $\lambda = 0.2, 0.4, .., 1$.

In the last iteration,

	min relative error	min relative residual	min relative solution difference	min discrepancy
λ	1	1	1	1

Figure 4.13: Reconstruction of the 128×128 MRI Head Phantom using Kaczmarz, Symmetric Kaczmarz, Randomized Kaczmarz and SART ($\lambda = 0.4$).

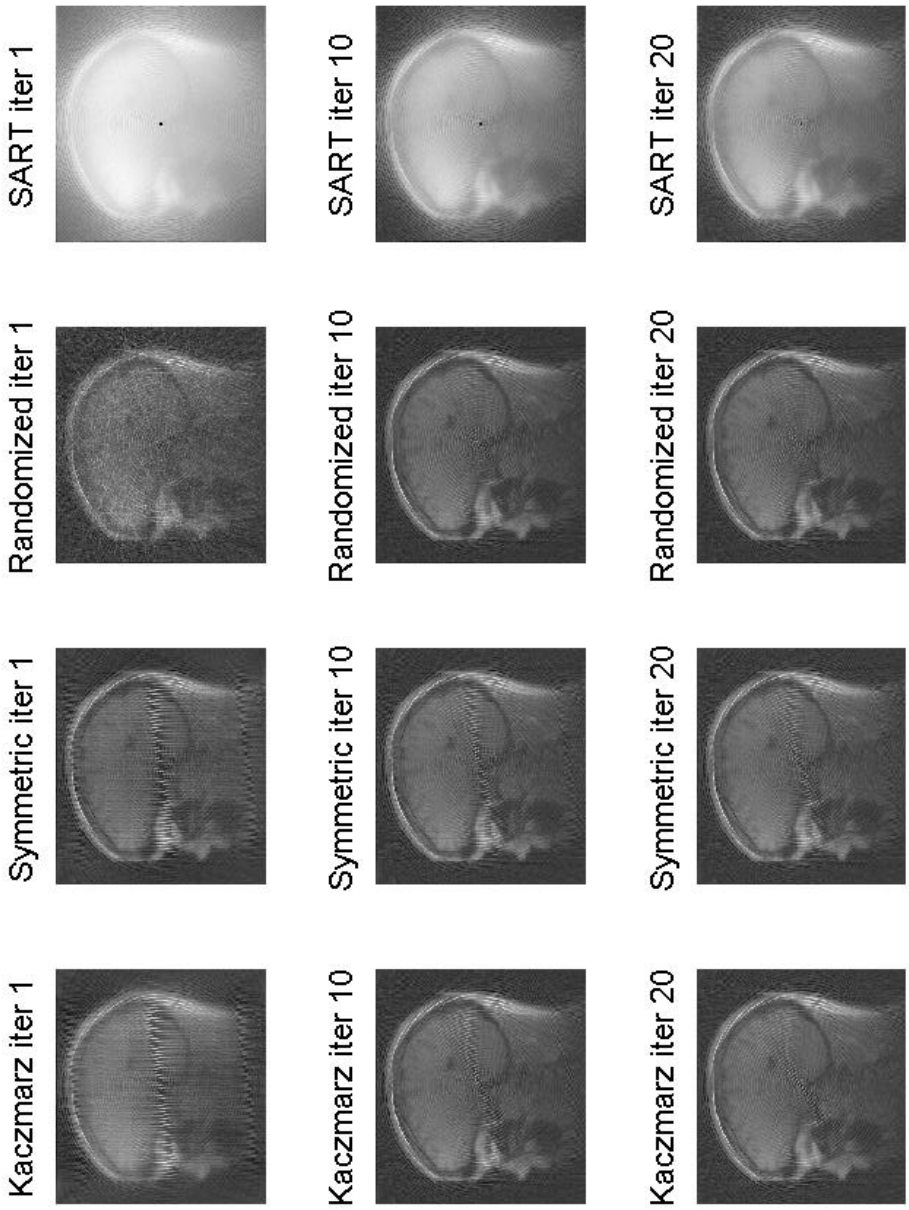

Figure 4.14: Reconstruction of the 256×256 MRI Head Phantom using Kaczmarz, Symmetric Kaczmarz, Randomized Kaczmarz and SART ($\lambda = 0.4$).

Figure 4.15: Reconstruction of the 512×512 MRI Head Phantom using Kaczmarz, Symmetric Kaczmarz, Randomized Kaczmarz and SART ($\lambda = 0.4$).

size	method	worst λ	max discrepancy	best λ	min discrepancy	time/iter(s)
128	Kacz.	1	0.3173	0.4	0.2854	6.46
	Symm.	1	0.3524	0.2	0.2771	10.55
	Rand.	0.2	0.2682	1	0.2351	9.22
	SART	0.2	0.6594	1	0.4157	0.01
256	Kacz.	1	0.5231	0.2	0.4712	43.34
	Symm.	1	0.5568	0.2	0.4791	102.43
	Rand.	0.2	0.4638	1	0.4620	38.66
	SART	0.2	0.6783	1	0.4845	0.05
512	Kacz.	1	0.6386	0.2	0.6074	171.72
	Symm.	1	0.6669	0.2	0.6084	355.11
	Rand.	0.2	0.6072	1	0.6067	213.81
	SART	0.2	0.6951	1	0.5614	0.25

Table 4.1: Experimental results of applying different methods to MRI Head phantom using relaxation parameters of $\lambda = 0.2, 0.4, .., 1$ for 20 number of iterations.

The experimental results shown in Table 4.1 are obtained from the Colsher's discrepancy measurement method [4] in such a way that, after applying different ART methods to different phantom sizes, for $\lambda = 0.2, 0.4, .., 1$, the minimum and the maximum discrepancies, which indicate the best and the worst relaxation parameters, are found in iteration number 20.

As it can be seen, the results for the overdetermined system corresponding to 128×128 Head phantom are different from the results achieved for two underdetermined systems corresponding to 256×256 and 512×512 MRI Head phantom image sizes. It is obvious that the results for both underdetermined systems follow the same pattern for their best and worst relaxation parameters, for various image reconstruction techniques.

Head, Kaczmrarz, 128×128 **image,** $\lambda = 1, 1.2, .., 1.8$

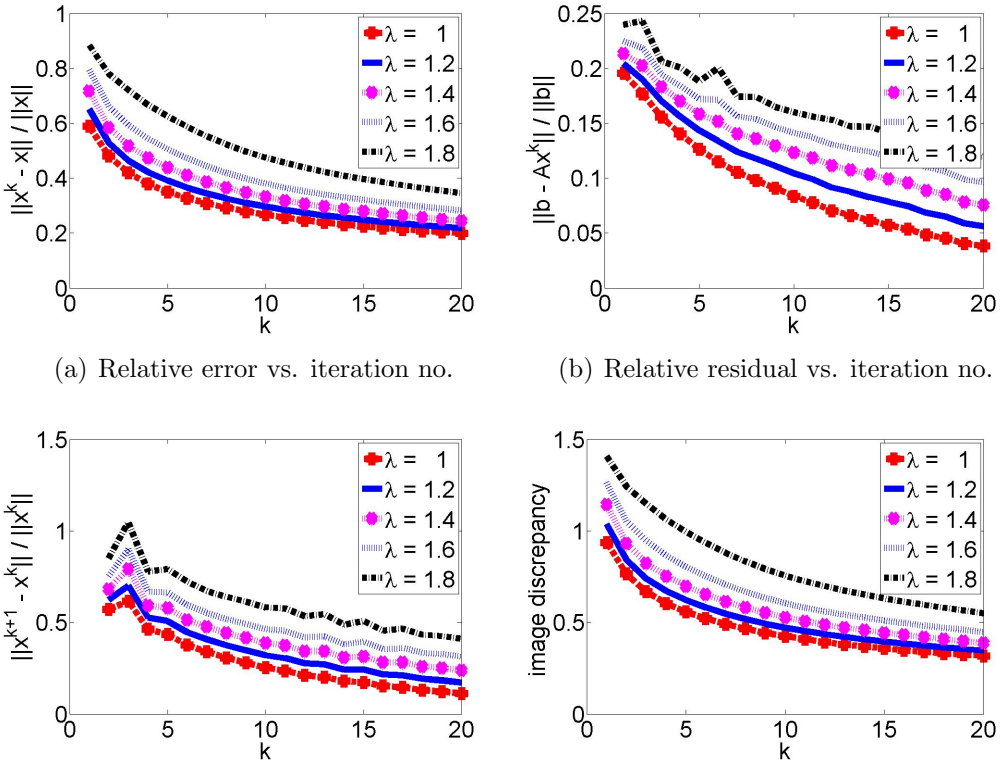

(a) Relative error vs. iteration no.

(b) Relative residual vs. iteration no.

(c) Relative solution difference vs. iteration no.

(d) Image discrepancy vs. iteration no.

Figure 4.16: ART(Kaczmrarz's method) applied to MRI Head Phantom for a 128×128 image and $\lambda = 1, 1.2, .., 1.8$.

In the last iteration,

	min relative error	min relative residual	min relative solution difference	min discrepancy
λ	1	1	1	1

.

Head, Symmetric Kaczmrarz, 128×128 **image,** $\lambda = 1, 1.2, .., 1.8$

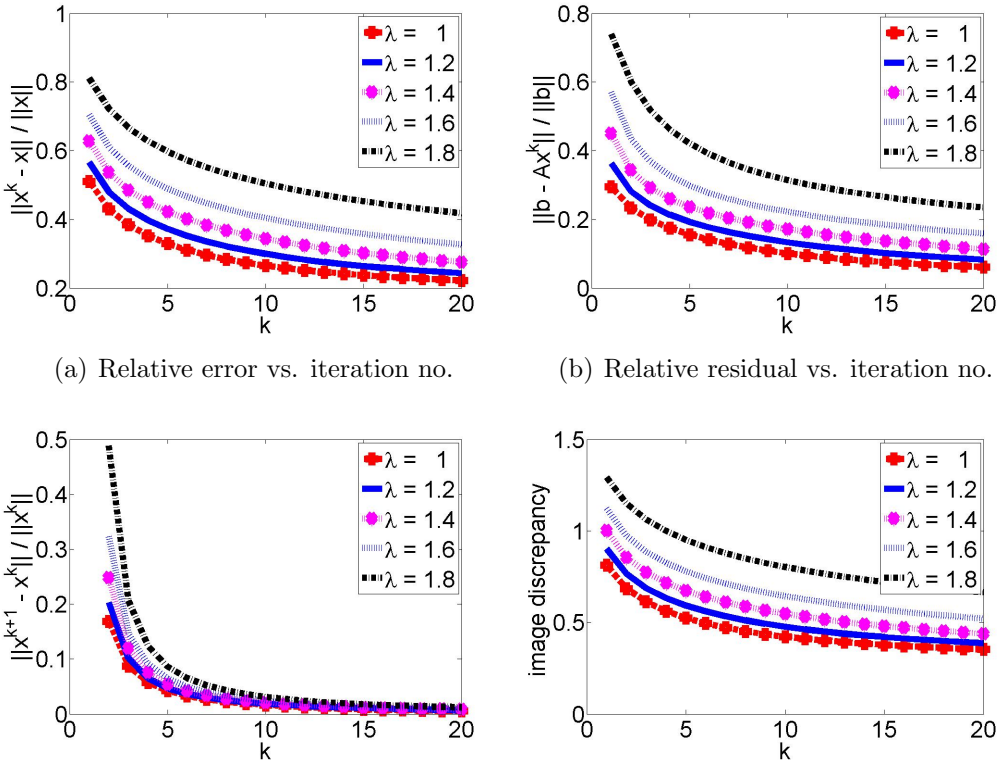

(a) Relative error vs. iteration no.

(b) Relative residual vs. iteration no.

(c) Relative solution difference vs. iteration no.

(d) Image discrepancy vs. iteration no.

Figure 4.17: Symmetric Kaczmarz's method applied to MRI Head Phantom for a 128 $\times$ 128 image and $\lambda = 1, 1.2, .., 1.8$.

In the last iteration,

	min relative error	min relative residual	min relative solution difference	min discrepancy
λ	1	1	1	1

Head, Randomized Kaczmrarz, 128×128 **image,** $\lambda = 1, 1.2, .., 1.8$

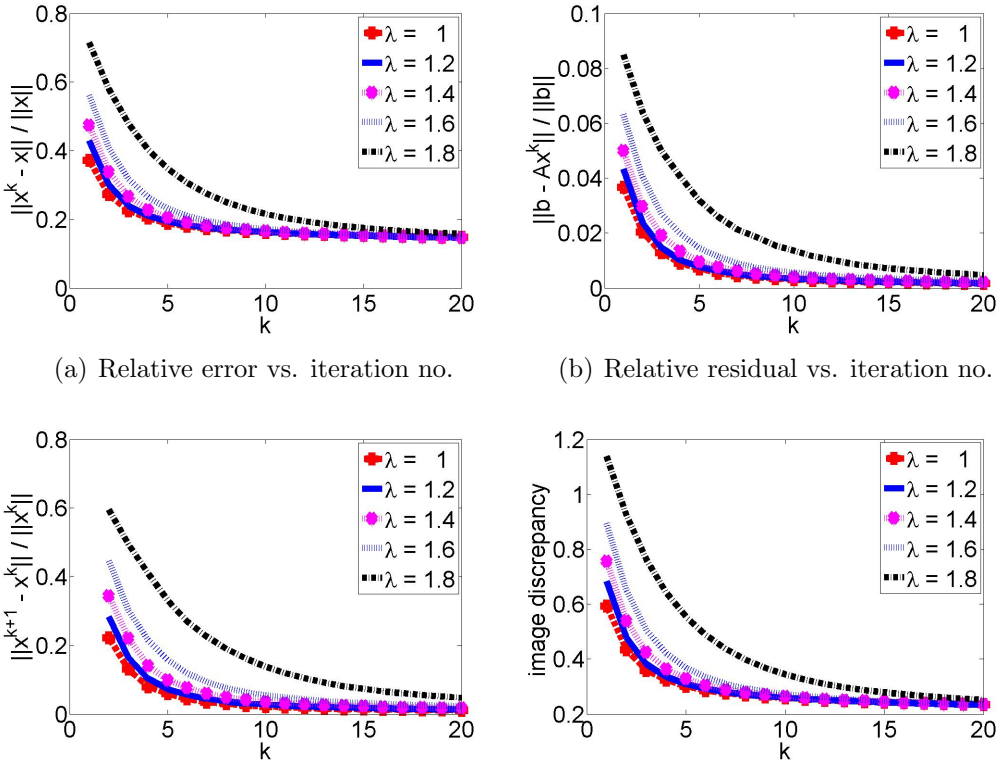

(a) Relative error vs. iteration no.

(b) Relative residual vs. iteration no.

(c) Relative solution difference vs. iteration no.

(d) Image discrepancy vs. iteration no.

Figure 4.18: Randomized Kaczmarz's method applied to MRI Head Phantom for a 128×128 image and $\lambda = 1, 1.2, .., 1.8$.

In the last iteration,

	min relative error	min relative residual	min relative solution difference	min discrepancy
λ	1	1	1	1.2

Head, SART, 128×128 **image,** $\lambda = 1, 1.2, .., 1.8$

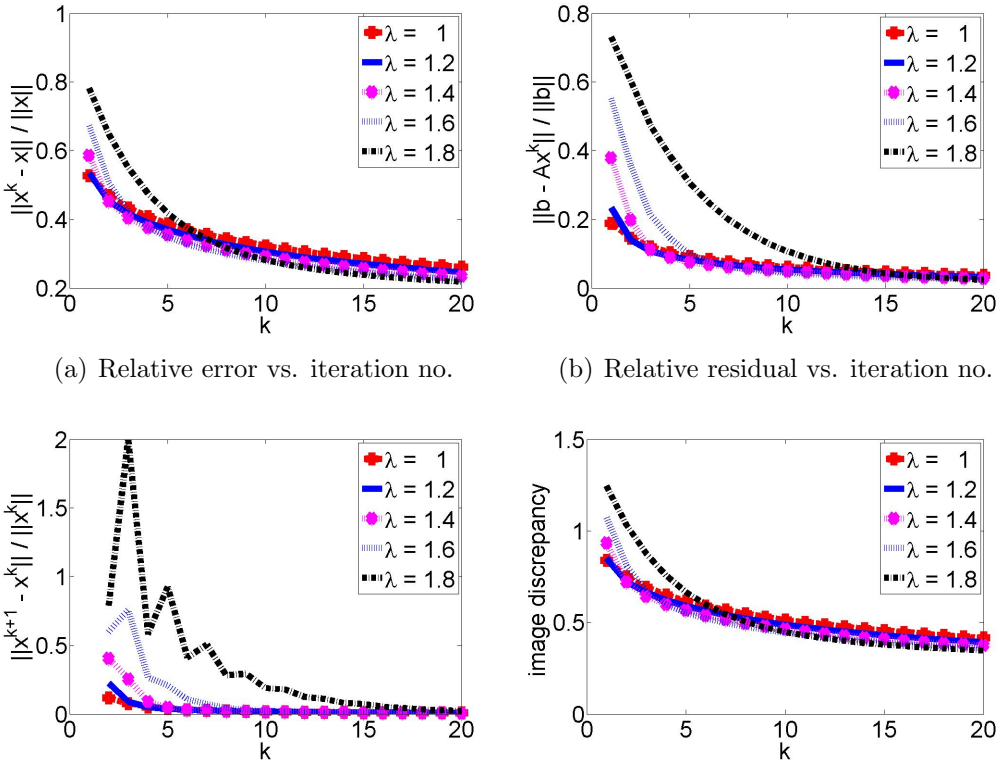

(a) Relative error vs. iteration no.

(b) Relative residual vs. iteration no.

(c) Relative solution difference vs. iteration no.

(d) Image discrepancy vs. iteration no.

Figure 4.19: SART method applied to MRI Head Phantom for a 128×128 image and $\lambda = 1, 1.2, .., 1.8$.

In the last iteration,

	min relative error	min relative residual	min relative solution difference	min discrepancy
λ	1.8	1.8	1.8	1.8

Head, Kaczmrarz, 256×256 **image,** $\lambda = 1, 1.2, .., 1.8$

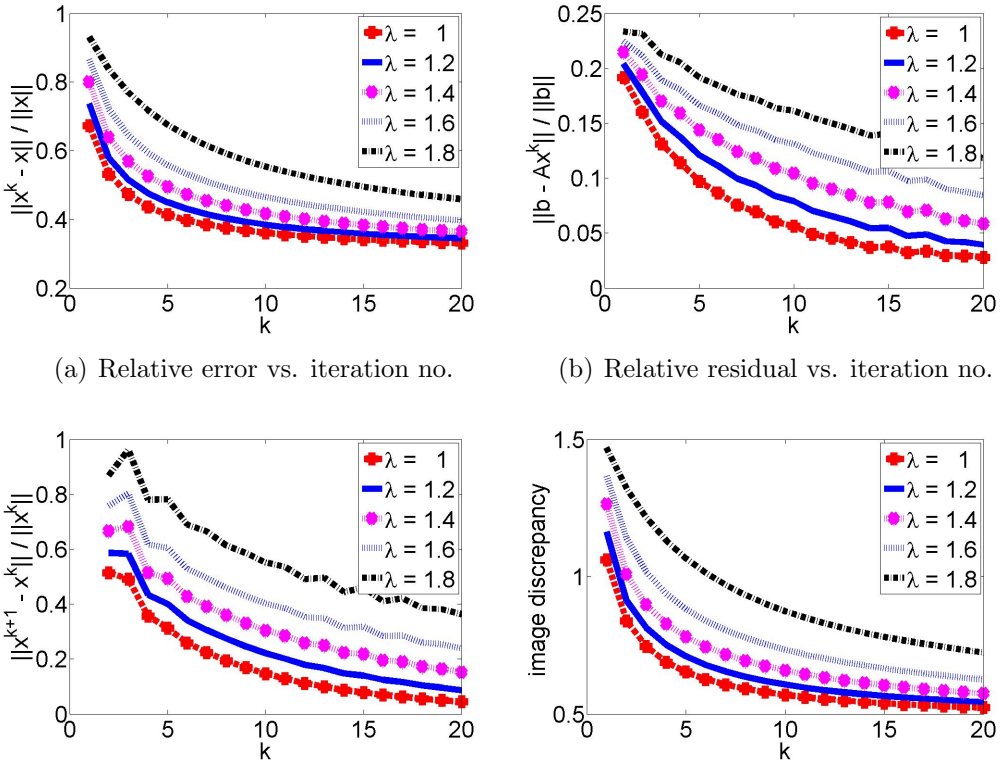

(a) Relative error vs. iteration no.

(b) Relative residual vs. iteration no.

(c) Relative solution difference vs. iteration no.

(d) Image discrepancy vs. iteration no.

Figure 4.20: ART(Kaczmrarz's method) applied to MRI Head Phantom for a 256×256 image and $\lambda = 1, 1.2, .., 1.8$.

In the last iteration,

	min relative error	min relative residual	min relative solution difference	min discrepancy
λ	1	1	1	1

Head, Symmetric Kaczmrarz, 256×256 **image,** $\lambda = 1, 1.2, .., 1.8$

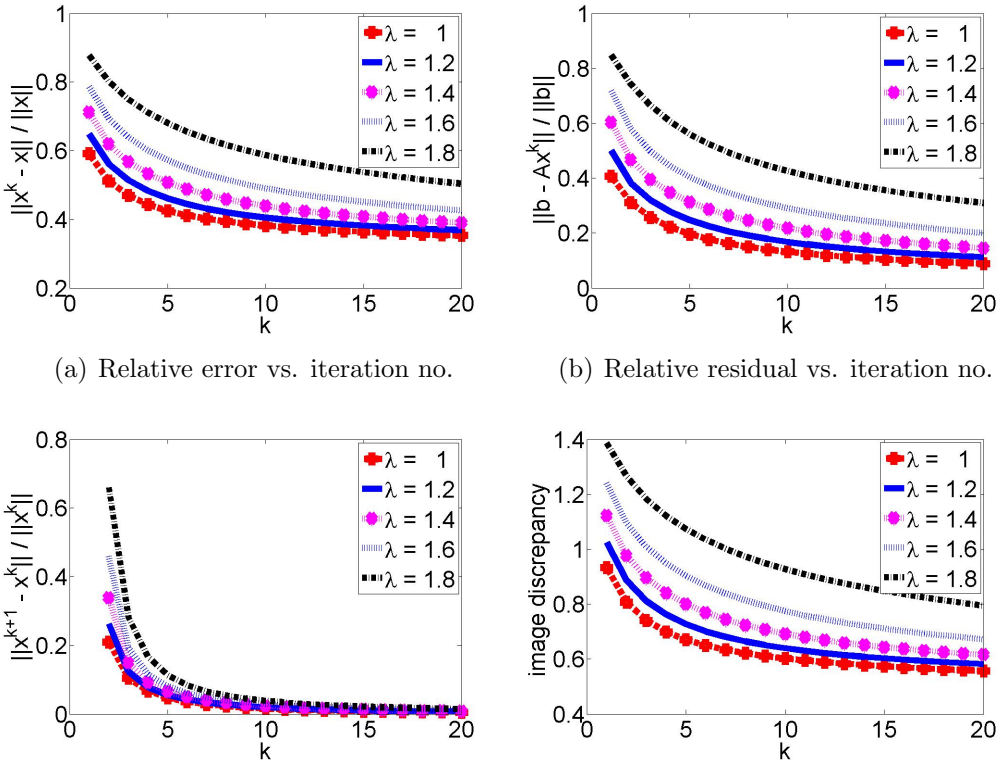

(a) Relative error vs. iteration no.

(b) Relative residual vs. iteration no.

(c) Relative solution difference vs. iteration no.

(d) Image discrepancy vs. iteration no.

Figure 4.21: Symmetric Kaczmarz's method applied to MRI Head Phantom for a 256 $\times$ 256 image and $\lambda = 1, 1.2, .., 1.8$.

In the last iteration,

	min relative error	min relative residual	min relative solution difference	min discrepancy
λ	1	1	1	1

Head, Randomized Kaczmrarz, 256×256 **image,** $\lambda = 1, 1.2, .., 1.8$

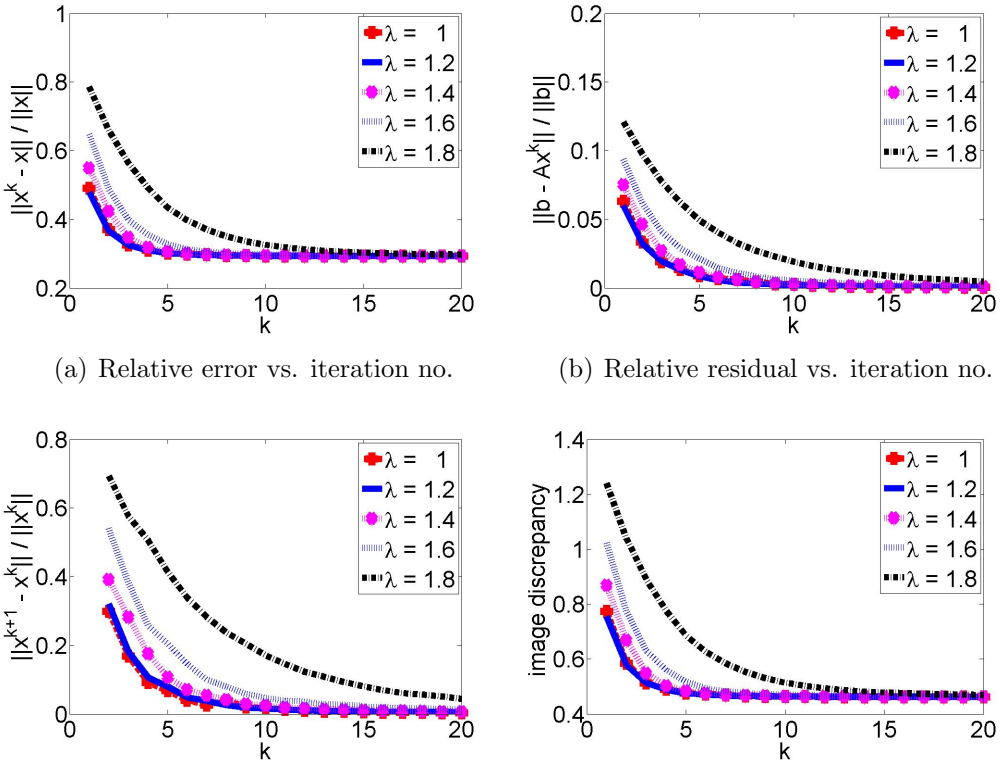

(a) Relative error vs. iteration no.

(b) Relative residual vs. iteration no.

(c) Relative solution difference vs. iteration no.

(d) Image discrepancy vs. iteration no.

Figure 4.22: Randomized Kaczmarz's method applied to MRI Head Phantom for a 256×256 image and $\lambda = 1, 1.2, .., 1.8$.

In the last iteration,

	min relative error	min relative residual	min relative solution difference	min discrepancy
λ	1	1	1	1

Head, SART, 256×256 **image,** $\lambda = 1, 1.2, .., 1.8$

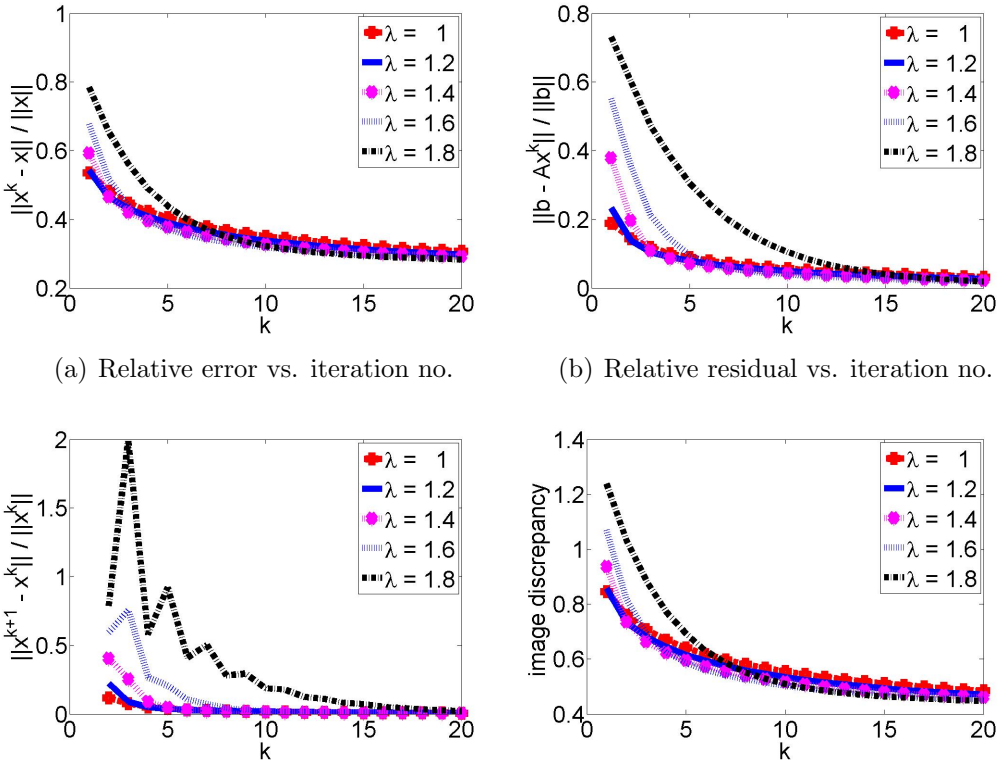

(a) Relative error vs. iteration no.

(b) Relative residual vs. iteration no.

(c) Relative solution difference vs. iteration no.

(d) Image discrepancy vs. iteration no.

Figure 4.23: SART method applied to MRI Head Phantom for a 256×256 image and $\lambda = 1, 1.2, .., 1.8$.

In the last iteration,

	min relative error	min relative residual	min relative solution difference	min discrepancy
λ	1.8	1.8	1.8	1.8

Head, Kaczmarz, 512×512 **image,** $\lambda = 1, 1.2, .., 1.8$

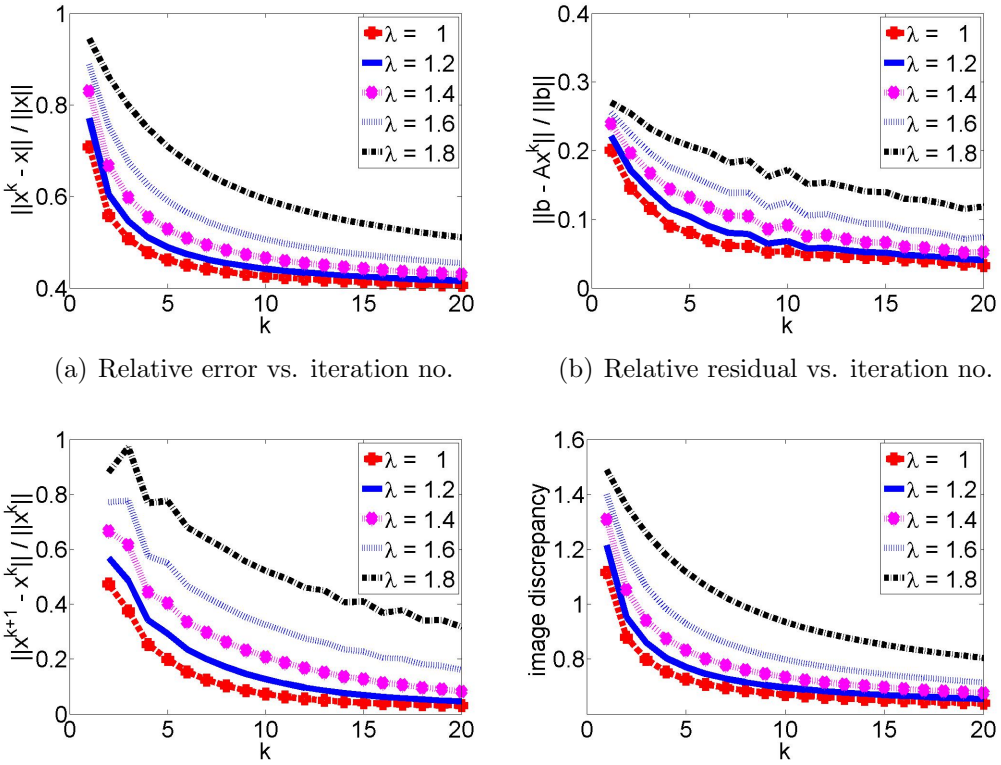

(a) Relative error vs. iteration no.

(b) Relative residual vs. iteration no.

(c) Relative solution difference vs. iteration no.

(d) Image discrepancy vs. iteration no.

Figure 4.24: ART(Kaczmrarz's method) applied to MRI Head Phantom for a 512×512 image and $\lambda = 1, 1.2, .., 1.8$.

In the last iteration,

	min relative error	min relative residual	min relative solution difference	min discrepancy
λ	1	1	1	1

Head, Symmetric Kaczmarz, 512×512 **image,** $\lambda = 1, 1.2, .., 1.8$

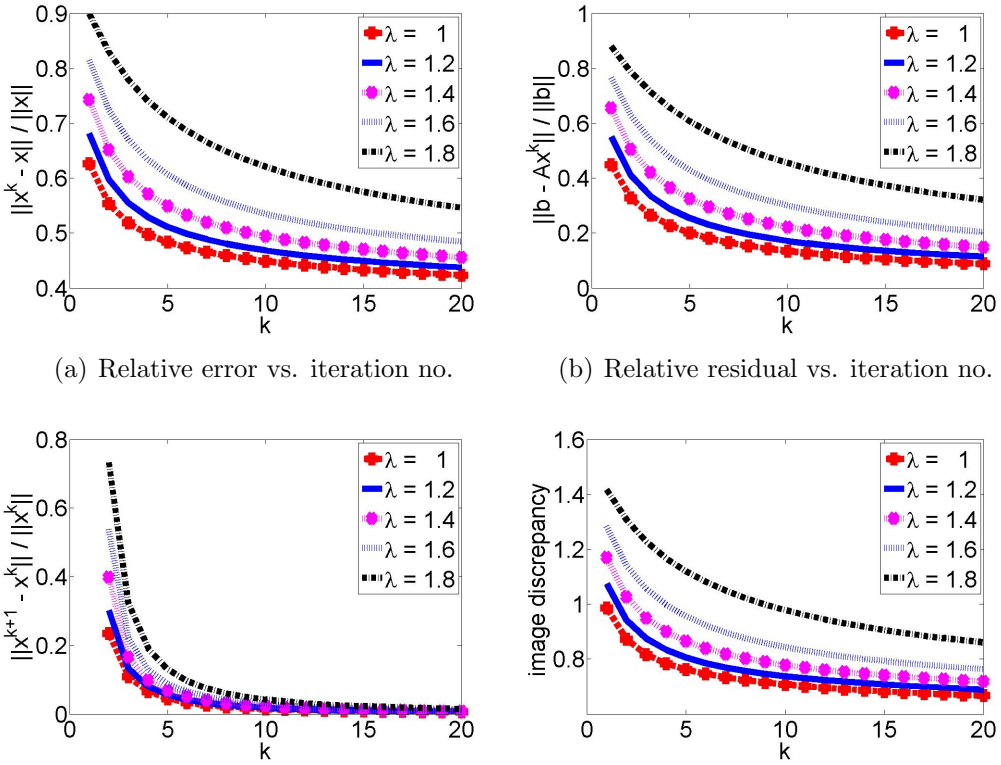

(a) Relative error vs. iteration no.

(b) Relative residual vs. iteration no.

(c) Relative solution difference vs. iteration no.

(d) Image discrepancy vs. iteration no.

Figure 4.25: Symmetric Kaczmarz's method applied to MRI Head Phantom for a 512 $\times$ 512 image and $\lambda = 1, 1.2, .., 1.8$.

In the last iteration,

	min relative error	min relative residual	min relative solution difference	min discrepancy
λ	1	1	1	1

Head, Randomized Kaczmarz, 512×512 **image,** $\lambda = 1, 1.2, .., 1.8$

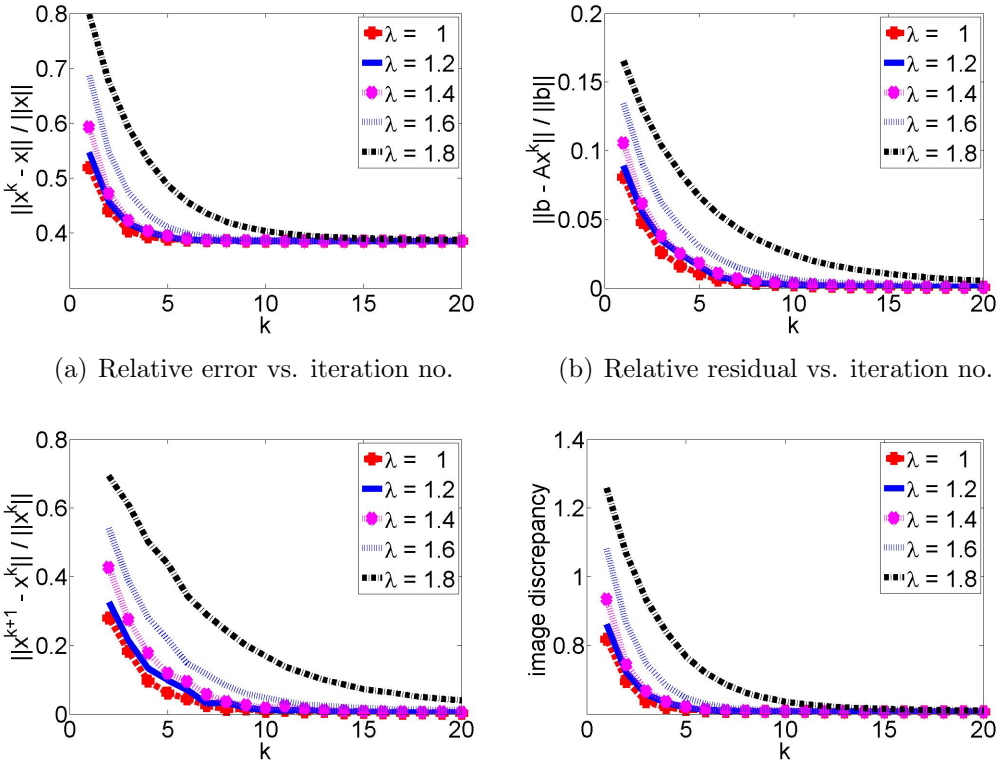

(a) Relative error vs. iteration no.

(b) Relative residual vs. iteration no.

(c) Relative solution difference vs. iteration no.

(d) Image discrepancy vs. iteration no.

Figure 4.26: Randomized Kaczmarz's method applied to MRI Head Phantom for a 512×512 image and $\lambda = 1, 1.2, .., 1.8$.

In the last iteration,

	min relative error	min relative residual	min relative solution difference	min discrepancy
λ	1	1	1	1

Head, SART, 512×512 **image,** $\lambda = 1, 1.2, .., 1.8$

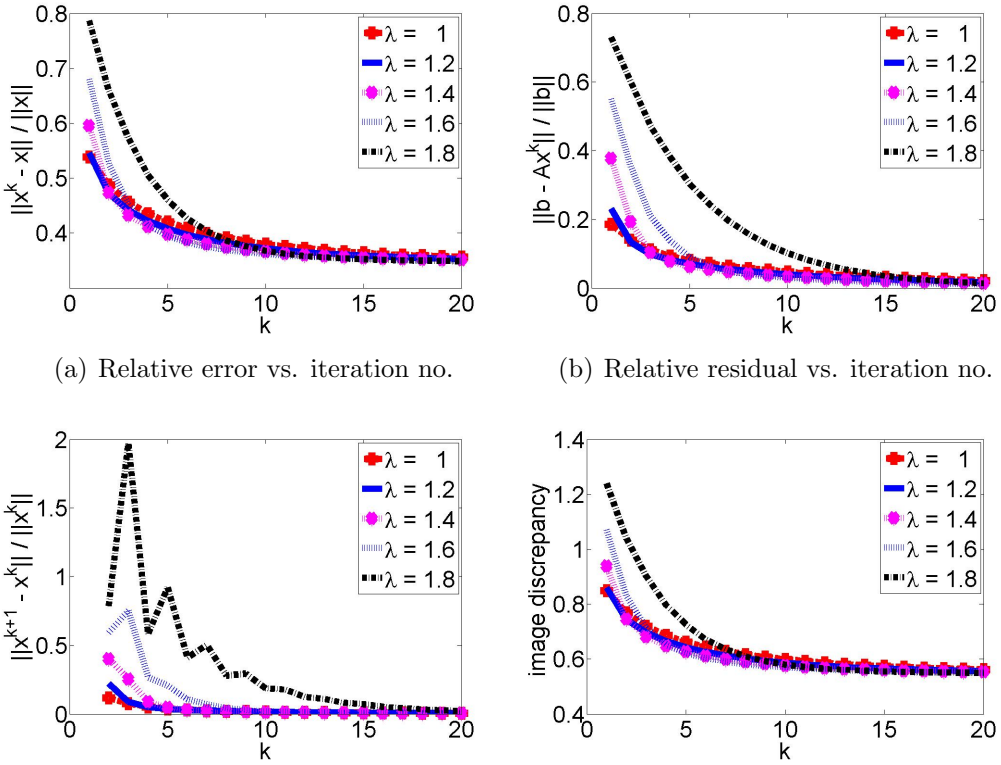

(a) Relative error vs. iteration no.

(b) Relative residual vs. iteration no.

(c) Relative solution difference vs. iteration no.

(d) Image discrepancy vs. iteration no.

Figure 4.27: SART method applied to MRI Head Phantom for a 512×512 image and $\lambda = 1, 1.2, .., 1.8$.

In the last iteration,

	min relative error	min relative residual	min relative solution difference	min discrepancy
λ	1.8	1.8	1.8	1.8

Figure 4.28: Reconstruction of the 128×128 MRI Head Phantom using Kaczmarz, Symmetric Kaczmarz, Randomized Kaczmarz and SART ($\lambda = 1.2$).

Figure 4.29: Reconstruction of the 256×256 MRI Head Phantom using Kaczmarz, Symmetric Kaczmarz, Randomized Kaczmarz and SART ($\lambda = 1.2$).

Figure 4.30: Reconstruction of the 512×512 MRI Head Phantom using Kaczmarz, Symmetric Kaczmarz, Randomized Kaczmarz and SART ($\lambda = 1.2$).

size	method	worst λ	max discrepancy	best λ	min discrepancy	time/iter(s)
128	Kacz.	1.8	0.5514	1	0.3173	6.45
	Symm.	1.8	0.6649	1	0.3524	18.28
	Rand.	1.8	0.2515	1.2	0.2334	15.26
	SART	1	0.4157	1.8	0.3467	0.02
256	Kacz.	1.8	0.7240	1	0.5231	33.34
	Symm.	1.8	0.7952	1	0.5568	91.54
	Rand.	1.8	0.4691	1	0.4621	48.34
	SART	1	0.4845	1.8	0.4473	0.06
512	Kacz.	1.8	0.8040	1	0.6386	194.63
	Symm.	1.8	0.8602	1	0.6669	420.44
	Rand.	1.8	0.6098	1	0.6067	205.14
	SART	1	0.5614	1.8	0.5495	0.32

Table 4.2: Experimental results of applying different methods to MRI Head phantom using relaxation parameters of $\lambda = 1, 1.2, .., 1.8$ for 20 number of iterations.

The experimental results shown in Table 4.2 are obtained from the Colsher's discrepancy measurement method [4] in such a way that, after applying different ART methods to different phantom sizes, for $\lambda = 1, 1.2, .., 1.8$, the minimum and the maximum discrepancies, which indicate the best and the worst relaxation parameters, are found in iteration number 20.

As you see, the results for the overdetermined system corresponding to 128×128 MRI Head phantom, when Randomized Kaczmarz's method is applied, are different from the results achieved for two underdetermined systems corresponding to 256×256 and 512×512 MRI Head phantom image sizes. It is obvious that the results for both underdetermined systems follow the same pattern for their best and worst relaxation parameters, for various image reconstruction techniques.

Based on the Tables A.1, A.2, 4.1, 4.2, B.3 and B.4 which are the experimental results of applying different ART methods to our three Shepp-Logan, MRI Head and MRI Knee test phantoms, for the overdetermined systems which corresponds to 128×128 phantom, no matter what the test phantom is, Randomized Kaczmarz's method has the minimum Colsher's discrepancy error in comparison with the other used methods in 20 iterations.

On the other hand, for the underdetermined systems which correspond to 256×256 and 512×512 image size phantoms, Randomized Kaczmarz/SART and SART methods have the least Colsher's discrepancy error measurements in comparison with the other image reconstruction techniques, respectively.

As it is clear in all the above mentioned tables, the execution time of SART method is much less than the rest of the methods execution times though as it is claimed in Chapter 3 , its time complexity is as like as the other methods. The reason of this contradiction is simply that MATLAB deals with vector products in a much more efficient and faster way. From the numerical results, it can also be concluded that the smaller the size of the phantom is, the better the performance of ART methods is.

4.5 Choosing Good Relaxation Parameter

For each iteration of ART methods studied here, ideally a separate relaxation parameter λ_k is required, and it is already claimed that by carefully adjusting the ART relaxation parameter, we can obtain high quality images [18]. However, up to now, several methods have been proposed for finding an optimum and fixed relaxation

parameter λ for all iterations, no particular method is generally accepted. In [6] two strategies are introduced to choose the relaxation parameter, which are basically derived for SIRT methods and cannot be used for ART methods.

4.5.1 A New Strategy For finding Relaxation Parameters

In this thesis, we have proposed a new technique that for each iterative method, Kaczmarz's, Symmetric Kaczmarz's, Randomized Kaczmarz's and SART methods, no matter what the test problem is, can find a good value of relaxation parameters (λ) for all iterations, and also the best value of λ in each iteration. Since it is more practical to deal with larger size images, we apply the proposed technique only to 256×256 and 512×512 image size phantoms.

This technique is done by running each iterative method for the first iteration for r particular relaxation parameters, which must be all between 0 and 2. After applying the iterative method for one iteration and getting r separate error measurements related to each of the used relaxation parameters, by means of interpolation, we can determine a good relaxation parameter for the first iteration with respect to its minimum error measurement. Using the best found relaxation parameter in iteration one and getting the solution for this specific relaxation parameter, we can proceed to the next iteration.

Again, we run the same iterative method for the second iteration for the same r particular relaxation parameters. Using interpolation, we find the best λ according to its minimum error measurement. After getting the solution for the best relaxation

parameter in iteration number two, we perform exactly the same steps for the next iterations up to the desired number of iterations.

All the above steps for finding λ for all iterations and also λ in each iteration have been implemented in MATLAB for previously discussed ART methods with different resulting image quality measurements. These implementations are available as a MATLAB package, through the author. In our proposed strategy, we have used spline interpolation.

4.5.2 Numerical Results of Our Strategy

To assess our proposed technique for finding a good relaxation parameter for both all iterations and each iteration, we have applied it to our three test phantoms. The numerical results are shown in Tables 4.3-4.8 for different phantoms and two various image sizes. According to the above mentioned tables, each test phantom has distinct best chosen relaxation parameter in each iteration.

In Tables 4.3, 4.5 and 4.7, which belong to Shepp-Logan, MRI Head and MRI Knee phantoms for 256×256 image size, respectively, the chosen relaxation parameters for Shepp-Logan phantom are a bit different from the results obtained for Head and Knee real test phantoms. On the other hand, in Tables 4.4, 4.6 and 4.8 belonging to Shepp-Logan, Head and Knee test phantoms, respectively for 512×512 image size, the best relaxation parameters in each iteration for Shepp-Logan phantom are also somewhat different from the chosen relaxation parameters for the other two real test problems.

As a matter of fact, based on the numerical results, we can claim that the obtained experimental results of MRI Head and Knee real test phantoms are much closer and more similar to each other in their corresponding iteration and in spite of the fact that the phantoms are totally different from each other, but they behave similarly to each other.

iter.	selected λ(Kacz.)	selected λ(Symm.)	selected λ(Rand.)	selected λ(SART.)
1	0.3252	0.2981	0.5820	2.0000
2	0.6462	0.5587	0.8018	1.9950
3	0.3277	0.1936	1.2227	1.9745
4	0.5900	0.2437	1.1735	1.9627
5	0.3341	0.2110	1.0170	1.9563
6	0.3231	0.2082	0.9955	1.9515
7	0.2992	0.1984	1.0081	1.9485
8	0.2853	0.1925	1.1676	1.9458
9	0.2723	0.1864	0.9921	1.9443
10	0.2622	0.1811	0.8855	1.9426
11	0.2542	0.1762	1.1652	1.9418
12	0.2474	0.1716	1.2304	1.9406
13	0.2418	0.1673	1.1993	1.9403
14	0.2370	0.1633	1.1804	1.9395
15	0.2328	0.1595	1.1890	1.9394
16	0.2292	0.1560	1.1854	1.9388
17	0.2260	0.1526	1.1511	1.9390
18	0.2232	0.1494	1.4137	1.9385
19	0.2208	0.1465	1.1827	1.9389
20	0.2186	0.1437	0.9969	1.9385
Average	0.2998	0.2029	1.0870	1.9508

Table 4.3: Experimental results of choosing the best λ in each iteration by applying different methods to Shepp-Logan phantom for a 256×256 image.

iter.	selected λ(Kacz.)	selected λ(Symm.)	selected λ(Rand.)	selected λ(SART.)
1	0.3433	0.3033	0.6451	2.0000
2	0.6959	0.3757	1.2019	1.9855
3	0.4412	0.2317	0.8077	1.9648
4	0.3426	0.2288	1.2270	1.9531
5	0.3050	0.2139	0.6141	1.9467
6	0.2845	0.2065	1.0642	1.9417
7	0.2676	0.2005	0.8096	1.9387
8	0.2557	0.1959	1.1239	1.9359
9	0.2467	0.1925	0.8907	1.9342
10	0.2399	0.1898	0.9939	1.9324
11	0.2349	0.1877	0.9044	1.9314
12	0.2314	0.1861	0.9708	1.9301
13	0.2292	0.1848	1.4175	1.9295
14	0.2281	0.1839	1.0231	1.9285
15	0.2281	0.1832	0.7463	1.9281
16	0.2291	0.1826	1.0124	1.9274
17	0.2310	0.1823	1.2334	1.9271
18	0.2337	0.1820	0.8431	1.9265
19	0.2373	0.1818	1.1931	1.9264
20	0.2415	0.1817	0.9890	1.9258
Average	0.2873	0.2087	0.9856	1.9407

Table 4.4: Experimental results of choosing the best λ in each iteration by applying different methods to Shepp-Logan phantom for a 512×512 image.

iter.	selected λ(Kacz.)	selected λ(Symm.)	selected λ(Rand.)	selected λ(SART.)
1	0.2441	0.2369	0.2852	2.0000
2	0.5436	0.3086	1.0631	1.9394
3	0.2905	0.2117	0.8707	1.9327
4	0.3556	0.2129	0.8415	1.9300
5	0.3215	0.1937	1.0441	1.9285
6	0.3016	0.1877	1.0625	1.9274
7	0.2825	0.1792	1.2276	1.9268
8	0.2676	0.1734	0.9971	1.9262
9	0.2567	0.1676	0.9499	1.9259
10	0.2476	0.1628	0.7684	1.9256
11	0.2403	0.1582	1.2034	1.9255
12	0.2342	0.1541	1.1163	1.9252
13	0.2290	0.1503	1.2848	1.9252
14	0.2245	0.1468	1.1076	1.9251
15	0.2207	0.1436	1.0244	1.9252
16	0.2173	0.1407	1.1439	1.9251
17	0.2143	0.1379	1.1164	1.9252
18	0.2117	0.1355	1.5505	1.9252
19	0.2094	0.1332	1.3926	1.9254
20	0.2074	0.1311	0.9892	1.9254
Average	0.2660	0.1733	1.0520	1.9308

Table 4.5: Experimental results of choosing the best λ in each iteration by applying different methods to MRI Head phantom for a 256×256 image.

iter.	selected λ(Kacz.)	selected λ(Symm.)	selected λ(Rand.)	selected λ(SART.)
1	0.2575	0.2527	0.5869	2.0000
2	0.6268	0.2866	1.0224	1.9367
3	0.3564	0.2178	0.8181	1.9300
4	0.3155	0.2115	0.8370	1.9272
5	0.2833	0.2021	1.2090	1.9256
6	0.2644	0.1969	1.2227	1.9244
7	0.2512	0.1929	1.0018	1.9237
8	0.2416	0.1900	0.9824	1.9230
9	0.2344	0.1878	0.6850	1.9226
10	0.2291	0.1861	0.9951	1.9222
11	0.2255	0.1848	0.9959	1.9219
12	0.2231	0.1838	1.0023	1.9216
13	0.2219	0.1830	1.2032	1.9214
14	0.2218	0.1825	0.9726	1.9212
15	0.2226	0.1821	0.7861	1.9211
16	0.2243	0.1818	0.8255	1.9209
17	0.2268	0.1815	1.2802	1.9208
18	0.2301	0.1814	0.9076	1.9207
19	0.2341	0.1813	0.5998	1.9207
20	0.2388	0.1812	1.2584	1.9205
Average	0.2664	0.1974	0.9596	1.9273

Table 4.6: Experimental results of choosing the best λ in each iteration by applying different methods to MRI Head phantom for a 512×512 image.

iter.	selected λ(Kacz.)	selected λ(Symm.)	selected λ(Rand.)	selected λ(SART.)
1	0.2378	0.2282	0.5599	2.0000
2	0.5219	0.2885	0.9317	1.9368
3	0.3030	0.2088	1.1651	1.9300
4	0.3572	0.2088	1.2148	1.9274
5	0.3153	0.1927	1.2701	1.9260
6	0.3007	0.1867	0.7411	1.9251
7	0.2784	0.1791	0.9600	1.9245
8	0.2657	0.1736	0.8816	1.9241
9	0.2550	0.1682	1.0787	1.9238
10	0.2465	0.1635	0.9613	1.9235
11	0.2397	0.1592	1.3657	1.9234
12	0.2339	0.1552	1.0928	1.9233
13	0.2291	0.1516	1.2118	1.9233
14	0.2249	0.1483	1.2191	1.9232
15	0.2213	0.1452	0.8043	1.9232
16	0.2181	0.1424	1.2730	1.9232
17	0.2154	0.1398	1.3744	1.9233
18	0.2130	0.1375	1.2022	1.9233
19	0.2109	0.1354	1.4145	1.9235
20	0.2091	0.1335	0.7713	1.9235
Average	0.2648	0.1723	1.0747	1.9287

Table 4.7: Experimental results of choosing the best λ in each iteration by applying different methods to MRI Knee phantom for a 256×256 image.

iter.	selected λ(Kacz.)	selected λ(Symm.)	selected λ(Rand.)	selected λ(SART.)
1	0.2509	0.2453	0.2822	2.0000
2	0.5864	0.2709	0.9342	1.9345
3	0.3703	0.2179	0.9882	1.9278
4	0.3203	0.2108	0.8236	1.9252
5	0.2849	0.2022	1.1202	1.9238
6	0.2660	0.1971	1.1104	1.9229
7	0.2525	0.1933	0.9986	1.9223
8	0.2428	0.1904	1.1392	1.9218
9	0.2357	0.1882	0.9900	1.9215
10	0.2305	0.1866	0.9694	1.9212
11	0.2270	0.1853	1.3319	1.9210
12	0.2248	0.1844	1.3657	1.9208
13	0.2237	0.1837	0.5921	1.9206
14	0.2238	0.1832	0.7315	1.9205
15	0.2249	0.1828	0.9359	1.9204
16	0.2269	0.1825	0.8247	1.9203
17	0.2297	0.1824	1.3283	1.9202
18	0.2334	0.1823	1.0090	1.9201
19	0.2378	0.1822	0.8195	1.9201
20	0.2430	0.1823	1.2591	1.9200
Average	0.2668	0.1967	0.9777	1.9263

Table 4.8: Experimental results of choosing the best λ in each iteration by applying different methods to MRI Knee phantom for a 512×512 image.

Tables 4.3, 4.4, 4.5, 4.6,4.7 and 4.8 represent the numerical results of applying the new proposed technique for finding the optimal value of λ for all iterations and also the best value of λ in each iteration for different ART methods. In each of the above mentioned tables, the best relaxation parameter in each iteration is found by means of interpolation for 20 number of iterations and finally in the last row of each table for each particular image reconstruction method, the average amount of all the

selected relaxation parameters for different iterations is given.

λ can be defined as a function of iteration number, that for each particular iteration k there must be a real number λ_k between 0 and 2. To be able to define such this function we have to find a unique choice for the best relaxation parameter in each iteration which is not basically an easy task to do since there is not a unique choice.

phantom	size	mean λ(Kacz.)	mean λ(Symm.)	mean λ(Rand.)	mean λ(SART.)
Shepp	256	0.2998	0.2029	1.0870	1.9508
	512	0.2873	0.2087	0.9856	1.9407
Head	256	0.2660	0.1733	1.0520	1.9308
	512	0.2664	0.1974	0.9596	1.9273
Knee	256	0.2648	0.1723	1.0747	1.9287
	512	0.2668	0.1967	0.9777	1.9263

Table 4.9: Average amount of the selected λ in 20 iterations for Kaczmarz, Symmetric Kaczmarz, Randomized Kaczmarz and SART methods.

As it is clear from Table 4.9, the average amount of the selected relaxation parameters for different ART methods for Shepp-Logan phantom are a little different from the other phantoms. Indeed, the two real test phantoms of MRI Head and MRI knee have very similar chosen relaxation parameters. However, roughly speaking, the numerical results of all the test phantoms are close to each other, the results for real test phantoms are much closer to each other.

To compare the strategy proposed by Maria Saxild-Hansen in her Master's thesis [10], which is a training method for finding an optimal value for the relaxation parameter, with the method which is proposed in this thesis, using [10], and the associated

phantom	size	λ(Kacz.)	λ(Symm.)	λ(Rand.)	λ(SART.)
Shepp	256	0.1459	0.1033	0.1885	1.8115
	512	0.1459	0.1459	0.1459	1.6312
Head	256	0.0770	0.0344	0.1033	1.6049
	512	0.0770	0.1459	0.1459	1.5197
Knee	256	0.0770	0.0344	0.0770	1.5197
	512	0.0770	0.1033	0.1459	1.4508

Table 4.10: Hansen's selected λs in 20 iterations for Kaczmarz, Symmetric Kaczmarz, Randomized Kaczmarz and SART methods.

software, we have tried to find and choose the optimal value of λ for each specific ART methods. The numerical results of applying Hansen's method to our three different test phantoms for two various sizes are brought in Table 4.10.

Comparing Tables 4.9 and 4.10, it is clear that results are mostly different with each other, and the selected relaxation parameters for each ART method in Table 4.9 for various phantoms and sizes are much closer to each other.

4.5.3 Performance Comparisons

To evaluate the selected relaxation parameters obtained from Hansen's and our strategies for finding a fixed and optimal relaxation parameter for each of ART methods, we apply numerical results in Tables 4.9 and 4.10 to our three test phantoms to compare the reconstructed images, for each ART method, in terms of relative error, relative residual and image discrepancy for 512×512 images.

The experimental results shown in Tables 4.11, 4.12, 4.13 and 4.14 correspond to applying of Kaczmarz's, Symmetric Kaczmarz's, Randomized Kaczmarz's and SART

methods, respectively.

phantom	method	selected λ	relative error	relative residual	discrepancy
Shepp	Hansen's	0.1459	0.5830	0.0062	0.6729
	our	0.2873	0.5830	0.0065	0.6729
Head	Hansen's	0.0770	0.3867	0.0086	0.6091
	our	0.2664	0.3858	0.0067	0.6077
Knee	Hansen's	0.0770	0.3354	0.0078	0.5702
	our	0.2668	0.3345	0.0067	0.5687

Table 4.11: Comparison of Hansen's and our proposed method in iteration 20 by applying Kaczmarz's method to a 512×512 image.

Roughly speaking, in Tables 4.11 and 4.13, the results obtained from applying Kaczmarz's and Randomized Kaczmarz's methods using our strategy, for the relative error, relative residual and image discrepancy of the reconstructed images, are less than the results achieved from Hansen's strategy.

phantom	method	selected λ	relative error	relative residual	discrepancy
Shepp	Hansen's	0.1459	0.5829	0.0051	0.6728
	our	0.2087	0.5831	0.0096	0.6731
Head	Hansen's	0.1459	0.3855	0.0054	0.6073
	our	0.1974	0.3862	0.0093	0.6083
Knee	Hansen's	0.1033	0.3339	0.0032	0.5677
	our	0.1967	0.3350	0.0092	0.5695

Table 4.12: Comparison of Hansen's and our proposed method in iteration 20 by applying Symmetric Kaczmarz's method to a 512×512 image.

On the other hand, according to Tables 4.12 and 4.14, the numerical results, obtained from applying Symmetric Kaczmarz and SART methods using Hansen's

strategy, are less than the numerical results which are obtained from our strategy.

phantom	method	selected λ	relative error	relative residual	discrepancy
Shepp	Hansen's	0.1459	0.5835	0.0071	0.6736
	our	0.9856	0.5828	0.0006	0.6727
Head	Hansen's	0.1459	0.3857	0.0035	0.6076
	our	0.9596	0.3852	0.0004	0.6067
Knee	Hansen's	0.1459	0.3350	0.0034	0.5695
	our	0.9777	0.3340	0.0008	0.5678

Table 4.13: Comparison of Hansen's and our proposed method in iteration 20 by applying Randomized Kaczmarz's method to a 512×512 image.

phantom	method	selected λ	relative error	relative residual	discrepancy
Shepp	Hansen's	1.6312	0.5646	0.0242	0.6516
	our	1.9407	0.5813	0.2530	0.6709
Head	Hansen's	1.5197	0.3500	0.0114	0.5513
	our	1.9273	0.3876	0.2026	0.6105
Knee	Hansen's	1.4508	0.2897	0.0102	0.4925
	our	1.9263	0.3362	0.1998	0.5715

Table 4.14: Comparison of Hansen's and our proposed method in iteration 20 by applying SART method to a 512×512 image.

The experimental results of comparing Hansen's and our proposed methods for finding an optimal relaxation parameter for each ART method indicate that however the obtained numerical results are generally close to each other, our proposed strategy for finding a suitable fixed relaxation parameter in Kaczmarz's and Randomized Kaczmarz's methods plays a better role in terms of relative error, relative residual and image discrepancy of the reconstructed image.

Chapter 5

Numerical Study of FBP Algorithm

5.1 Test Phantoms

In this chapter, to assess FBP algorithm we have used our three previously discussed phantoms which are Shepp-Logan phantom, Figure 4.1, whose structure is completely defined by mathematical formulas, MRI Head phantom which is the para-sagittal MRI scan of a head, Figure 4.2 and MRI Knee phantom which is the sagittal MRI scan image of a knee, Figure 4.3.

5.2 Measuring Image Quality

To measure the quality of the reconstructed images obtained by means of FBP algorithm for each of the test phantoms, two ways of error measuring, which are in common with ART methods error measuring ways, are basically used in this chapter.

The first one is the relative error of the reconstructed image, Equation 4.4, and the second one is the discrepancy between the exact phantom and the reconstructed image, Equation 4.5, which is also called Colsher's discrepancy metric [4].

5.3 Experimental Results of Test Phantoms

Experimental results of applying filtered back projection algorithm to Shepp-Logan, MRI Head and MRI Knee phantoms for three different image sizes are shown in Table 5.1. In the above mentioned table, the relative error and Colsher's discrepancy of each of the reconstructed images are brought.

phantom	size	relative error	discrepancy
Shepp	128	0.4746	0.6867
	256	0.5104	0.6733
	512	0.5005	0.6284
Head	128	0.1162	0.3772
	256	0.0851	0.2707
	512	0.0573	0.1794
Knee	128	0.0850	0.2719
	256	0.0613	0.1817
	512	0.0544	0.1370

Table 5.1: Numerical results of applying FBP to three test phantoms.

As it is clear from Table 5.1, the smaller the sizes of the phantoms are, the greater the relative errors and Colsher's discrepancies of the reconstructed images become.

(a) Exact Shepp-Logan phantom

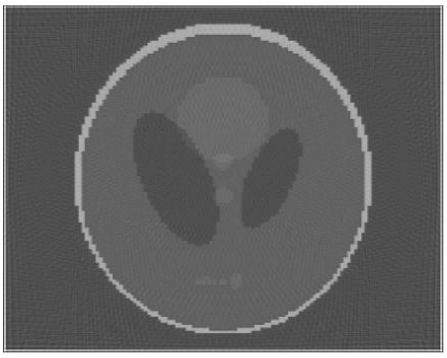

(b) Reconstructed Shepp-Logan phantom

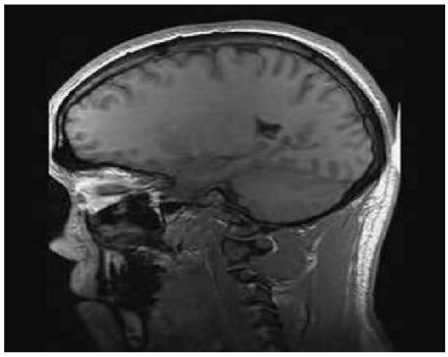

(c) Exact MRI Head phantom

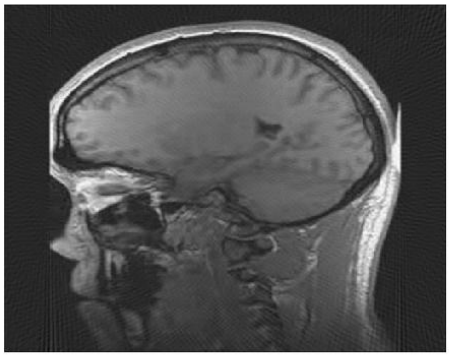

(d) Reconstructed MRI Head phantom

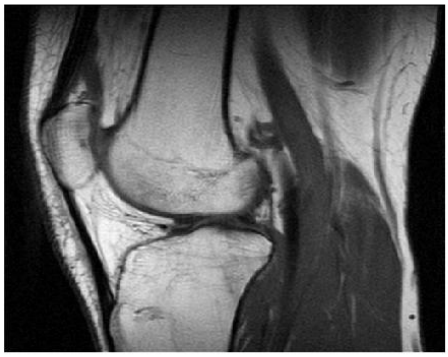

(e) Exact MRI Knee phantom

(f) Reconstructed MRI Knee phantom

Figure 5.1: Reconstructed images after applying FBP to our test phantoms for 512×512 images.

(a) Exact Shepp-Logan phantom

(b) Reconstructed Shepp-Logan phantom

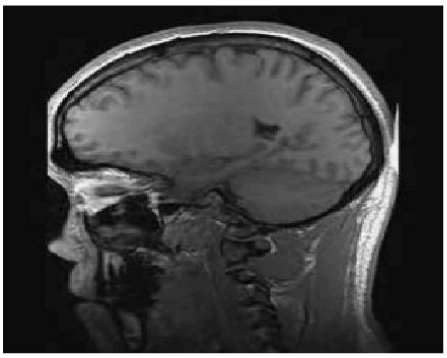

(c) Exact MRI Head phantom

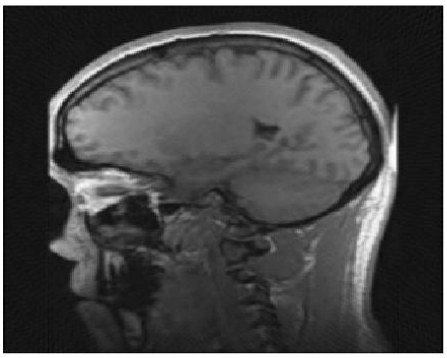

(d) Reconstructed MRI Head phantom

(e) Exact MRI Knee phantom

(f) Reconstructed MRI Knee phantom

Figure 5.2: Reconstructed images after applying FBP to our test phantoms for 256×256 images.

(a) Exact Shepp-Logan phantom

(b) Reconstructed Shepp-Logan phantom

(c) Exact MRI Head phantom

(d) Reconstructed MRI Head phantom

(e) Exact MRI Knee phantom

(f) Reconstructed MRI Knee phantom

Figure 5.3: Reconstructed images after applying FBP to our test phantoms for 128×128 images.

The reconstructed images of applying FBP to our three test phantoms for 512×512, 256×256 and 128×128 image sizes are represented in Figures 5.1, 5.2 and 5.3, respectively. However, Table 5.1 indicates that the less the sizes of the images become, the more the errors of the reconstructed images are, the resulting images in the above figures are in contradiction with the numerical results achieved in Table 5.1. As a matter of fact, the smaller the size of the phantom is, the more visible and smooth the reconstructed image becomes even though losing its sharpness.

phantom	size	Kacz.	Symm.	Rand.	SART	FBP
Shepp	256	0.5560	0.5567	0.5531	0.5603	0.6733
	512	0.6730	0.6732	0.6727	0.6522	0.6284
Head	256	0.4742	0.4780	0.4619	0.4563	0.2707
	512	0.6077	0.6087	0.6067	0.5572	0.1794
Knee	256	0.4245	0.4295	0.4070	0.3957	0.1817
	512	0.5687	0.5700	0.5678	0.5011	0.1370

Table 5.2: Comparison of Colsher's discrepancy between ART methods and FBP algorithm for three test phantoms.

To assess the image quality of the reconstructed images obtained using FBP algorithm and different ART methods which were previously discussed and inspected in chapter 4, we have compared their corresponding Colsher's discrepancies which is the most significant error measuring strategy in our thesis.

According to Table 5.2, generally speaking, FBP has the least discrepancy error in comparison with all the iterative methods, specially in MRI Head and Knee phantoms which are our two practical test phantoms.

Chapter 6

Conclusion

6.1 ART versus FBP

As said earlier, the first CT scanners essentially used an ART approach for their image reconstruction processes. However, today's commercial scanners are programmed to use transform based methods since Fourier transform methods are generally faster to implement on computer.

On the other hand, Algebraic Reconstruction Technique (ART) methods simply get applied to a smaller set of equations and unlike the transform based methods like Filtered Back-Projection (FBP), based on a continuous model, does not necessarily require complete X-ray data collection.

As a matter of fact, there are situations where it is not possible to measure a large number of projections or the projections are not uniformly distributed over 180 or 360

degrees and indeed the range of angles used in a CT scan is restricted. Hence, transform based methods like FBP that rely on convolution cannot get applied without the completion of data, so for problems of this type, it is more amenable to have solution by ART such a concrete situation is earth resources imaging using cross bore-hole measurements [7].

However, ART simply gets applied to a smaller set of equations in case of incomplete X-ray data collection, it converges too slowly, and based on the numerical results of this thesis in comparison with transform based methods like Filtered Back Projection have more relative error and discrepancy error measurements. Roughly speaking, ART methods lack the accuracy and speed of implementation, while the Filtered Back Projection can be adapted fairly easily to any desired level of accuracy and is faster than all ART methods, accroding to its complexity shown in Table 3.1.

6.2 Thesis Results

In the overdetermined systems corresponding to 128×128 image size in our three test phantoms, among Kaczmarz's, Symmetric Kaczmarz's, Randomized Kaczmarz and SART methods, Randomized Kaczmarz's methods shows the least Colsher's discrepancy and relative error.

On the other hand, in the underdetermined systems corresponding to 256×256 and 512×512 image sizes, Randomized Kaczmarz/SART and SART methods have the least Colsher's discrepancy error measurements in comparison with the other ART methods.

Experimental results of applying our proposed strategy for finding an adaptive and optimal relaxation parameter for each of ART methods showed that the obtained numerical results of MRI Head and Knee real test phantoms are closer to each other in their corresponding iteration and indeed follow the same pattern in spite of the fact that the phantoms are totally different from each other. It can also be concluded that the ranges of the selected relaxation parameters for Kaczmarz's, Symmetric Kaczmarz's, Randomized Kaczmarz's and SART methods can be reduced to $(0.2, 0.7)$, $(0.1, 0.6)$, $(0.5, 1.5)$ and $(1.9, 2)$, respectively.

Relaxation parameter (λ) should idealistically be defined as a function of iteration number, that for each particular iteration k there must be a real number $\lambda^{(k)}$ between 0 and 2. But, since the result for each iteration can vary from a test phantom to another one and essentially there is not a unique choice for the best relaxation parameter, it is not an easy task to find a unique choice for the best relaxation parameter in each iteration.

Comparing numerical results obtained from our proposed strategy and the previously proposed strategy by Maria Saxild-Hansen, for finding a fixed relaxation parameter, showed that the selected relaxation parameters are different from each other. Running all ART methods with their corresponding selected relaxation parameter from each of the proposed strategies led to this fact that our proposed strategy, for finding a fixed relaxation parameter, in Kaczmarz's and Randomized Kaczmarz's methods has slightly a better performance in terms of relative error, relative residual

and image discrepancy of the reconstructed image. But generally speaking, different λs obtained from Hansen's and our strategies, for each phantom and image size, produce nearly the same numerical results.

6.3 Suggestions for Future Work

There are some issues about ART methods that can be worked on in future works as following:

- To have a better understanding whether selected relaxation parameters in each ART method relatively follow the same pattern no matter what the image size is, we can test the phantoms for a higher resolution of 1024×1024.
- Try to find a function according to the selected relaxation parameters obtained by applying our proposed strategy for finding the best relaxation parameter in each iteration.
- Try to find an adaptive strategy for finding the relaxation parameters for similar phantoms.
- To speed up the implementation time for ART methods, GPU programming for iterative methods is also an interest.

Appendix A

Experimental Results on Shepp-Logan Test Phantom

Experimental results, obtained by applying Kaczmarz's, Symmetric Kaczmarz's, Randomized Kaczmarz's and SART methods to an overdetermined system corresponding to 128×128 image size and two underdetermined system corresponding to 256×256 and 512×512 Shepp-Logan phantom image sizes, are plotted in Figures A.1—A.4, A.5–A.8 and A.9–A.12, respectively. The results in these Figures A.1–A.12 are computed for relaxation parameters, $\lambda = 0.2, 0.4, .., 1$, for 20 iterations.

Reconstructed images of 128×128, 256×256 and 512×512 Shepp-Logan phantoms using Kaczmarz, Symmetric Kaczmarz, Randomized Kaczmarz and SART for relaxation parameter $\lambda = 0.4$ are given in Figures A.13, A.14 and A.15, respectively for three different iterations.

Consecutively, to compute numerical results for other relaxation parameters,

$\lambda = 1, 1.2, .., 1.8$, for 20 iterations, we have applied these methods to overdetermined system corresponding to 128×128 image size and underdetermined systems corresponding to 256×256 and 512×512 Shepp-Logan phantom image sizes. The plots are shown in Figures A.16–A.19, A.20–A.23 and A.24–A.27, respectively. Related Reconstructed images of 128×128, 256×256 and 512×512 Shepp-Logan phantoms using Kaczmarz, Symmetric Kaczmarz, Randomized Kaczmarz and SART for relaxation parameter $\lambda = 1.2$ are shown in Figures A.28, A.29 and A.30, respectively for three different iterations.

Shepp Logan, Kaczmarz, 128×128 **image,** $\lambda = 0.2, 0.4, .., 1$

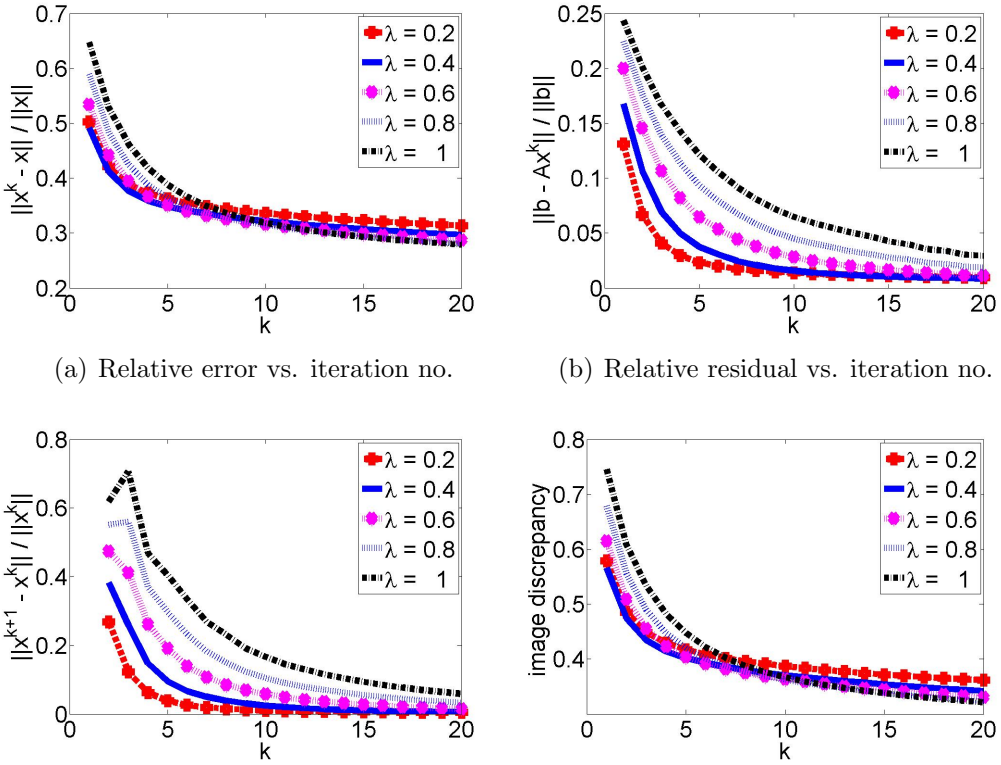

(a) Relative error vs. iteration no.

(b) Relative residual vs. iteration no.

(c) Relative solution difference vs. iteration no.

(d) Image discrepancy vs. iteration no.

Figure A.1: ART(Kaczmarz's method) applied to Shepp-Logan phantom for a 128×128 image and $\lambda = 0.2, 0.4, .., 1$.

In the last iteration,

	min relative error	min relative residual	min relative solution difference	min discrepancy
λ	1	0.2	0.2	1

Shepp Logan, Symmetric Kaczmarz, 128×128 **image,** $\lambda = 0.2, 0.4, .., 1$

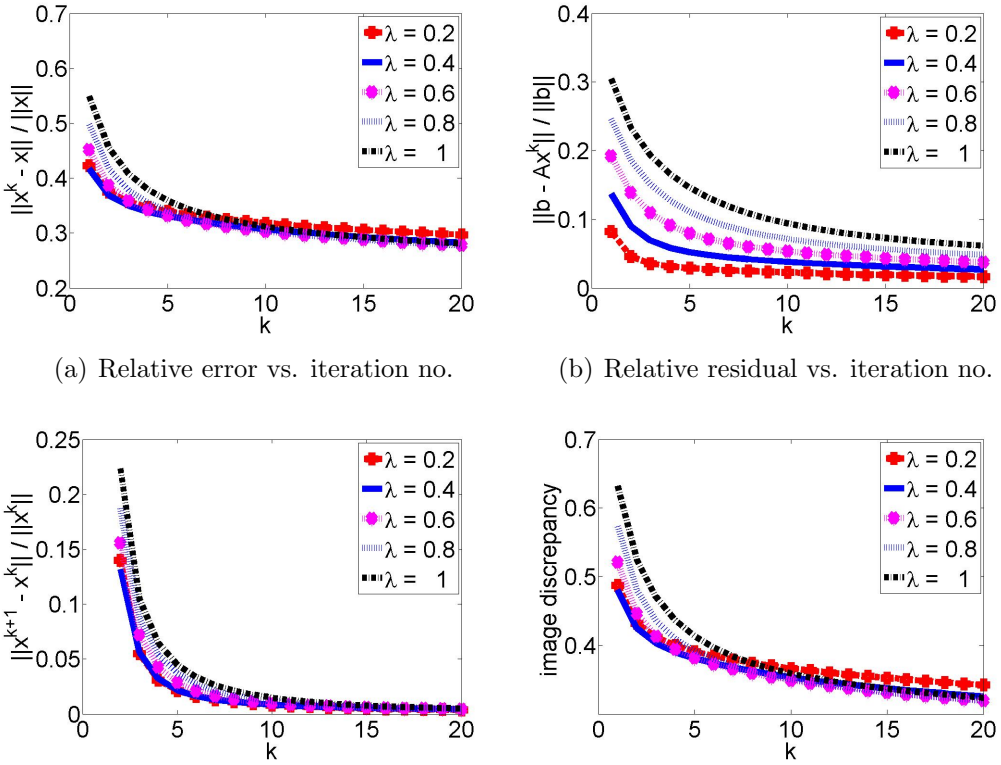

(a) Relative error vs. iteration no.

(b) Relative residual vs. iteration no.

(c) Relative solution difference vs. iteration no.

(d) Image discrepancy vs. iteration no.

Figure A.2: Symmetric Kaczmarz's method applied to Shepp-Logan phantom for a 128×128 image and $\lambda = 0.2, 0.4, .., 1$.

In the last iteration,

	min relative error	min relative residual	min relative solution difference	min discrepancy
λ	0.8	0.2	0.2	0.8

Shepp Logan, Randomized Kaczmarz, 128×128 **image,** $\lambda = 0.2, 0.4, .., 1$

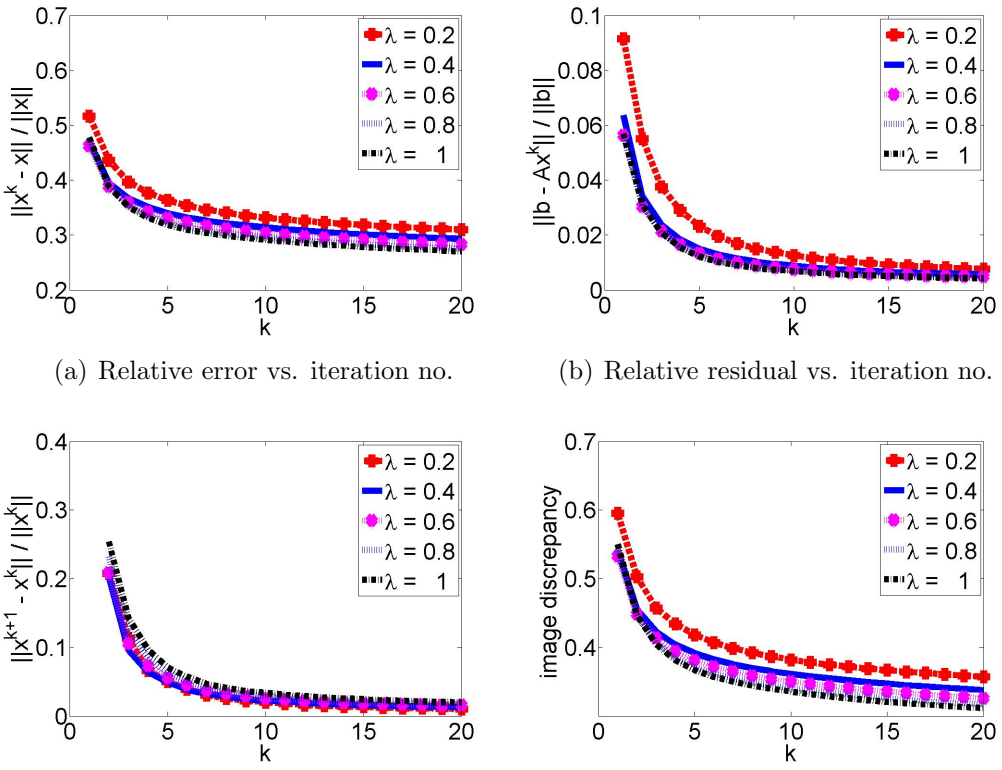

(a) Relative error vs. iteration no.

(b) Relative residual vs. iteration no.

(c) Relative solution difference vs. iteration no.

(d) Image discrepancy vs. iteration no.

Figure A.3: Randomized Kaczmarz's method applied to Shepp-Logan phantom for a 128×128 image and $\lambda = 0.2, 0.4, .., 1$.

In the last iteration,

	min relative error	min relative residual	min relative solution difference	min discrepancy
λ	1	1	0.2	1

Shepp Logan, SART, 128×128 **image,** $\lambda = 0.2, 0.4, .., 1$

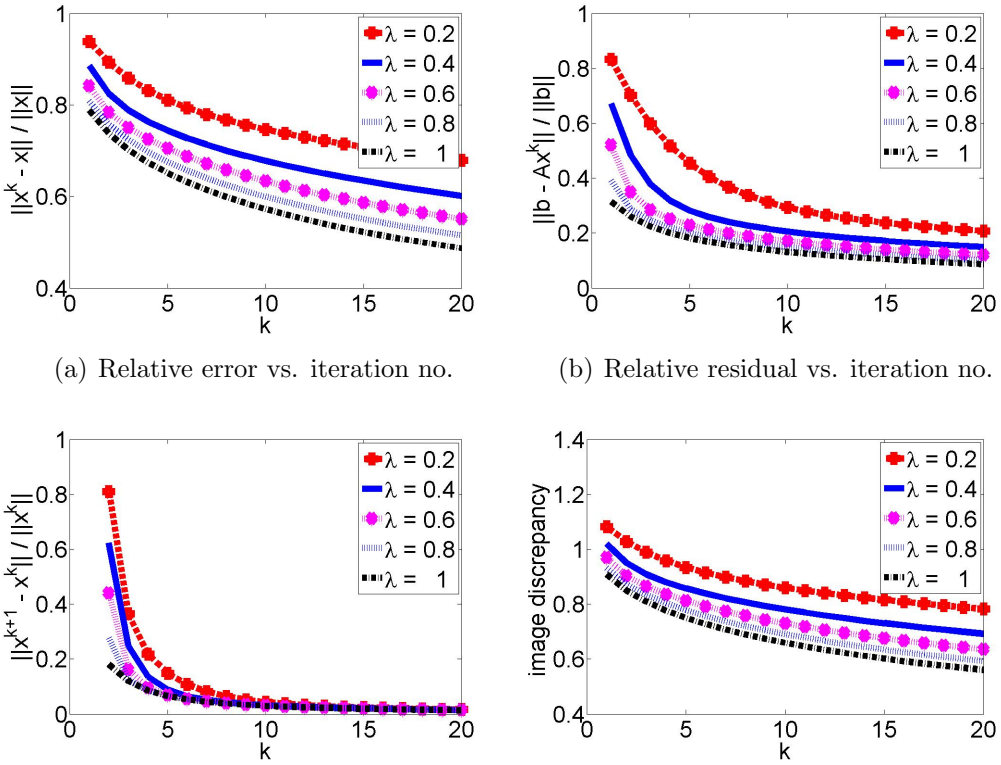

(a) Relative error vs. iteration no.

(b) Relative residual vs. iteration no.

(c) Relative solution difference vs. iteration no.

(d) Image discrepancy vs. iteration no.

Figure A.4: SART method applied to Shepp-Logan phantom for a 128×128 image and $\lambda = 0.2, 0.4, .., 1$.

In the last iteration,

	min relative error	min relative residual	min relative solution difference	min discrepancy
λ	1	1	1	1

Shepp Logan, Kaczmarz's, 256×256 **image,** $\lambda = 0.2, 0.4, .., 1$

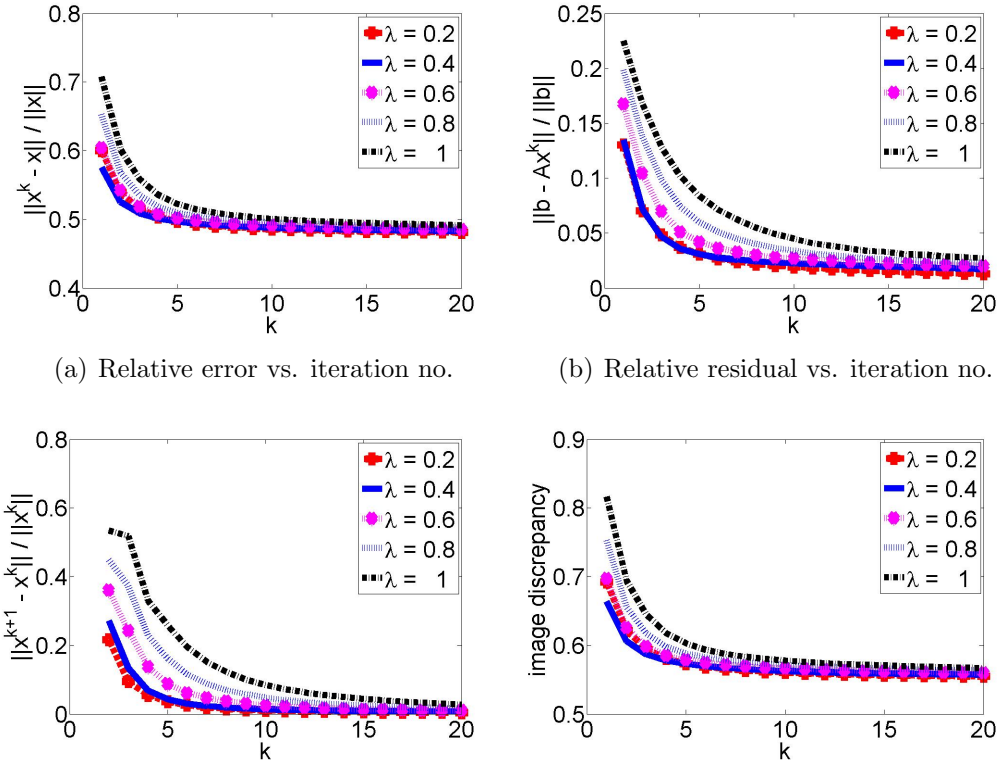

(a) Relative error vs. iteration no.

(b) Relative residual vs. iteration no.

(c) Relative solution difference vs. iteration no.

(d) Image discrepancy vs. iteration no.

Figure A.5: ART(Kaczmarz's method) applied to Shepp-Logan phantom for a 256×256 image and $\lambda = 0.2, 0.4, .., 1$.

In the last iteration,

	min relative error	min relative residual	min relative solution difference	min discrepancy
λ	0.2	0.2	0.2	0.2

Shepp Logan, Symmetric Kaczmarz, 256×256 **image,** $\lambda = 0.2, 0.4, .., 1$

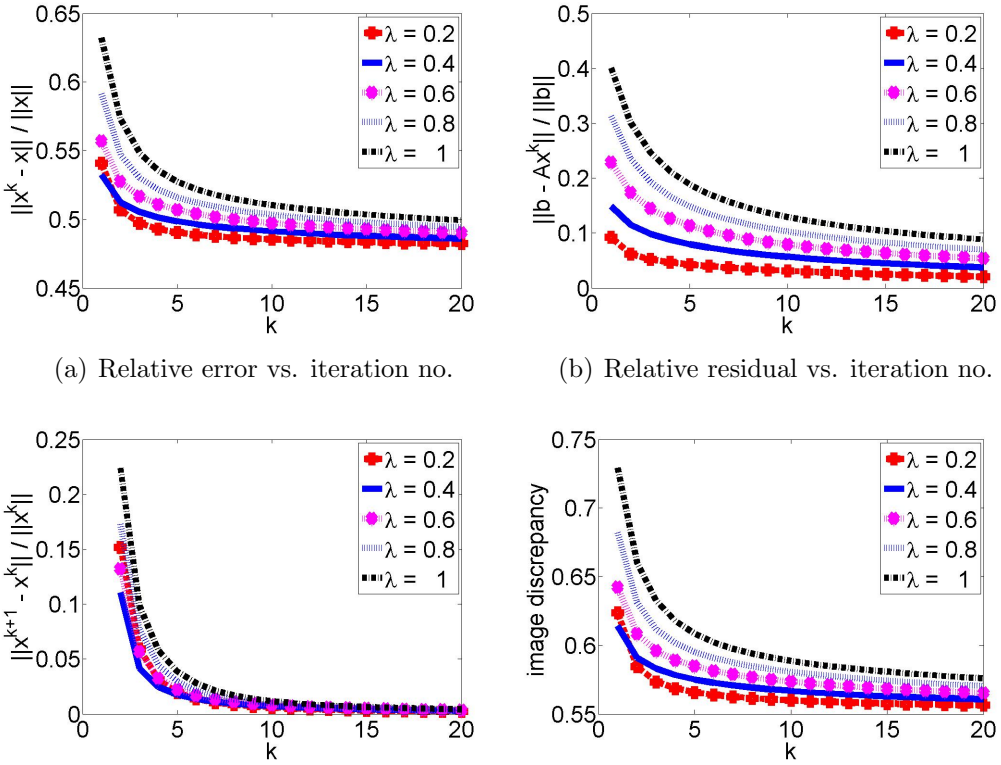

(a) Relative error vs. iteration no.

(b) Relative residual vs. iteration no.

(c) Relative solution difference vs. iteration no.

(d) Image discrepancy vs. iteration no.

Figure A.6: Symmetric Kaczmarz's method applied to Shepp-Logan phantom for a 256×256 image and $\lambda = 0.2, 0.4, .., 1$.

In the last iteration,

	min relative error	min relative residual	min relative solution difference	min discrepancy
λ	0.2	0.2	0.2	0.2

Shepp Logan, Randomized Kaczmarz, 256×256 **image,** $\lambda = 0.2, 0.4, .., 1$

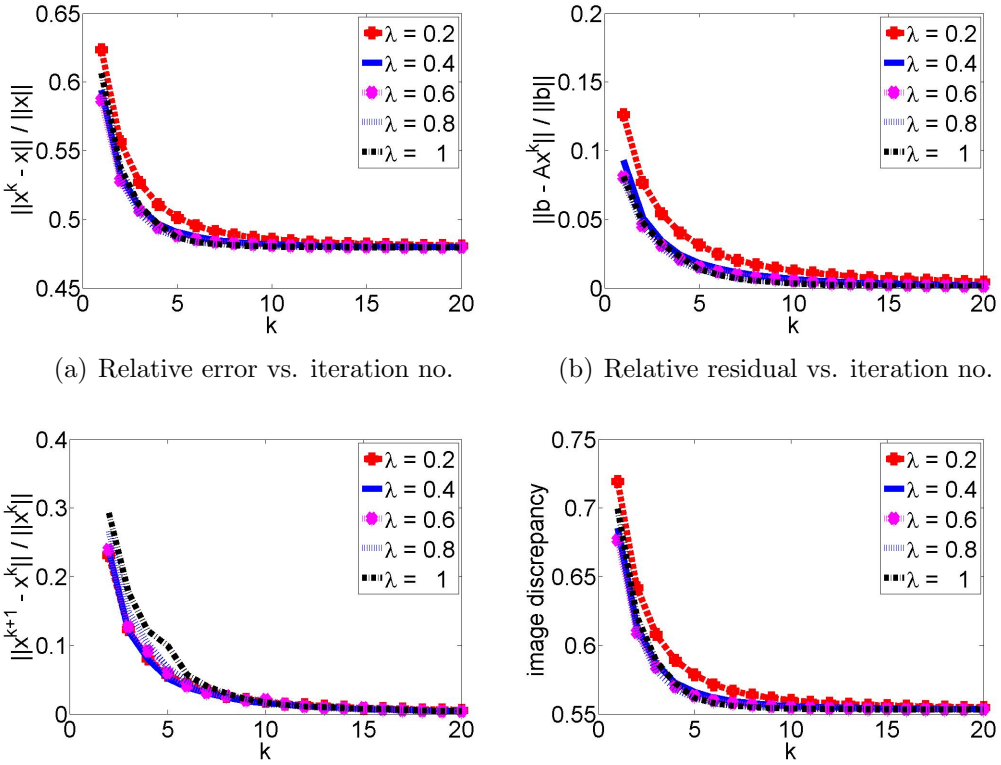

(a) Relative error vs. iteration no.

(b) Relative residual vs. iteration no.

(c) Relative solution difference vs. iteration no.

(d) Image discrepancy vs. iteration no.

Figure A.7: Randomized Kaczmarz's method applied to Shepp-Logan phantom for a 256×256 image and $\lambda = 0.2, 0.4, .., 1$.

In the last iteration,

	min relative error	min relative residual	min relative solution difference	min discrepancy
λ	1	1	1	1

Shepp Logan, SART, 256×256 **image,** $\lambda = 0.2, 0.4, .., 1$

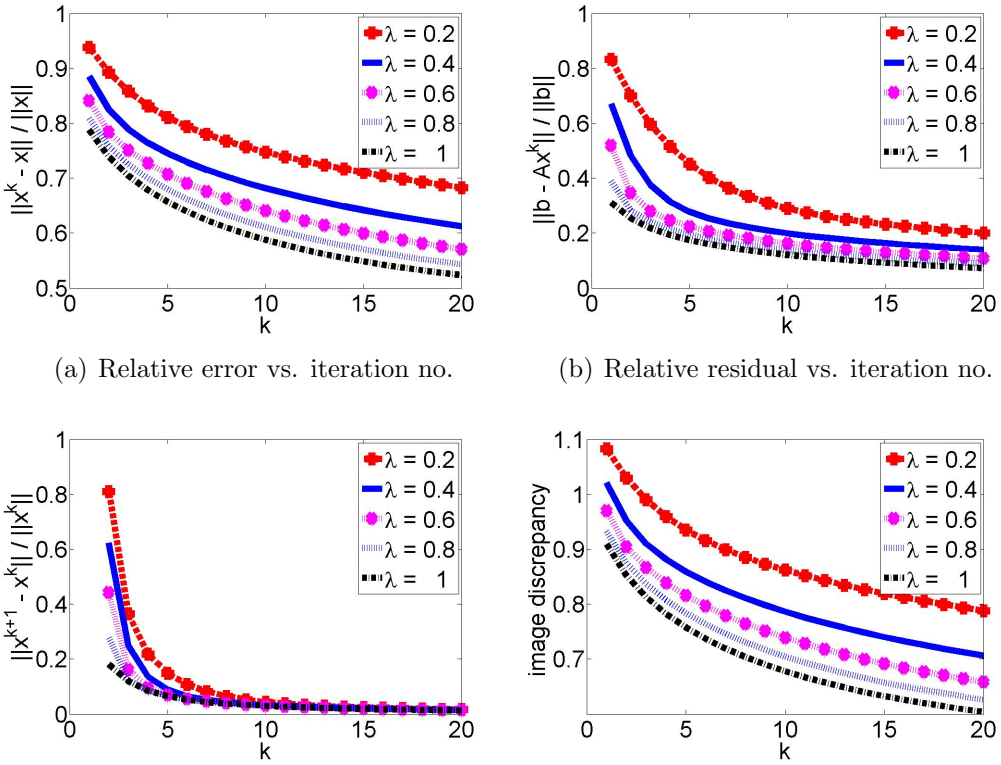

(a) Relative error vs. iteration no.

(b) Relative residual vs. iteration no.

(c) Relative solution difference vs. iteration no.

(d) Image discrepancy vs. iteration no.

Figure A.8: SART method applied to Shepp-Logan phantom for a 256×256 image and $\lambda = 0.2, 0.4, .., 1$.

In the last iteration,

	min relative error	min relative residual	min relative solution difference	min discrepancy
λ	1	1	1	1

Shepp Logan, Kaczmarz, 512×512 **image,** $\lambda = 0.2, 0.4, .., 1$

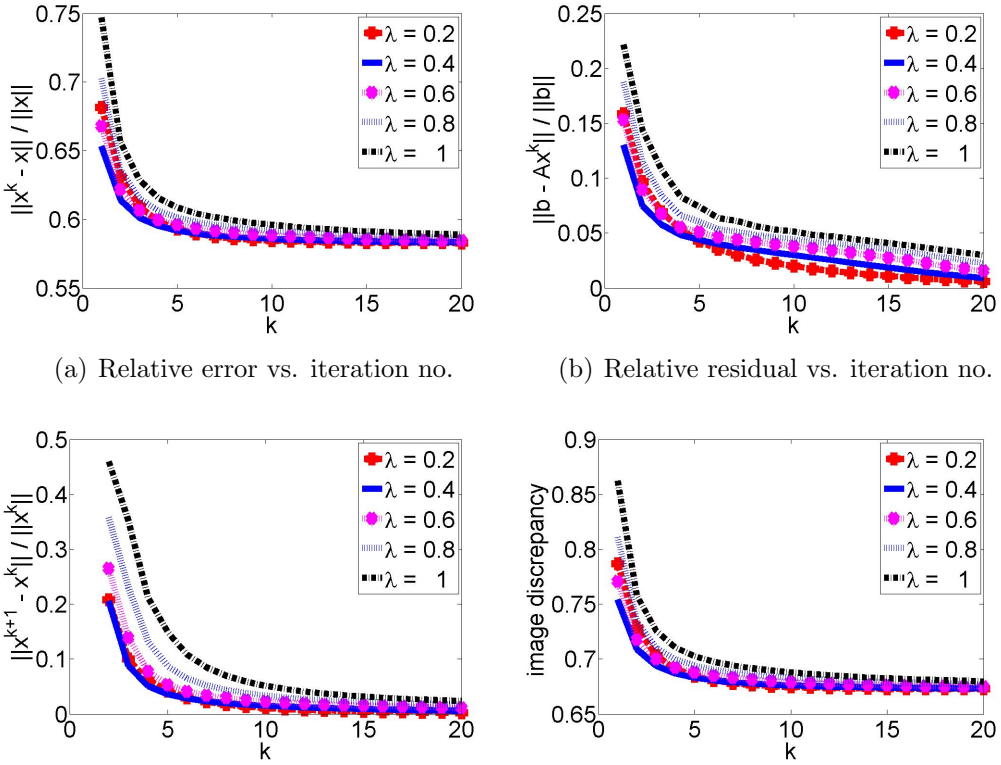

(a) Relative error vs. iteration no.

(b) Relative residual vs. iteration no.

(c) Relative solution difference vs. iteration no.

(d) Image discrepancy vs. iteration no.

Figure A.9: ART(Kaczmarz's method) applied to Shepp-Logan phantom for a 512×512 image and $\lambda = 0.2, 0.4, .., 1$.

In the last iteration,

	min relative error	min relative residual	min relative solution difference	min discrepancy
λ	0.2	0.2	0.2	0.2

Shepp Logan, Symmetric Kaczmarz, 512×512 **image,** $\lambda = 0.2, 0.4, .., 1$

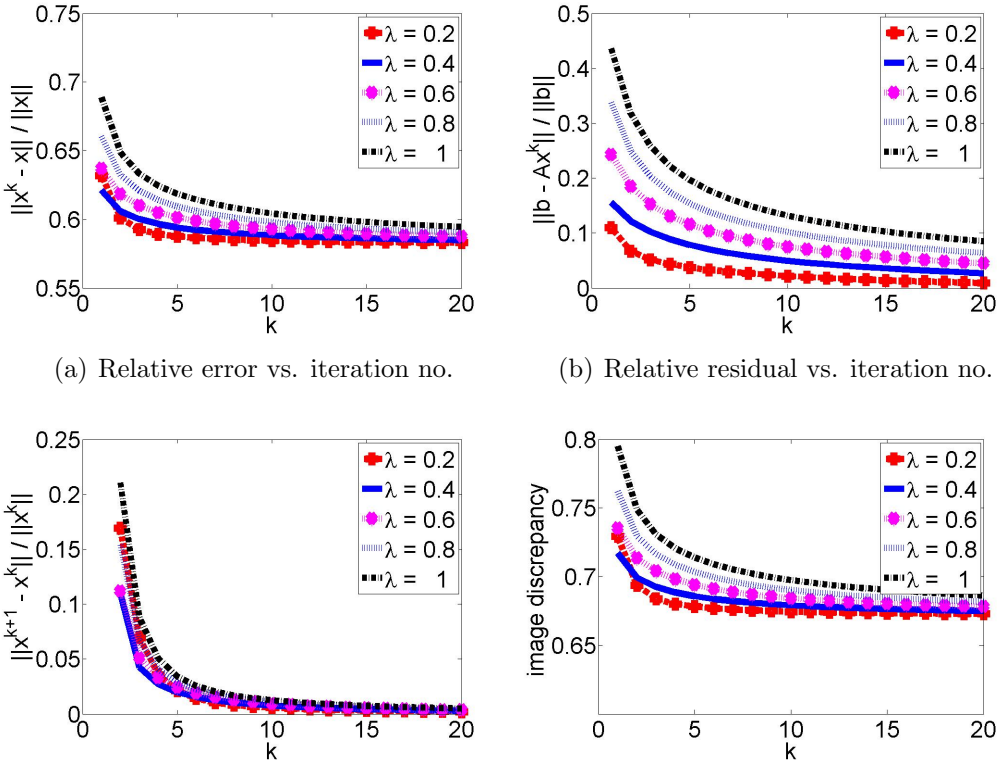

(a) Relative error vs. iteration no.

(b) Relative residual vs. iteration no.

(c) Relative solution difference vs. iteration no.

(d) Image discrepancy vs. iteration no.

Figure A.10: Symmetric Kaczmarz's method applied to Shepp-Logan phantom for a 512×512 image and $\lambda = 0.2, 0.4, .., 1$.

In the last iteration,

	min relative error	min relative residual	min relative solution difference	min discrepancy
λ	0.2	0.2	0.2	0.2

Shepp Logan, Randomized Kaczmarz, 512×512 **image,** $\lambda = 0.2, 0.4, .., 1$

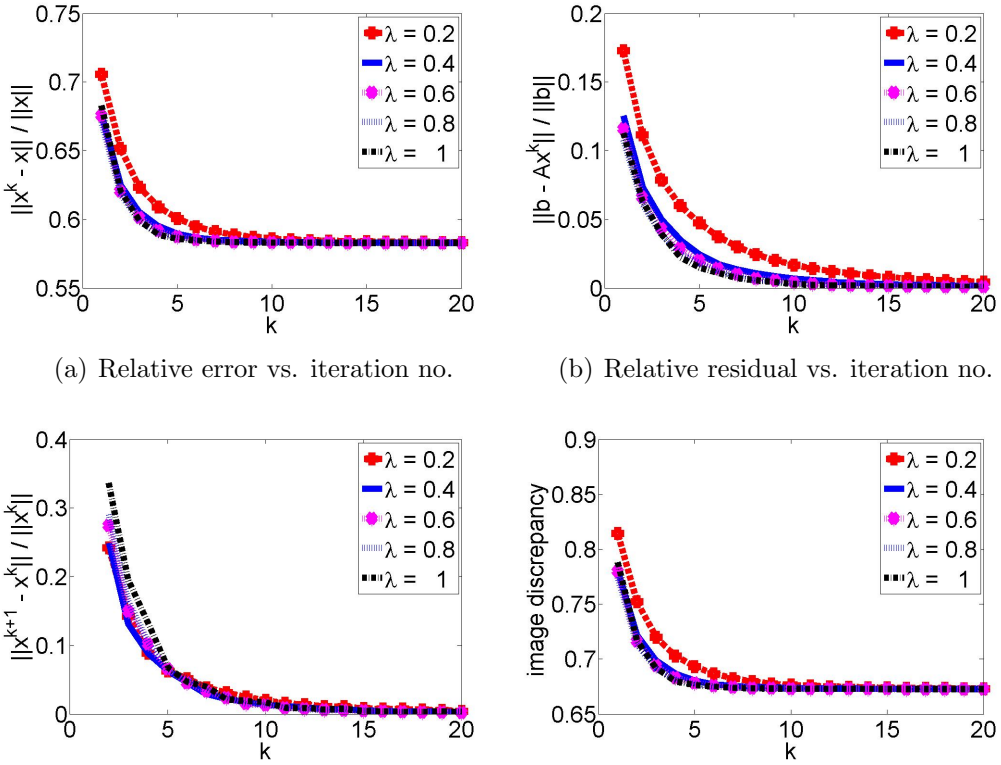

(a) Relative error vs. iteration no.

(b) Relative residual vs. iteration no.

(c) Relative solution difference vs. iteration no.

(d) Image discrepancy vs. iteration no.

Figure A.11: Randomized Kaczmarz's method applied to Shepp-Logan phantom for a 512×512 image and $\lambda = 0.2, 0.4, .., 1$.

In the last iteration,

	min relative error	min relative residual	min relative solution difference	min discrepancy
λ	1	1	1	1

Shepp Logan, SART, 512×512 **image,** $\lambda = 0.2, 0.4, .., 1$

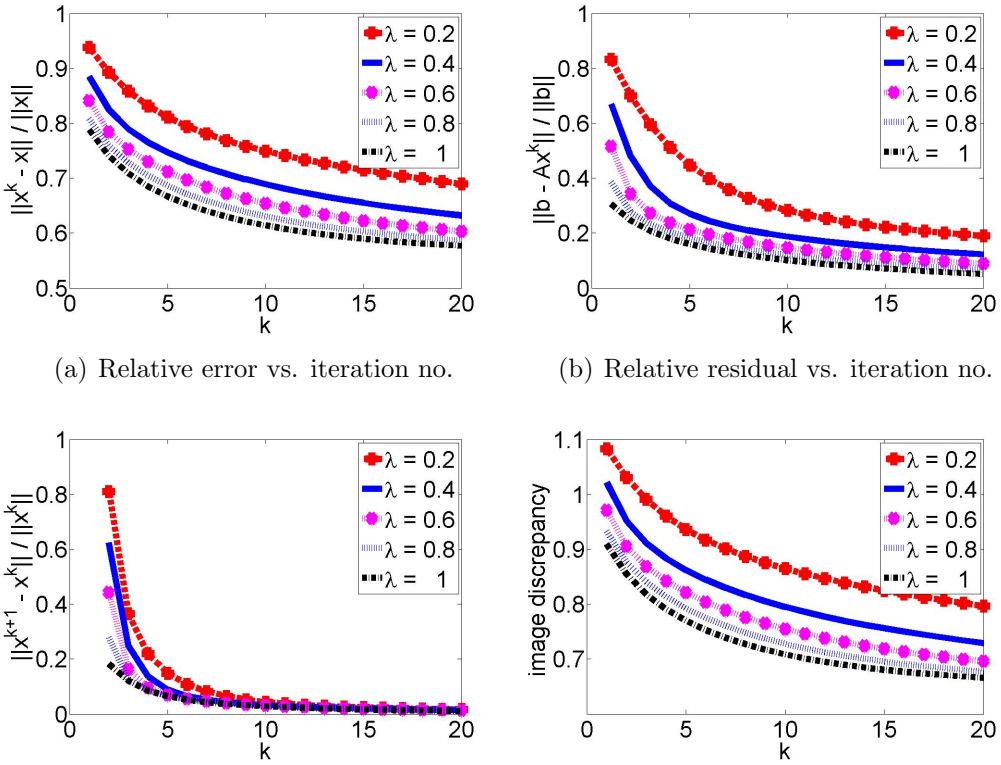

(a) Relative error vs. iteration no.

(b) Relative residual vs. iteration no.

(c) Relative solution difference vs. iteration no.

(d) Image discrepancy vs. iteration no.

Figure A.12: SART method applied to Shepp-Logan phantom for a 512×512 image and $\lambda = 0.2, 0.4, .., 1$.

In the last iteration,

	min relative error	min relative residual	min relative solution difference	min discrepancy
λ	1	1	1	1

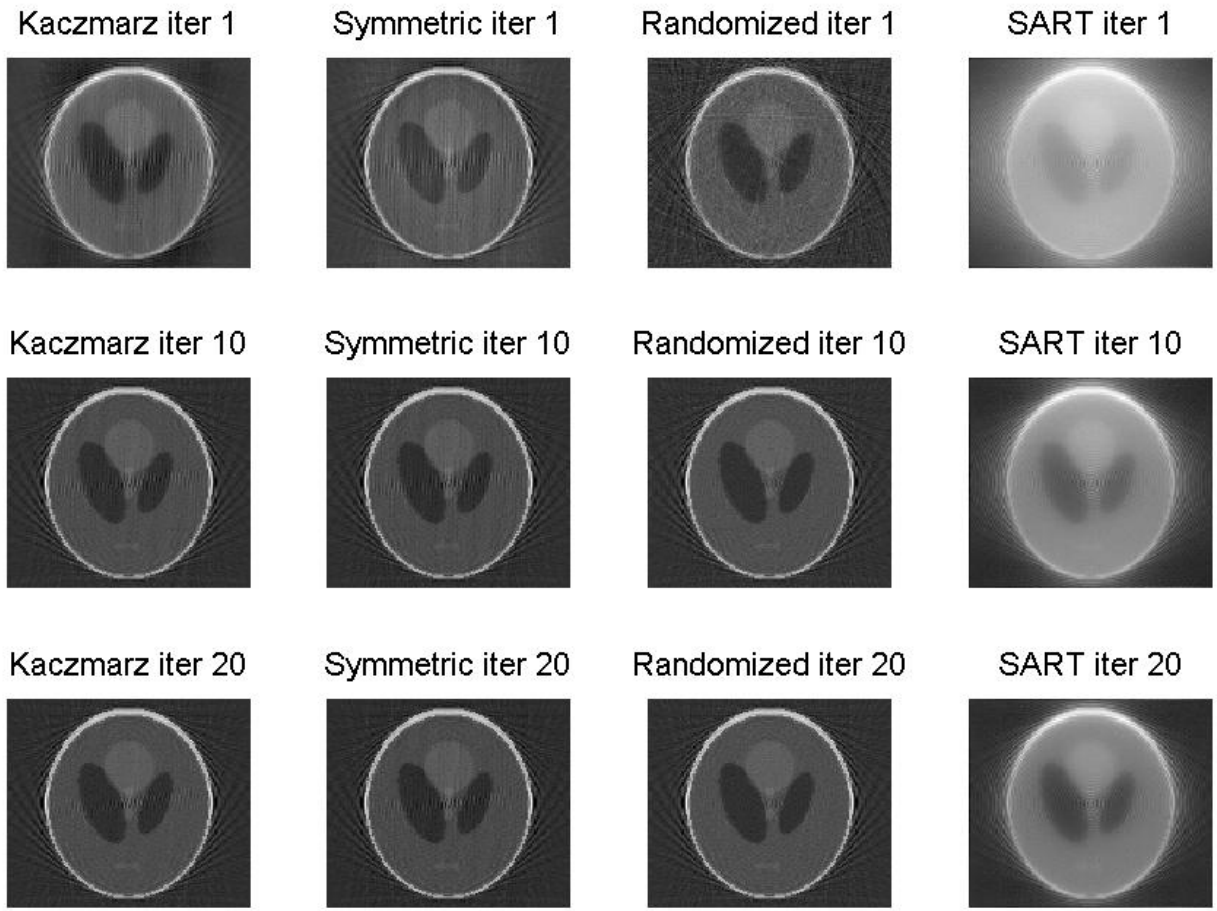

Figure A.13: Reconstruction of the 128×128 Shepp-Logan Phantom using Kaczmarz, Symmetric Kaczmarz, Randomized Kaczmarz and SART ($\lambda = 0.4$).

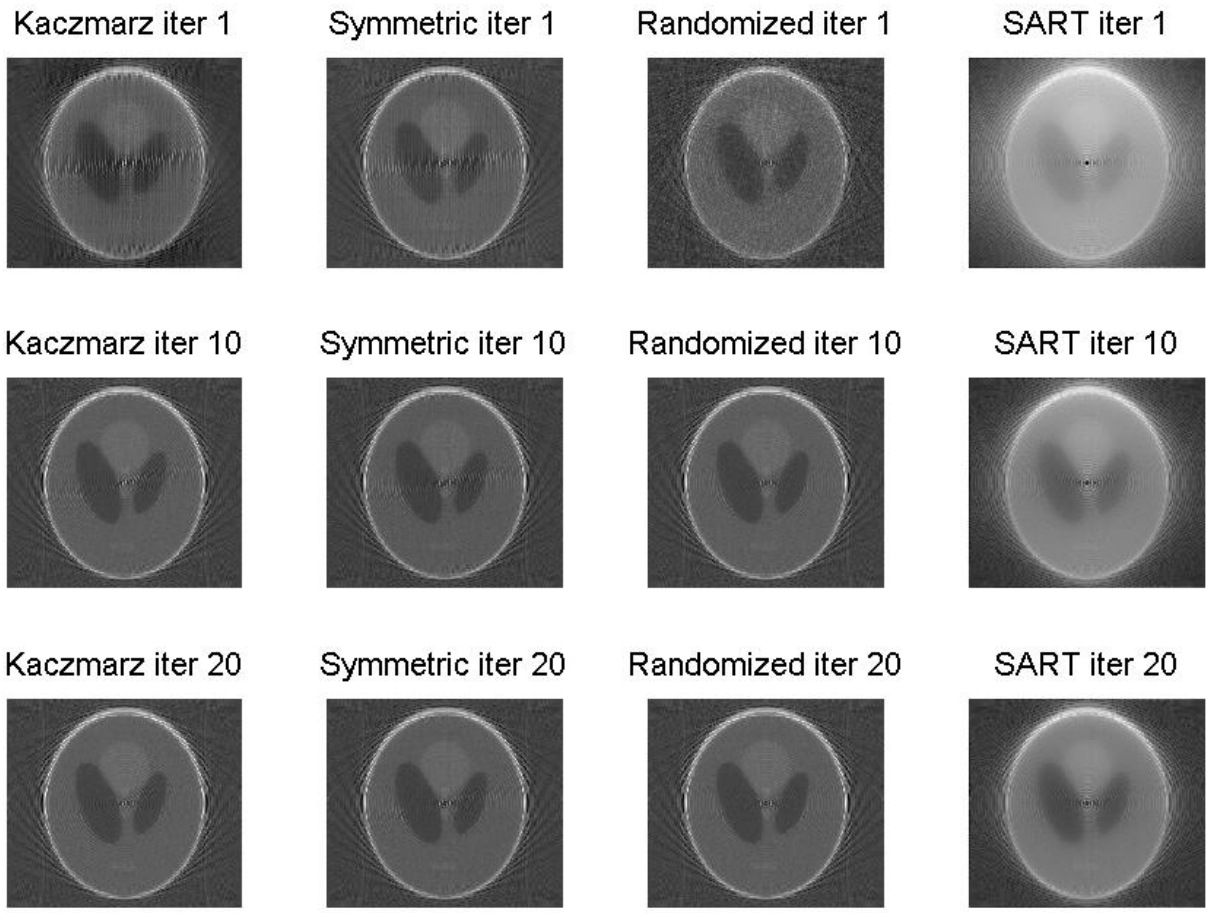

Figure A.14: Reconstruction of the 256×256 Shepp-Logan Phantom using Kaczmarz, Symmetric Kaczmarz, Randomized Kaczmarz and SART ($\lambda = 0.4$).

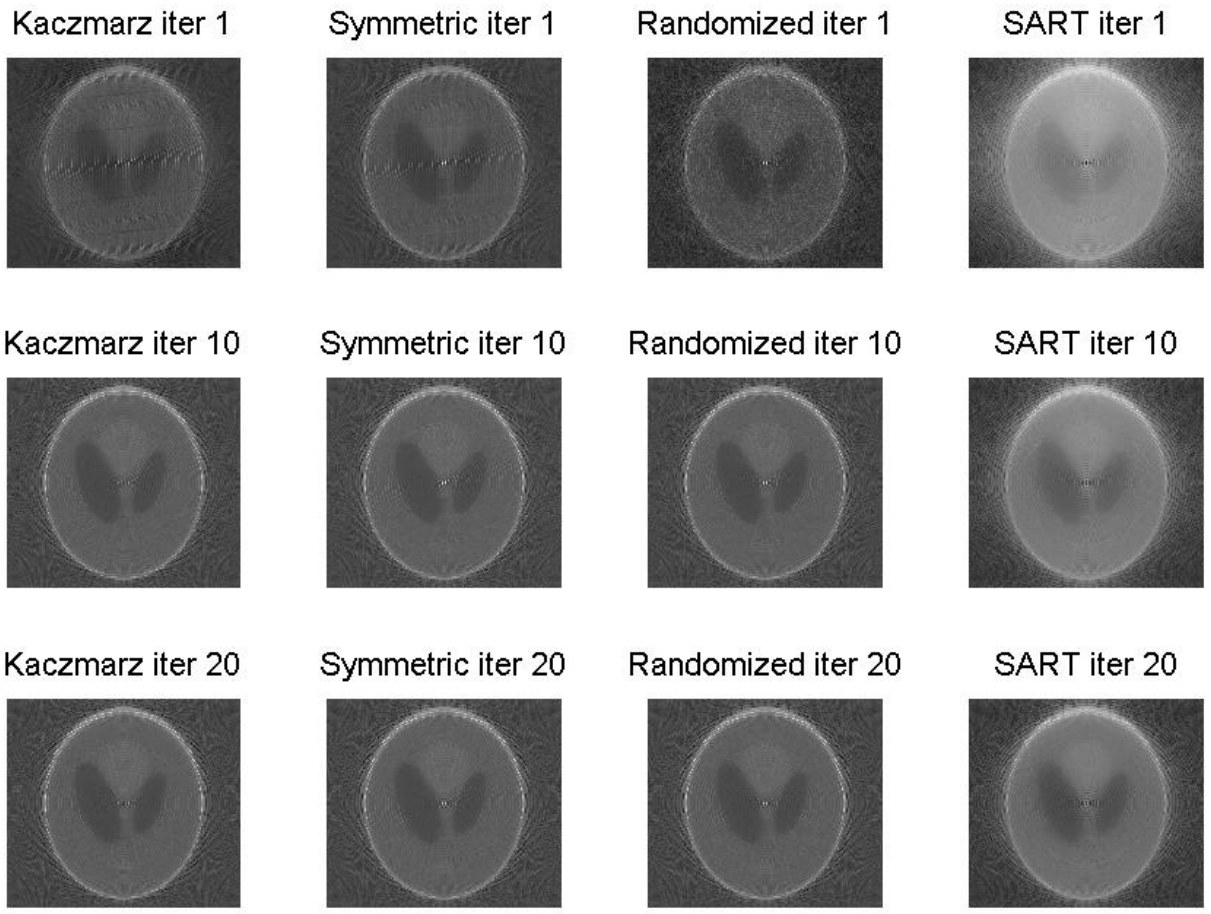

Figure A.15: Reconstruction of the 512×512 Shepp-Logan Phantom using Kaczmarz, Symmetric Kaczmarz, Randomized Kaczmarz and SART ($\lambda = 0.4$).

size	method	worst λ	max discrepancy	best λ	min discrepancy	time/iter(s)
128	Kacz.	0.2	0.3615	1	0.3209	9.6
	Symm.	0.2	0.3422	0.8	0.3191	18.81
	Rand.	0.2	0.3570	1	0.3112	18.517
	SART	0.2	0.7822	1	0.5608	0.024
256	Kacz.	1	0.5666	0.2	0.5551	36.23
	Symm.	1	0.5760	0.2	0.5564	65.49
	Rand.	0.2	0.5546	1	0.5532	41.71
	SART	0.2	0.7878	1	0.6036	0.067
512	Kacz.	1	0.6795	0.2	0.6728	151.95
	Symm.	1	0.6862	0.2	0.6730	406.54
	Rand.	0.2	0.6731	1	0.6727	189.84
	SART	0.2	0.7964	1	0.6658	0.25

Table A.1: Experimental results of applying different methods to Shepp-Logan phantom using relaxation parameters of $\lambda = 0.2, 0.4, .., 1$ for 20 number of iterations.

The experimental results shown in Table A.1 are obtained from the Colsher's discrepancy measurement method [4] in such a way that, after applying different ART methods to different phantom sizes, for $\lambda = 0.2, 0.4, .., 1$, the minimum and the maximum discrepancies, which indicate the best and the worst relaxation parameters, are found in iteration number 20.

As it can be seen, the results for the overdetermined system corresponding to 128×128 Shepp-Logan phantom are different from the results achieved for two underdetermined systems corresponding to 256×256 and 512×512 Shepp-Logan phantom image sizes. It is obvious that the results for both underdetermined systems follow the same pattern for their best and worst relaxation parameters, for various image reconstruction techniques.

Shepp Logan, Kaczmarz, 128×128 **image,** $\lambda = 1, 1.2, .., 1.8$

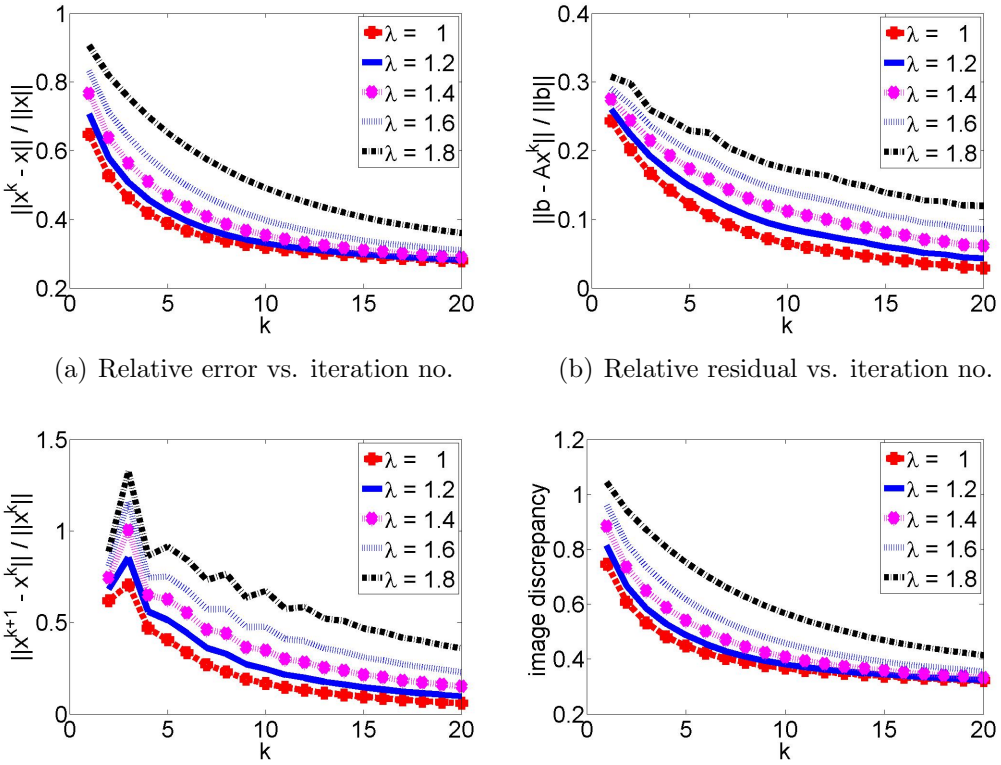

(a) Relative error vs. iteration no.

(b) Relative residual vs. iteration no.

(c) Relative solution difference vs. iteration no.

(d) Image discrepancy vs. iteration no.

Figure A.16: ART(Kaczmarz's method) applied to Shepp-Logan phantom for a 128 $\times$ 128 image and $\lambda = 1, 1.2, .., 1.8$.

In the last iteration,

	min relative error	min relative residual	min relative solution difference	min discrepancy
λ	1	1	1	1

Shepp Logan, Symmetric Kaczmarz, 128×128 **image,** $\lambda = 1, 1.2, .., 1.8$

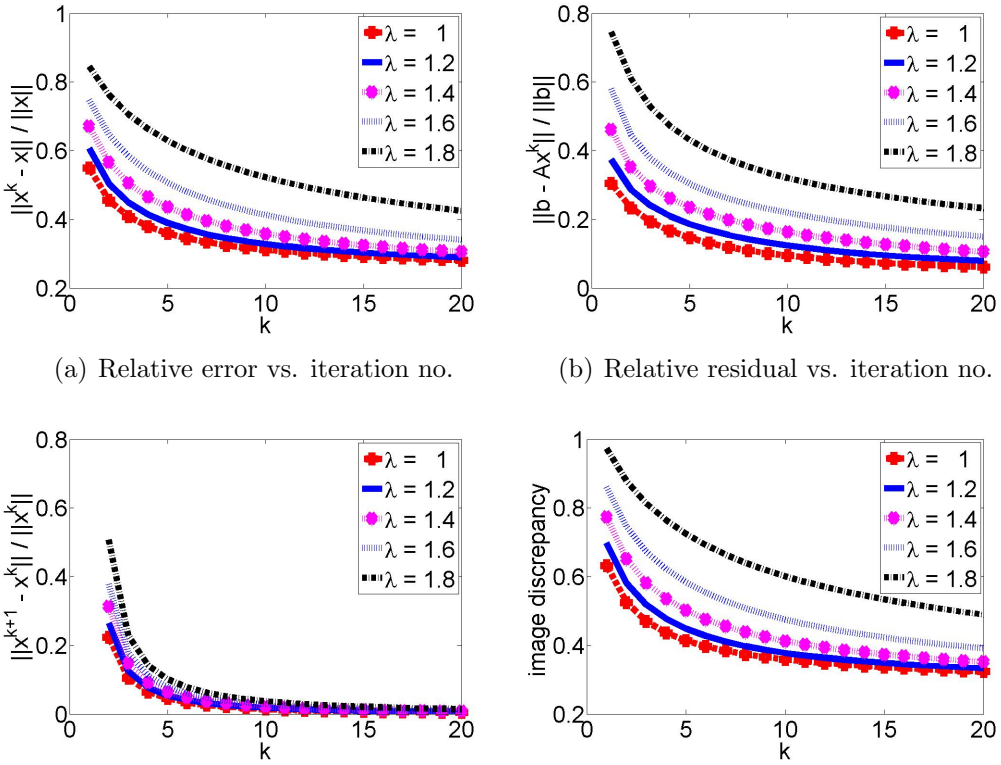

(a) Relative error vs. iteration no.

(b) Relative residual vs. iteration no.

(c) Relative solution difference vs. iteration no.

(d) Image discrepancy vs. iteration no.

Figure A.17: Symmetric Kaczmarz's method applied to Shepp-Logan phantom for a 128×128 image and $\lambda = 1, 1.2, .., 1.8$.

In the last iteration,

	min relative error	min relative residual	min relative solution difference	min discrepancy
λ	1	1	1	1

Shepp Logan, Randomized Kaczmarz, 128×128 **image,** $\lambda = 1, 1.2, .., 1.8$

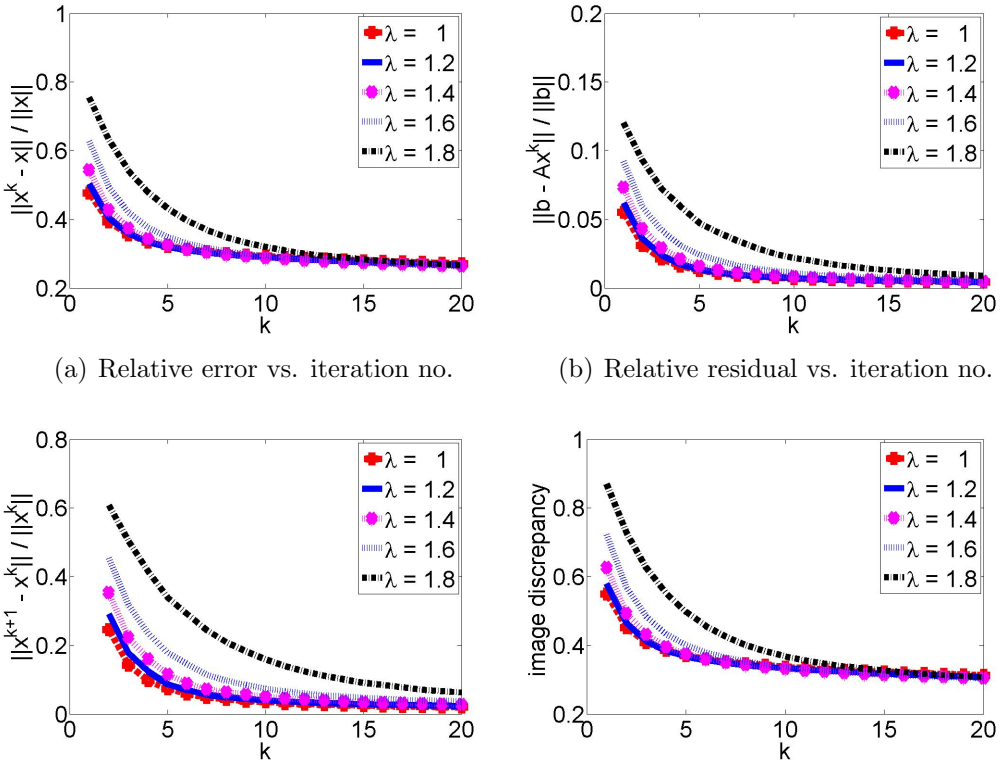

(a) Relative error vs. iteration no.

(b) Relative residual vs. iteration no.

(c) Relative solution difference vs. iteration no.

(d) Image discrepancy vs. iteration no.

Figure A.18: Randomized Kaczmarz's method applied to Shepp-Logan phantom for a 128×128 image and $\lambda = 1, 1.2, .., 1.8$.

In the last iteration,

	min relative error	min relative residual	min relative solution difference	min discrepancy
λ	1	1	1	1.6

Shepp Logan, SART, 128×128 **image,** $\lambda = 1, 1.2, .., 1.8$

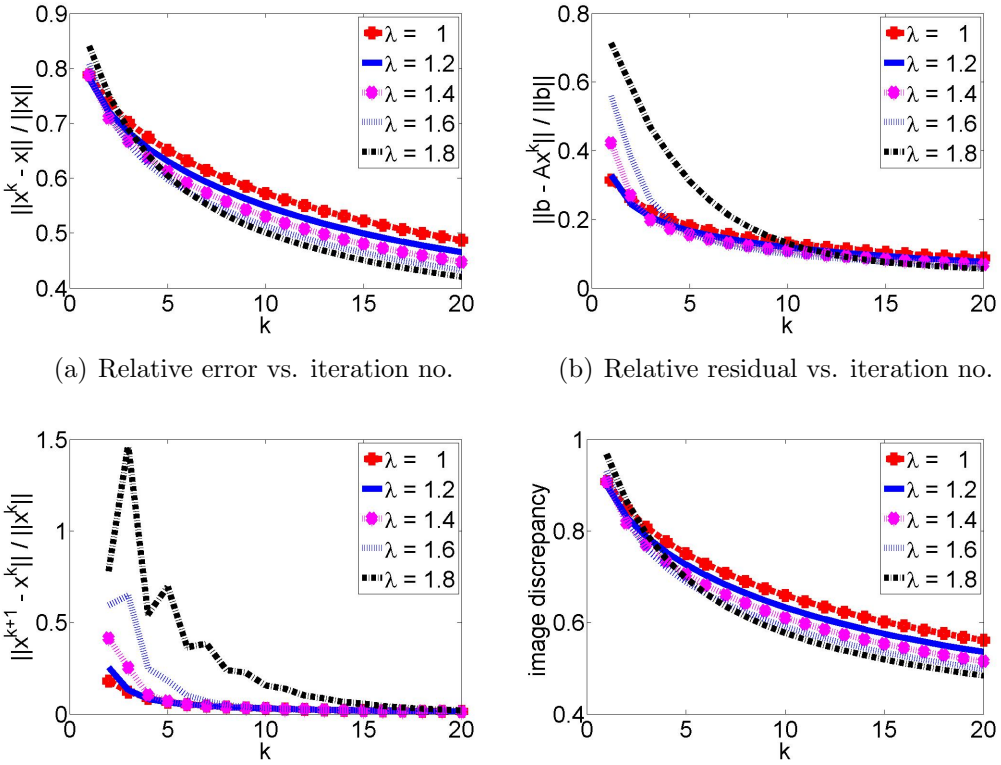

(a) Relative error vs. iteration no.

(b) Relative residual vs. iteration no.

(c) Relative solution difference vs. iteration no.

(d) Image discrepancy vs. iteration no.

Figure A.19: SART method applied to Shepp-Logan phantom for a 128×128 image and $\lambda = 1, 1.2, .., 1.8$.

In the last iteration,

	min relative error	min relative residual	min relative solution difference	min discrepancy
λ	1.8	1.8	1.8	1.8

Shepp Logan, Kaczmarz, 256×256 **image,** $\lambda = 1, 1.2, .., 1.8$

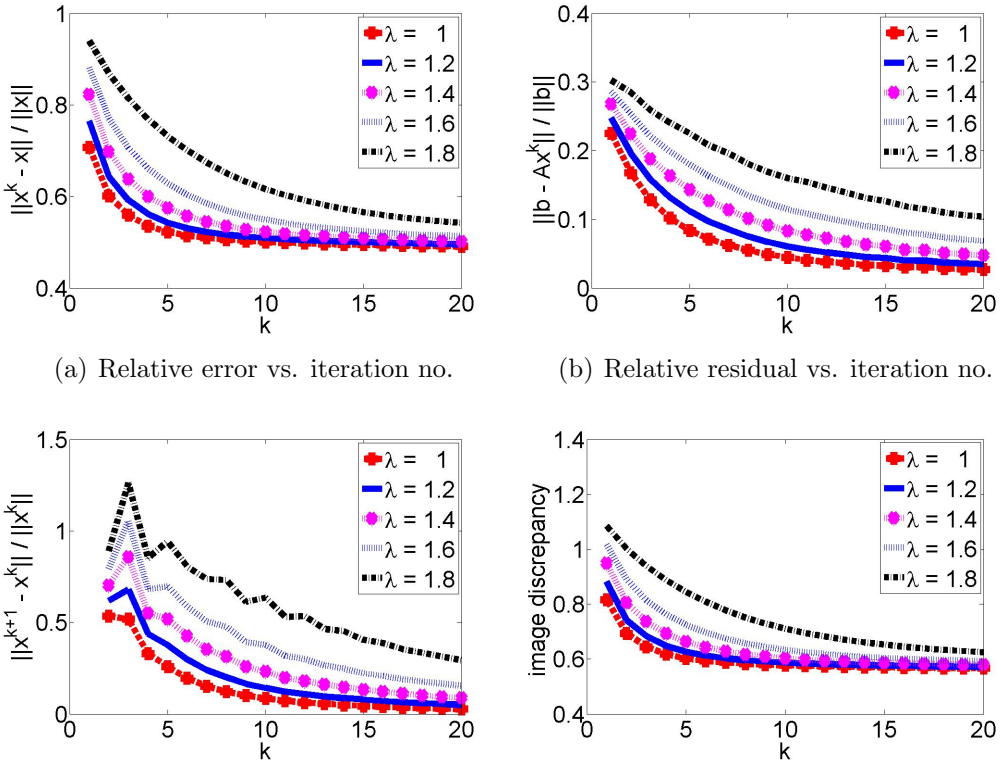

(a) Relative error vs. iteration no.

(b) Relative residual vs. iteration no.

(c) Relative solution difference vs. iteration no.

(d) Image discrepancy vs. iteration no.

Figure A.20: ART(Kaczmarz's method) applied to Shepp-Logan phantom for a 256 $\times$ 256 image and $\lambda = 1, 1.2, .., 1.8$.

In the last iteration,

	min relative error	min relative residual	min relative solution difference	min discrepancy
λ	1	1	1	1

Shepp Logan, Symmetric Kaczmarz, 256×256 **image,** $\lambda = 1, 1.2, .., 1.8$

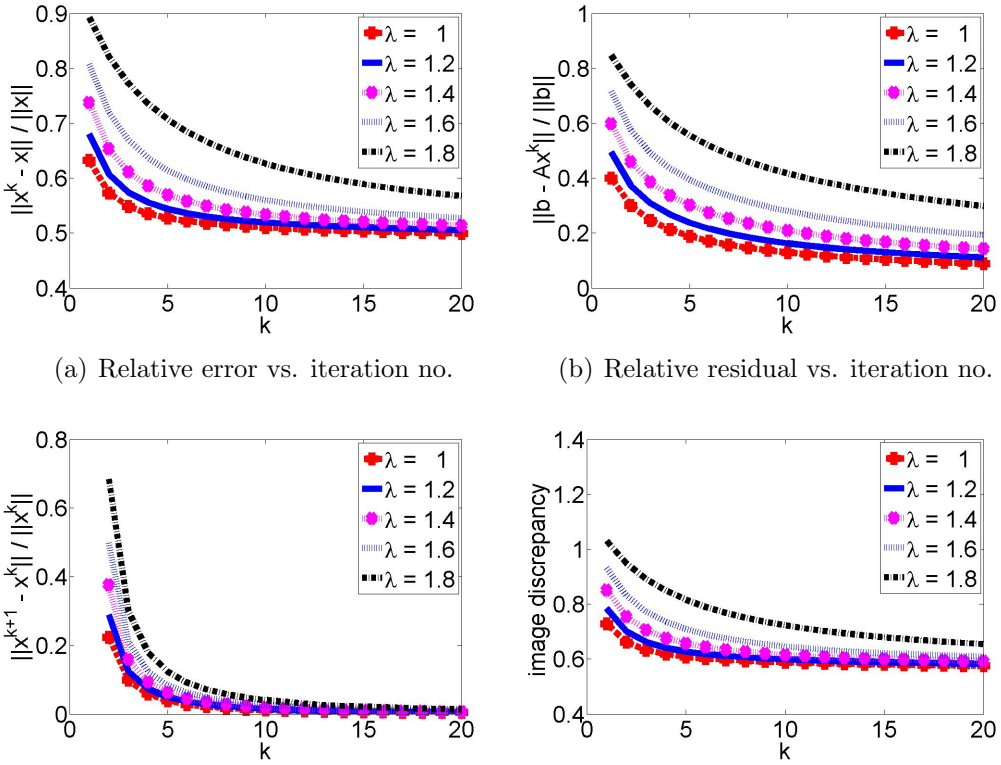

(a) Relative error vs. iteration no.

(b) Relative residual vs. iteration no.

(c) Relative solution difference vs. iteration no.

(d) Image discrepancy vs. iteration no.

Figure A.21: Symmetric Kaczmarz's method applied to Shepp-Logan phantom for a 256×256 image and $\lambda = 1, 1.2, .., 1.8$.

In the last iteration,

	min relative error	min relative residual	min relative solution difference	min discrepancy
λ	1	1	1	1

Shepp Logan, Randomized Kaczmarz, 256×256 **image,** $\lambda = 1, 1.2, .., 1.8$

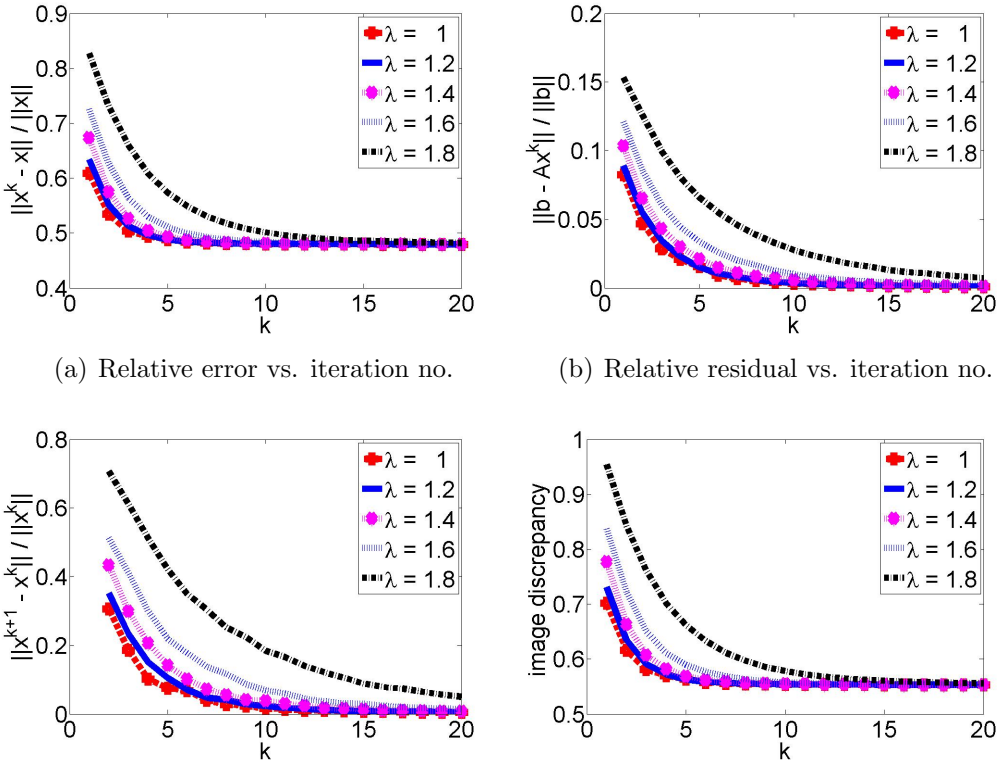

(a) Relative error vs. iteration no.

(b) Relative residual vs. iteration no.

(c) Relative solution difference vs. iteration no.

(d) Image discrepancy vs. iteration no.

Figure A.22: Randomized Kaczmarz's method applied to Shepp-Logan phantom for a 256×256 image and $\lambda = 1, 1.2, .., 1.8$.

In the last iteration,

	min relative error	min relative residual	min relative solution difference	min discrepancy
λ	1	1	1	1

Shepp Logan, SART, 256×256 **image,** $\lambda = 1, 1.2, .., 1.8$

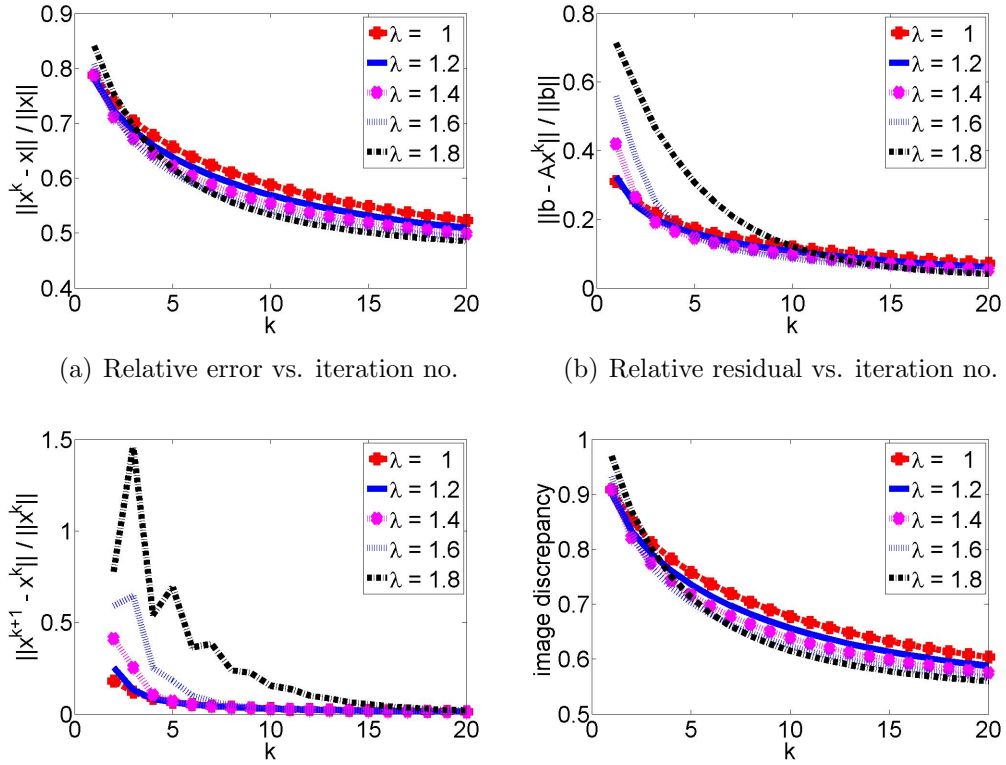

(a) Relative error vs. iteration no.

(b) Relative residual vs. iteration no.

(c) Relative solution difference vs. iteration no.

(d) Image discrepancy vs. iteration no.

Figure A.23: SART method applied to Shepp-Logan phantom for a 256×256 image and $\lambda = 1, 1.2, .., 1.8$.

In the last iteration,

	min relative error	min relative residual	min relative solution difference	min discrepancy
λ	1.8	1.8	1.8	1.8

Shepp Logan, Kaczmarz, 512×512 **image,** $\lambda = 1, 1.2, .., 1.8$

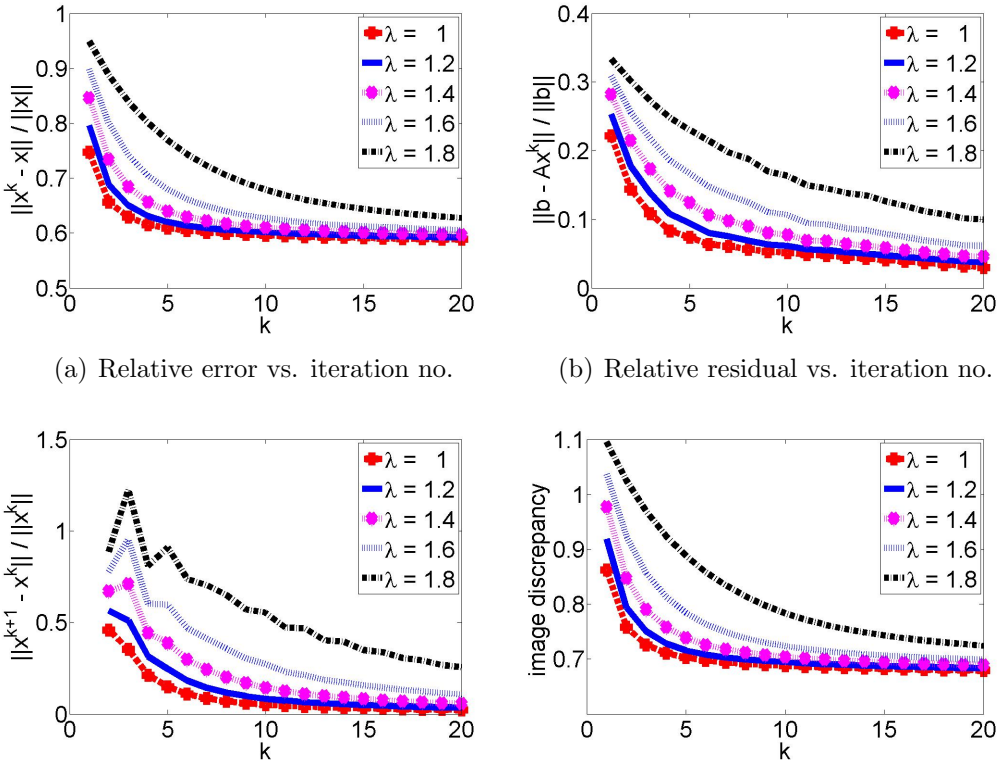

(a) Relative error vs. iteration no.

(b) Relative residual vs. iteration no.

(c) Relative solution difference vs. iteration no.

(d) Image discrepancy vs. iteration no.

Figure A.24: ART(Kaczmarz's method) applied to Shepp-Logan phantom for a 512 $\times$ 512 image and $\lambda = 1, 1.2, .., 1.8$.

In the last iteration,

	min relative error	min relative residual	min relative solution difference	min discrepancy
λ	1	1	1	1

Shepp Logan, Symmetric Kaczmarz, 512×512 **image,** $\lambda = 1, 1.2, .., 1.8$

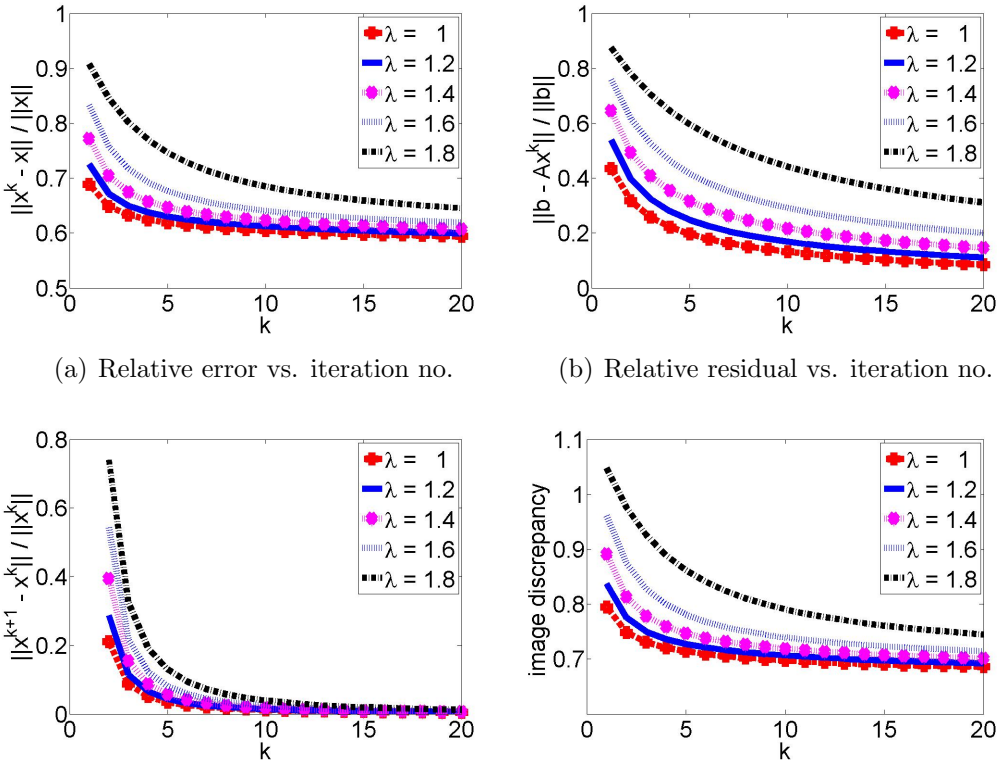

(a) Relative error vs. iteration no.

(b) Relative residual vs. iteration no.

(c) Relative solution difference vs. iteration no.

(d) Image discrepancy vs. iteration no.

Figure A.25: Symmetric Kaczmarz's method applied to Shepp-Logan phantom for a 512×512 image and $\lambda = 1, 1.2, .., 1.8$.

In the last iteration,

	min relative error	min relative residual	min relative solution difference	min discrepancy
λ	1	1	1	1

Shepp Logan, Randomized Kaczmarz, 512×512 **image,** $\lambda = 1, 1.2, .., 1.8$

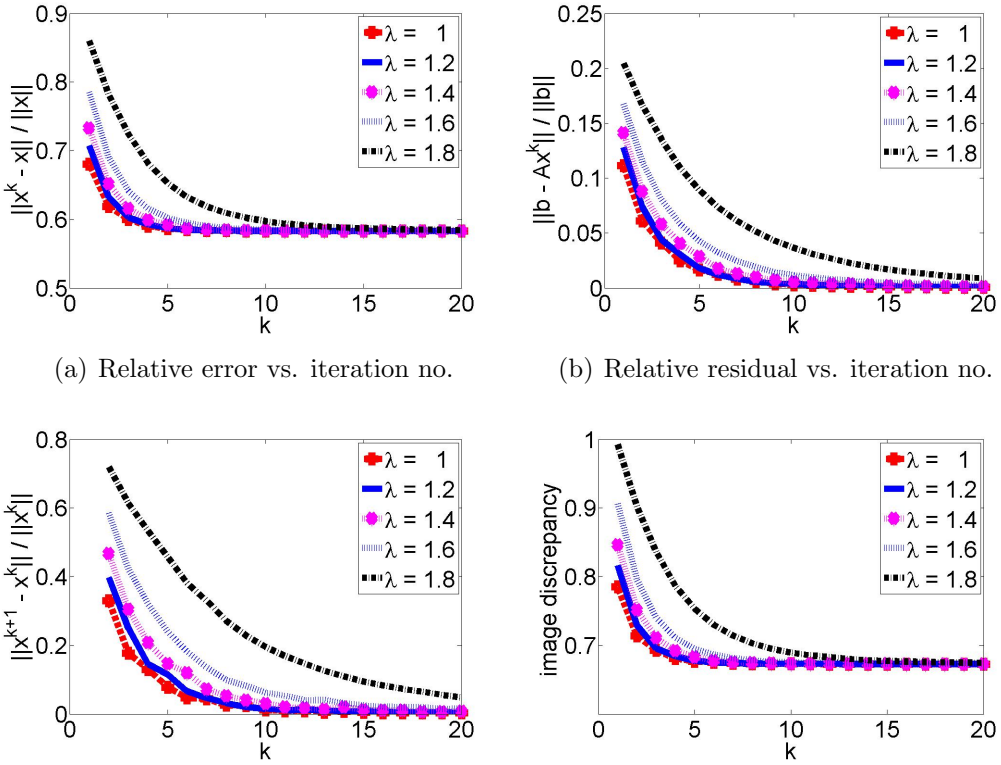

(a) Relative error vs. iteration no.

(b) Relative residual vs. iteration no.

(c) Relative solution difference vs. iteration no.

(d) Image discrepancy vs. iteration no.

Figure A.26: Randomized Kaczmarz's method applied to Shepp-Logan phantom for a 512×512 image and $\lambda = 1, 1.2, .., 1.8$.

In the last iteration,

	min relative error	min relative residual	min relative solution difference	min discrepancy
λ	1	1	1	1

Shepp Logan, SART, 512×512 **image,** $\lambda = 1, 1.2, .., 1.8$

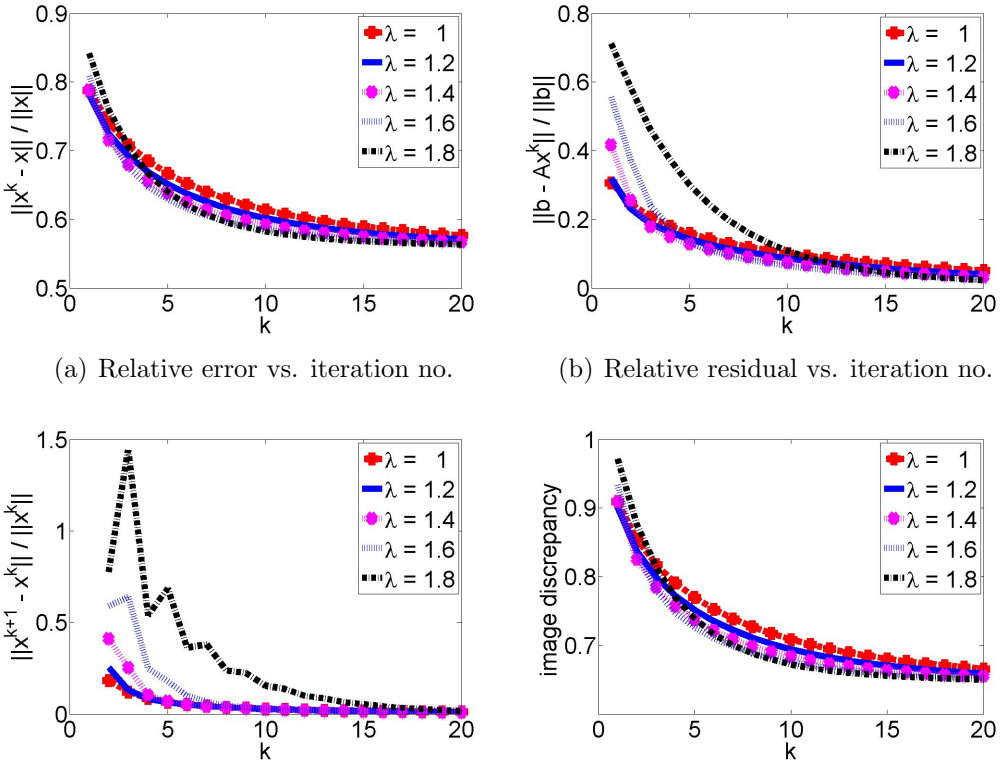

(a) Relative error vs. iteration no.

(b) Relative residual vs. iteration no.

(c) Relative solution difference vs. iteration no.

(d) Image discrepancy vs. iteration no.

Figure A.27: SART method applied to Shepp-Logan phantom for a 512×512 image and $\lambda = 1, 1.2, .., 1.8$.

In the last iteration,

	min relative error	min relative residual	min relative solution difference	min discrepancy
λ	1.8	1.8	1.8	1.8

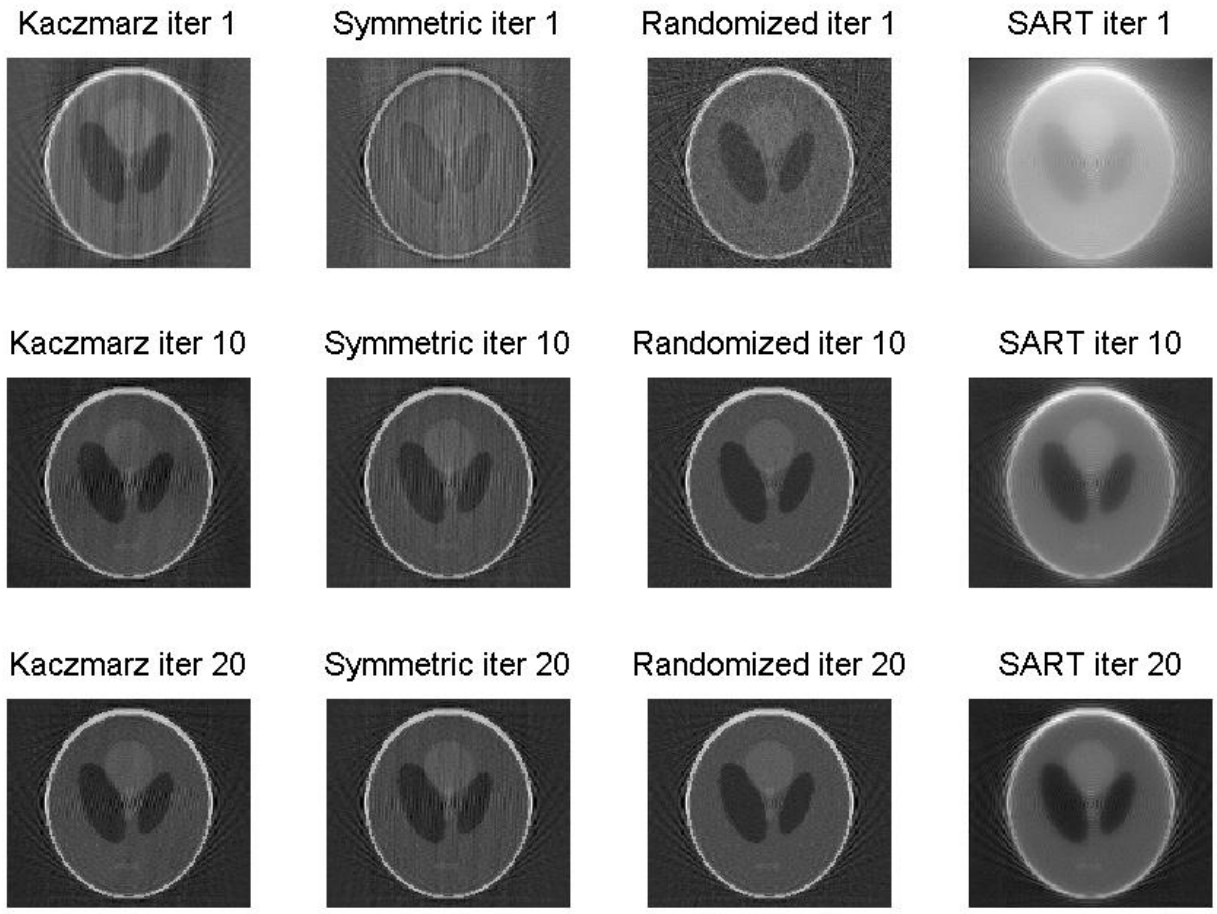

Figure A.28: Reconstruction of the 128×128 Shepp-Logan Phantom using Kaczmarz, Symmetric Kaczmarz, Randomized Kaczmarz and SART ($\lambda = 1.2$).

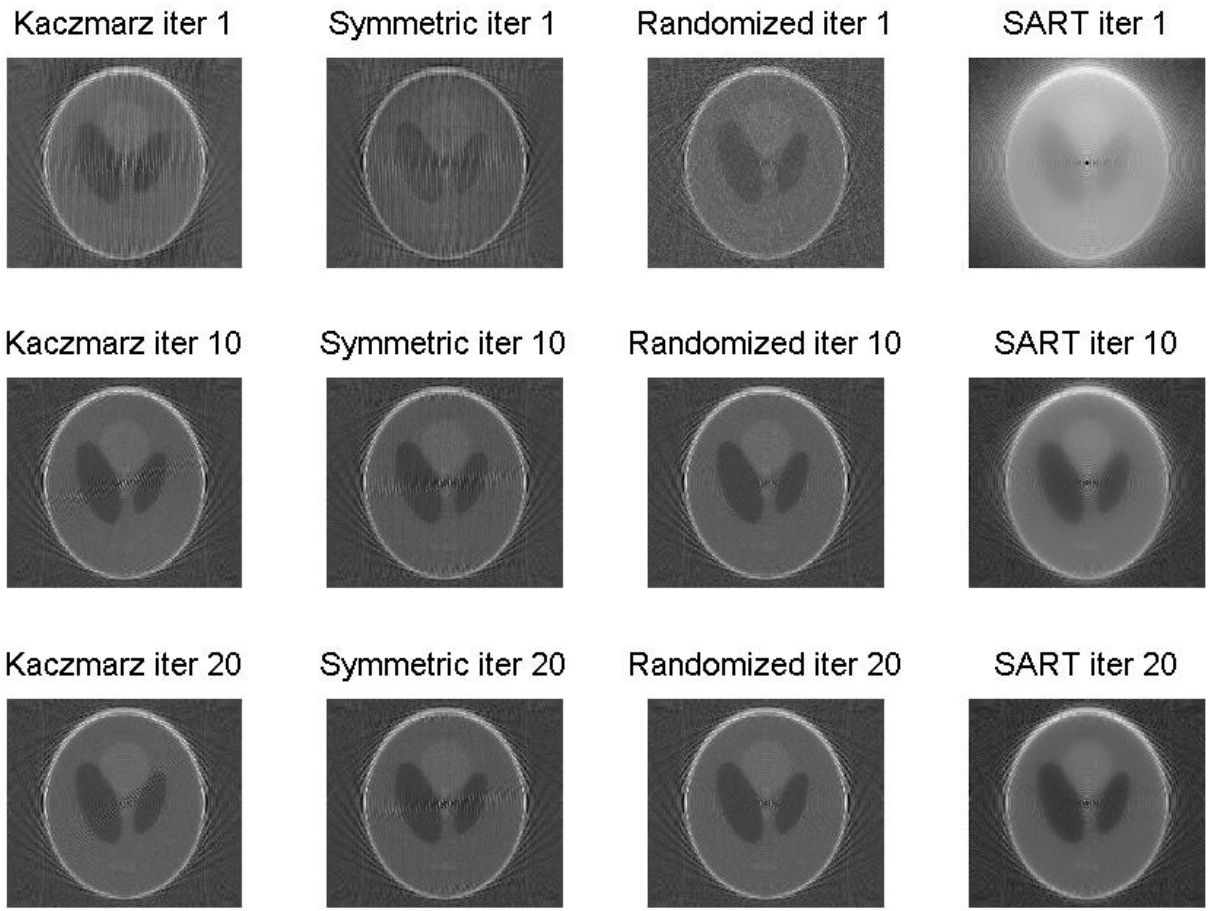

Figure A.29: Reconstruction of the 256×256 Shepp-Logan Phantom using Kaczmarz, Symmetric Kaczmarz, Randomized Kaczmarz and SART ($\lambda = 1.2$).

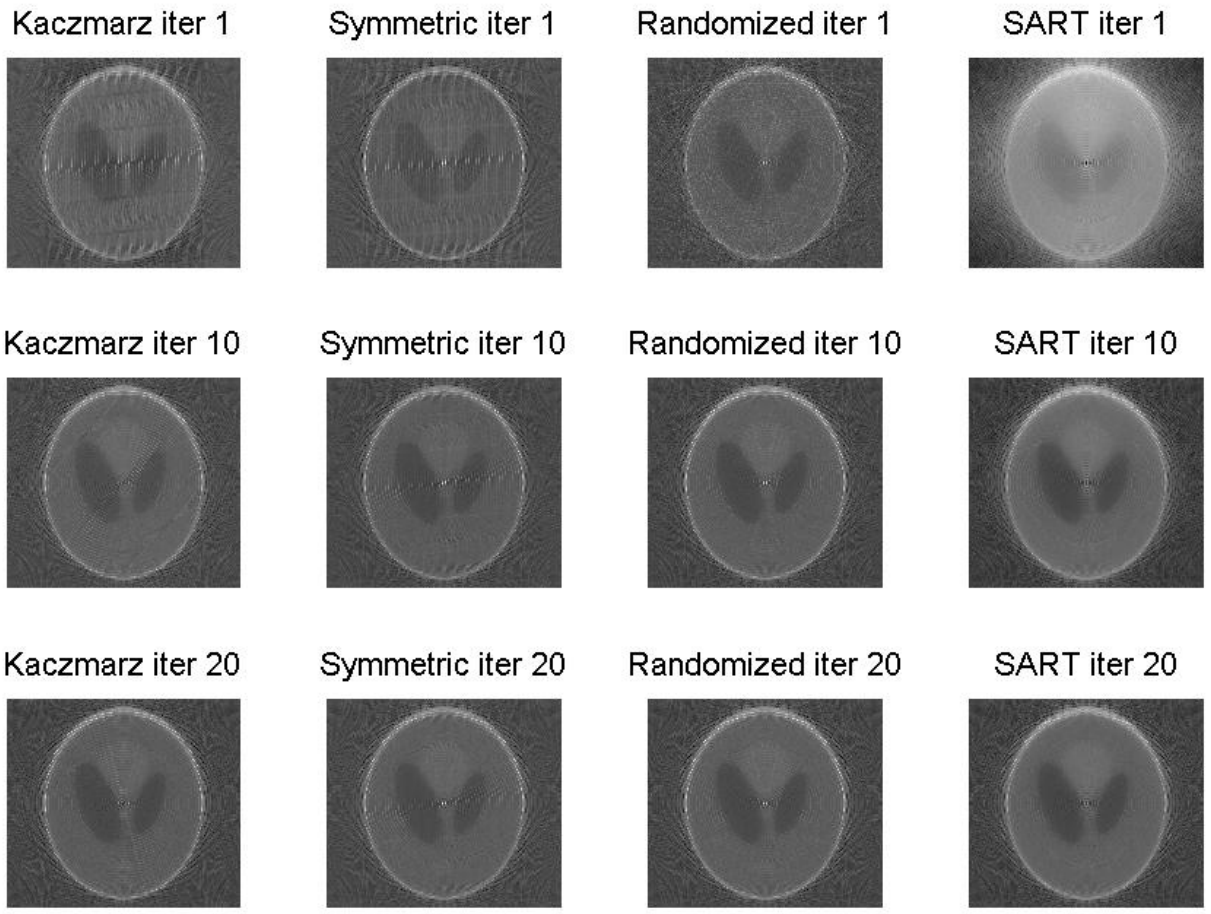

Figure A.30: Reconstruction of the 512×512 Shepp-Logan Phantom using Kaczmarz, Symmetric Kaczmarz, Randomized Kaczmarz and SART ($\lambda = 1.2$).

size	method	worst λ	max discrepancy	best λ	min discrepancy	time/iter(s)
128	Kacz.	1.8	0.4144	1	0.3209	9.14
	Symm.	1.8	0.4893	1	0.3234	18.46
	Rand.	1	0.3125	1.6	0.3041	13.56
	SART	1	0.5608	1.8	0.4839	0.02
256	Kacz.	1.8	0.6249	1	0.5666	32.87
	Symm.	1.8	0.6546	1	0.5760	62.71
	Rand.	1.8	0.5559	1	0.5532	34.63
	SART	1	0.6036	1.8	0.5595	0.05
512	Kacz.	1.8	0.7243	1	0.6795	205.38
	Symm.	1.8	0.7449	1	0.6862	454.46
	Rand.	1.8	0.6743	1	0.6727	212.17
	SART	1	0.6658	1.8	0.6502	0.24

Table A.2: Experimental results of applying different methods to Shepp-Logan phantom using relaxation parameters of $\lambda = 1, 1.2, .., 1.8$ for 20 number of iterations.

The experimental results shown in Table A.2 are obtained from the Colsher's discrepancy measurement method [4] in such a way that, after applying different ART methods to different phantom sizes, for $\lambda = 1, 1.2, .., 1.8$, the minimum and the maximum discrepancies, which indicate the best and the worst relaxation parameters, are found in iteration number 20.

As it can be seen, the results for the overdetermined system corresponding to 128×128 Shepp-Logan phantom, when Randomized Kaczmarz's method is applied, are different from the results achieved for two underdetermined systems corresponding to 256×256 and 512×512 Shepp-Logan phantom image sizes. It is obvious that the results for both underdetermined systems follow the same pattern for their best and worst relaxation parameters, for various image reconstruction techniques.

Appendix B

Experimental Results on MRI Knee Test Phantom

Experimental results, obtained by applying Kaczmarz's, Symmetric Kaczmarz's, Randomized Kaczmarz's and SART methods to an overdetermined system corresponding to 128×128 image size and two underdetermined system corresponding to 256×256 and 512×512 MRI Knee phantom image sizes, are plotted in Figures B.31–B.34, B.35–B.38 and B.39–B.42, respectively. The results in these Figures B.31–B.42 are computed for relaxation parameters, $\lambda = 0.2, 0.4, .., 1$, for 20 iterations.

Reconstructed images of 128×128, 256×256 and 512×512 MRI Knee phantoms using Kaczmarz, Symmetric Kaczmarz, Randomized Kaczmarz and SART for relaxation parameter $\lambda = 0.4$ are given in Figures B.43, B.44 and B.45, respectively for three different iterations.

Consecutively, to compute numerical results for other relaxation parameters,

$\lambda = 1, 1.2, .., 1.8$, for 20 iterations, we have applied these methods to overdetermined system corresponding to 128×128 image size and underdetermined systems corresponding to 256×256 and 512×512 MRI Knee phantom image sizes. The plots are shown in Figures B.46–B.49, B.50–B.53 and B.54–B.57, respectively. Related Reconstructed images of 128×128, 256×256 and 512×512 MRI Knee phantoms using Kaczmarz, Symmetric Kaczmarz, Randomized Kaczmarz and SART for relaxation parameter $\lambda = 1.2$ are represented in Figures B.58, B.59 and B.60, respectively for three different iterations.

Knee, Kaczmarz, 128×128 **image,** $\lambda = 0.2, 0.4, .., 1$

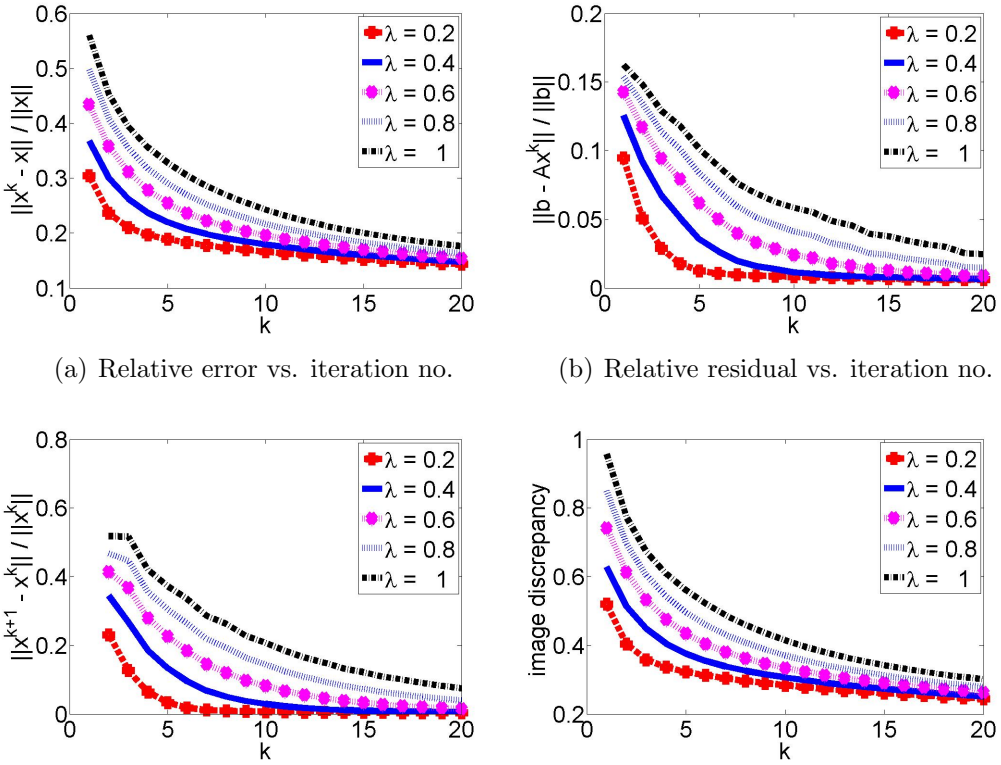

(a) Relative error vs. iteration no.

(b) Relative residual vs. iteration no.

(c) Relative solution difference vs. iteration no.

(d) Image discrepancy vs. iteration no.

Figure B.31: ART(Kaczmrarz's method) applied to MRI Knee Phantom for a 128×128 image and $\lambda = 0.2, 0.4, .., 1$.

In the last iteration,

	min relative error	min relative residual	min relative solution difference	min discrepancy
λ	0.2	0.2	0.2	0.2

Knee, Symmetric Kaczmarz, 128×128 **image,** $\lambda = 0.2, 0.4, .., 1$

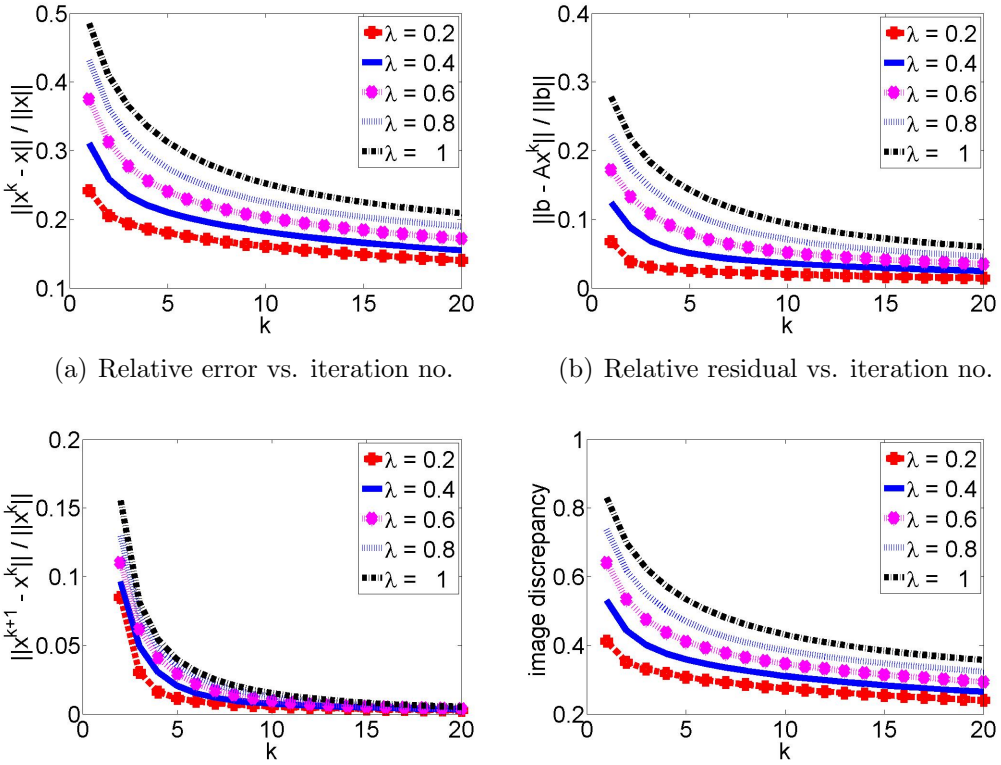

(a) Relative error vs. iteration no.

(b) Relative residual vs. iteration no.

(c) Relative solution difference vs. iteration no.

(d) Image discrepancy vs. iteration no.

Figure B.32: Symmetric Kaczmarz's method applied to MRI Knee Phantom for a 128×128 image and $\lambda = 0.2, 0.4, .., 1$.

In the last iteration,

	min relative error	min relative residual	min relative solution difference	min discrepancy
λ	0.2	0.2	0.2	0.2

Knee, Randomized Kaczmarz, 128×128 **image,** $\lambda = 0.2, 0.4, .., 1$

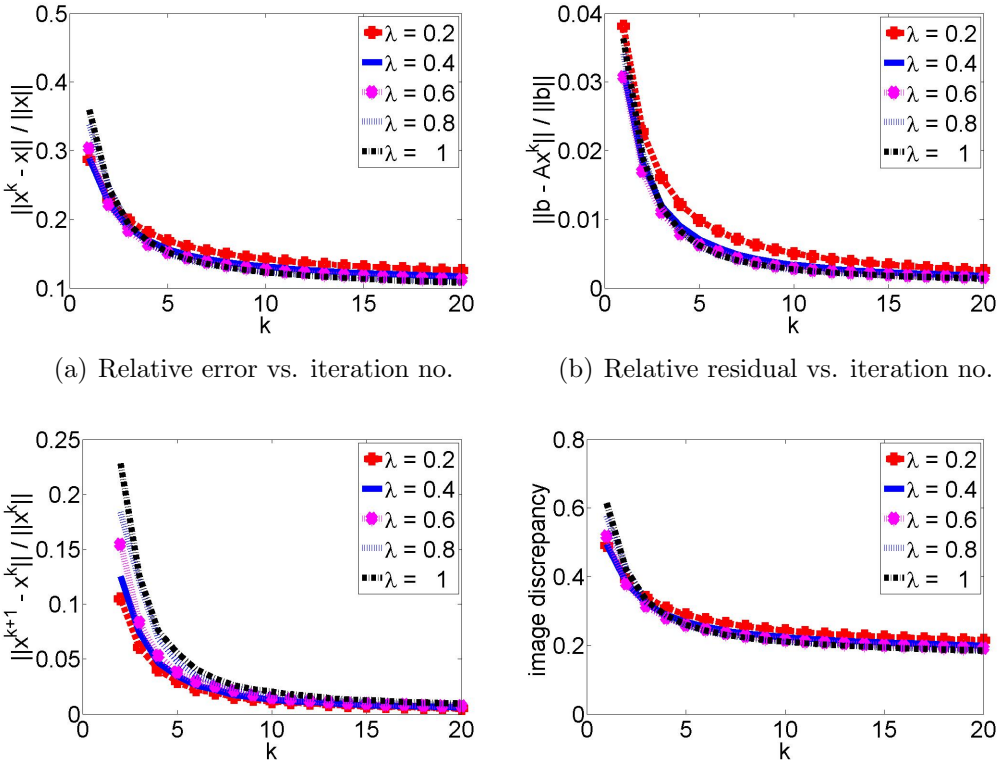

(a) Relative error vs. iteration no.

(b) Relative residual vs. iteration no.

(c) Relative solution difference vs. iteration no.

(d) Image discrepancy vs. iteration no.

Figure B.33: Randomized Kaczmarz's method applied to MRI Knee Phantom for a 128×128 image and $\lambda = 0.2, 0.4, .., 1$.

In the last iteration,

	min relative error	min relative residual	min relative solution difference	min discrepancy
λ	1	1	0.2	1

Knee, SART, 128×128 **image,** $\lambda = 0.2, 0.4, .., 1$

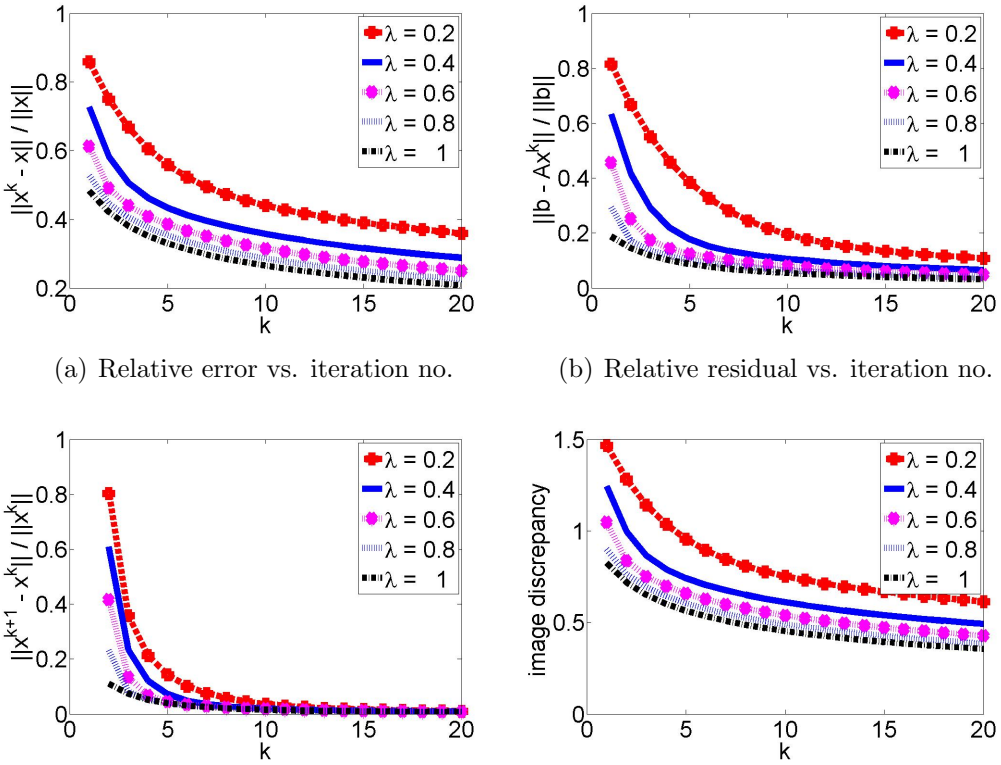

(a) Relative error vs. iteration no.

(b) Relative residual vs. iteration no.

(c) Relative solution difference vs. iteration no.

(d) Image discrepancy vs. iteration no.

Figure B.34: SART method applied to MRI Knee Phantom for a 128×128 image and $\lambda = 0.2, 0.4, .., 1$.

In the last iteration,

	min relative error	min relative residual	min relative solution difference	min discrepancy
λ	1	1	1	1

Knee, Kaczmrarz, 256×256 **image,** $\lambda = 0.2, 0.4, .., 1$

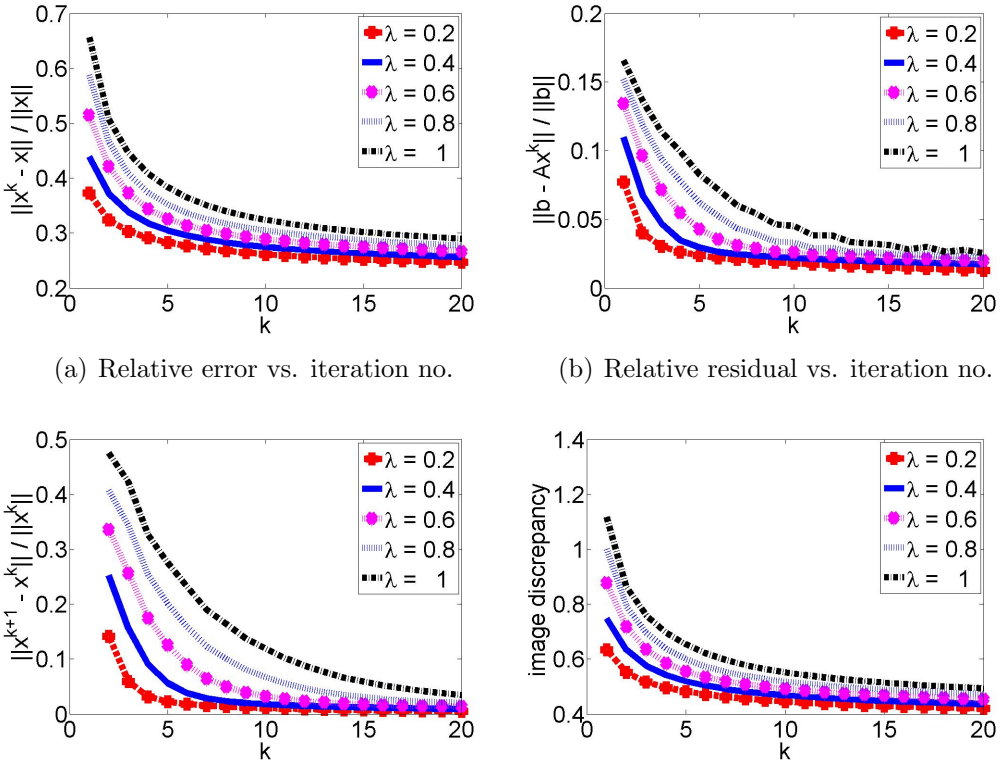

(a) Relative error vs. iteration no.

(b) Relative residual vs. iteration no.

(c) Relative solution difference vs. iteration no.

(d) Image discrepancy vs. iteration no.

Figure B.35: ART(Kaczmrarz's method) applied to MRI Knee Phantom for a 256×256 image and $\lambda = 0.2, 0.4, .., 1$.

In the last iteration,

	min relative error	min relative residual	min relative solution difference	min discrepancy
λ	0.2	0.2	0.2	0.2

Knee, Symmetric Kaczmrarz, 256×256 **image,** $\lambda = 0.2, 0.4, .., 1$

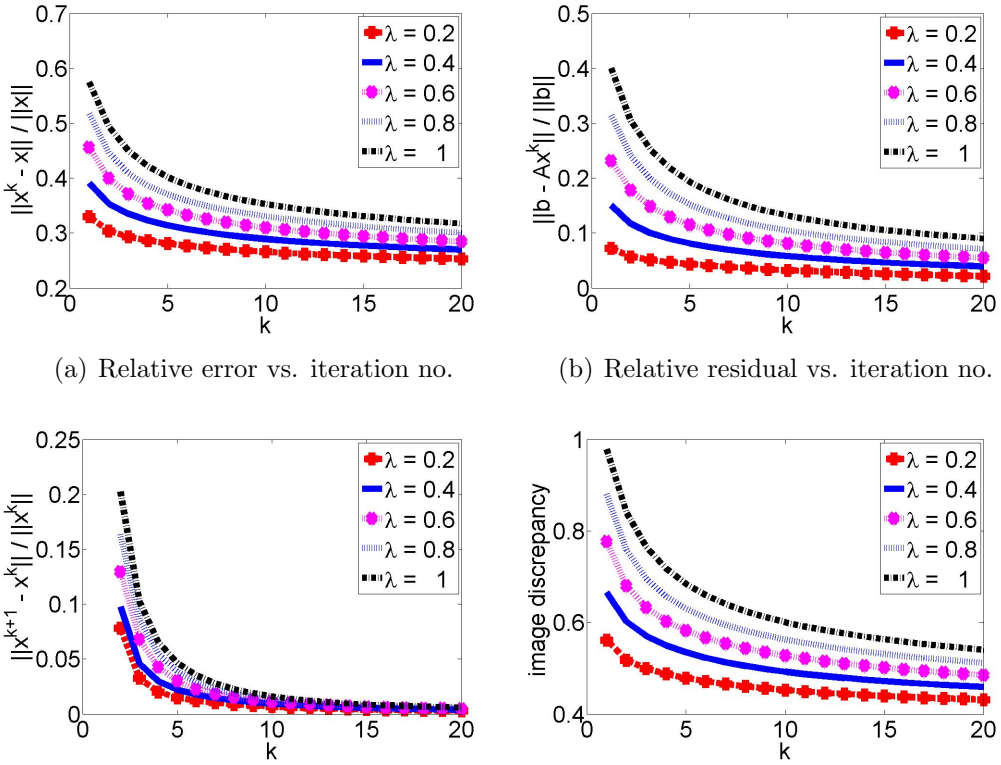

(a) Relative error vs. iteration no.

(b) Relative residual vs. iteration no.

(c) Relative solution difference vs. iteration no.

(d) Image discrepancy vs. iteration no.

Figure B.36: Symmetric Kaczmarz's method applied to MRI Knee Phantom for a 256×256 image and $\lambda = 0.2, 0.4, .., 1$.

In the last iteration,

	min relative error	min relative residual	min relative solution difference	min discrepancy
λ	0.2	0.2	0.2	0.2

Knee, Randomized Kaczmrarz, 256×256 **image,** $\lambda = 0.2, 0.4, .., 1$

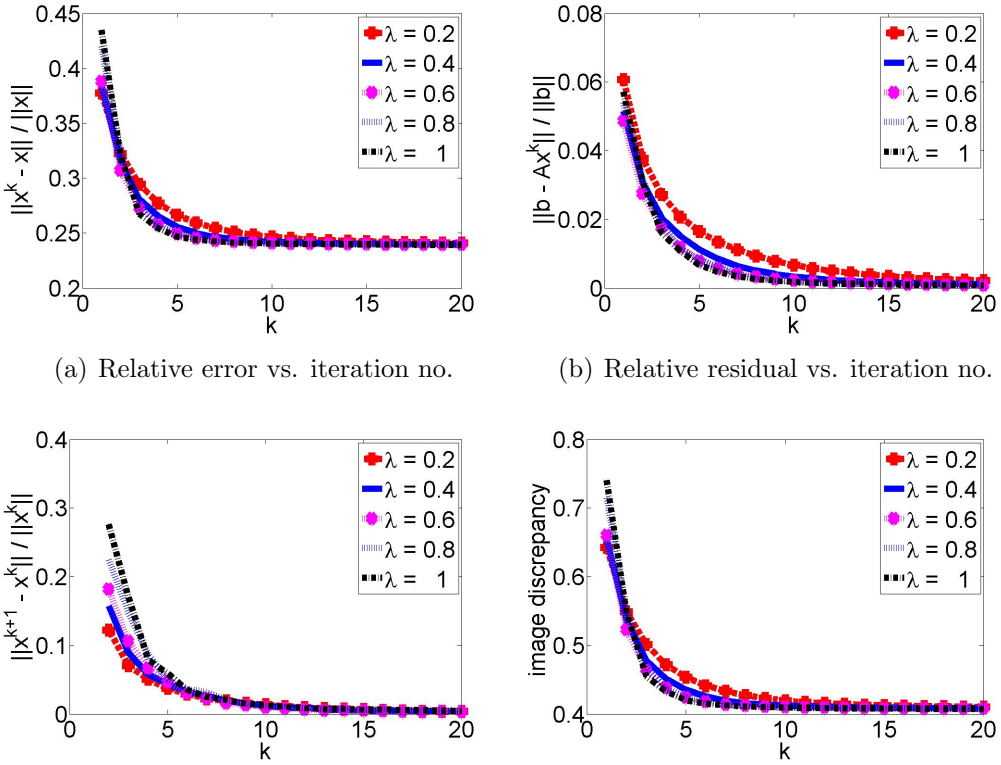

(a) Relative error vs. iteration no.

(b) Relative residual vs. iteration no.

(c) Relative solution difference vs. iteration no.

(d) Image discrepancy vs. iteration no.

Figure B.37: Randomized Kaczmarz's method applied to MRI Knee Phantom for a 256×256 image and $\lambda = 0.2, 0.4, .., 1$.

In the last iteration,

	min relative error	min relative residual	min relative solution difference	min discrepancy
λ	1	1	1	1

Knee, SART, 256×256 **image,** $\lambda = 0.2, 0.4, .., 1$

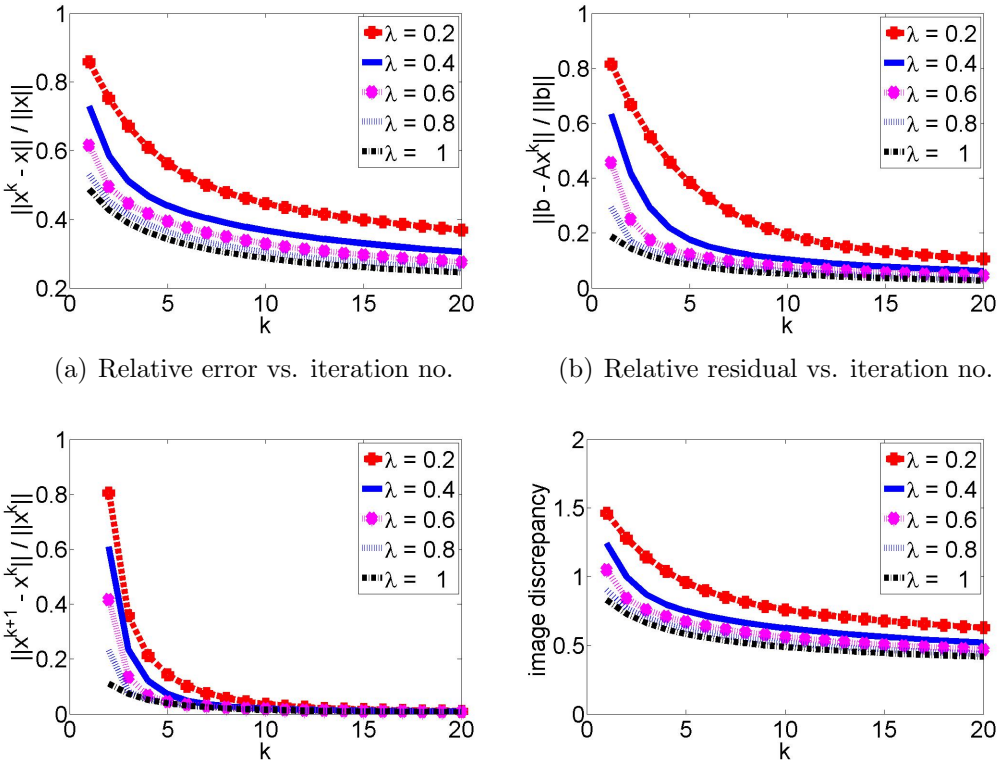

(a) Relative error vs. iteration no.

(b) Relative residual vs. iteration no.

(c) Relative solution difference vs. iteration no.

(d) Image discrepancy vs. iteration no.

Figure B.38: SART method applied to MRI Knee Phantom for a 256×256 image and $\lambda = 0.2, 0.4, .., 1$.

In the last iteration,

	min relative error	min relative residual	min relative solution difference	min discrepancy
λ	1	1	1	1

Knee, Kaczmrarz, 512×512 **image,** $\lambda = 0.2, 0.4, .., 1$

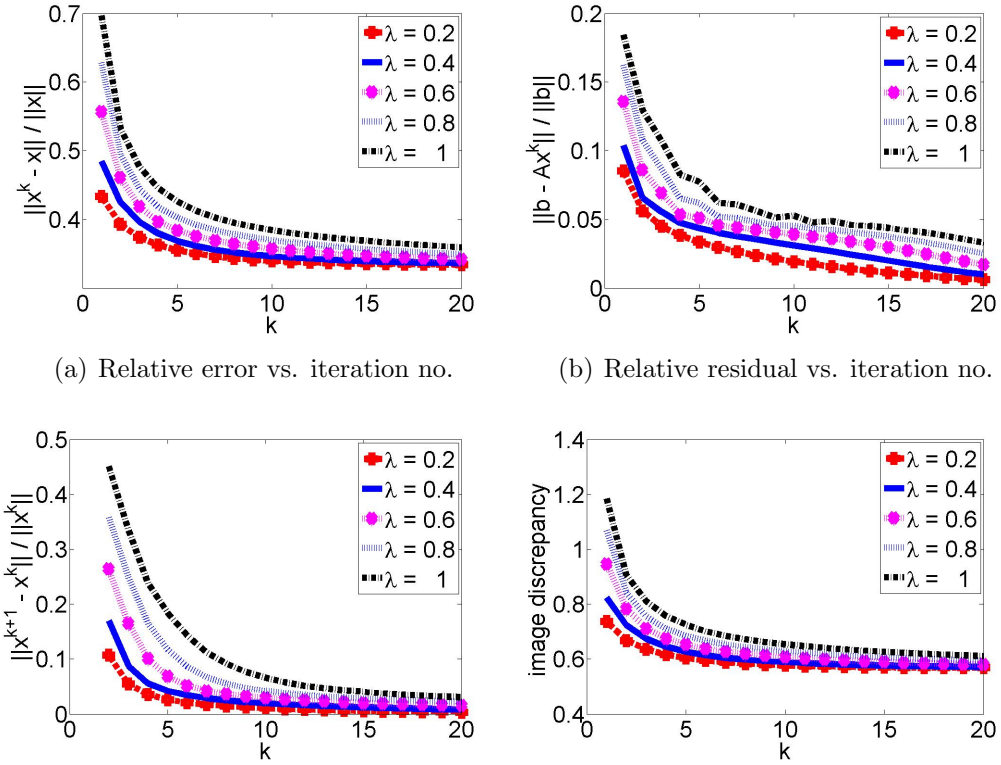

(a) Relative error vs. iteration no.

(b) Relative residual vs. iteration no.

(c) Relative solution difference vs. iteration no.

(d) Image discrepancy vs. iteration no.

Figure B.39: ART(Kaczmrarz's method) applied to MRI Knee Phantom for a 512×512 image and $\lambda = 0.2, 0.4, .., 1$.

In the last iteration,

	min relative error	min relative residual	min relative solution difference	min discrepancy
λ	0.2	0.2	0.2	0.2

Knee, Symmetric Kaczmarz, 512×512 **image,** $\lambda = 0.2, 0.4, .., 1$

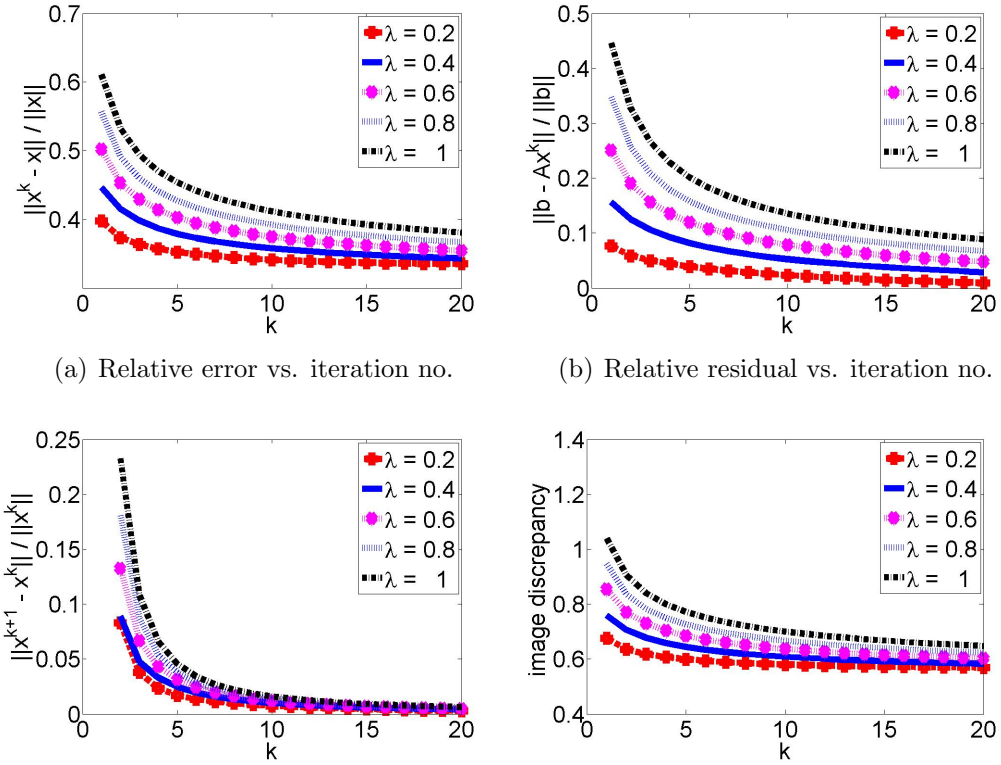

(a) Relative error vs. iteration no.

(b) Relative residual vs. iteration no.

(c) Relative solution difference vs. iteration no.

(d) Image discrepancy vs. iteration no.

Figure B.40: Symmetric Kaczmarz's method applied to MRI Knee Phantom for a 512×512 image and $\lambda = 0.2, 0.4, .., 1$.

In the last iteration,

	min relative error	min relative residual	min relative solution difference	min discrepancy
λ	0.2	0.2	0.2	0.2

Knee, Randomized Kaczmarz, 512×512 **image,** $\lambda = 0.2, 0.4, .., 1$

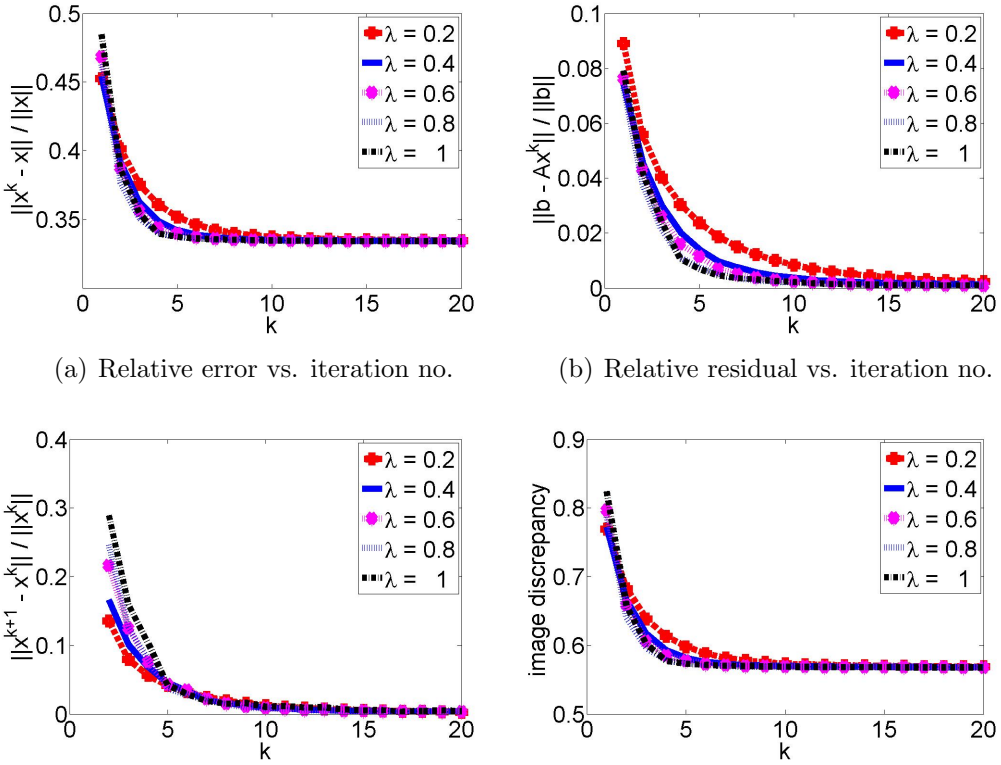

(a) Relative error vs. iteration no.

(b) Relative residual vs. iteration no.

(c) Relative solution difference vs. iteration no.

(d) Image discrepancy vs. iteration no.

Figure B.41: Randomized Kaczmarz's method applied to MRI Knee Phantom for a 512×512 image and $\lambda = 0.2, 0.4, .., 1$.

In the last iteration,

	min relative error	min relative residual	min relative solution difference	min discrepancy
λ	1	1	1	1

Knee, SART, 512×512 **image,** $\lambda = 0.2, 0.4, .., 1$

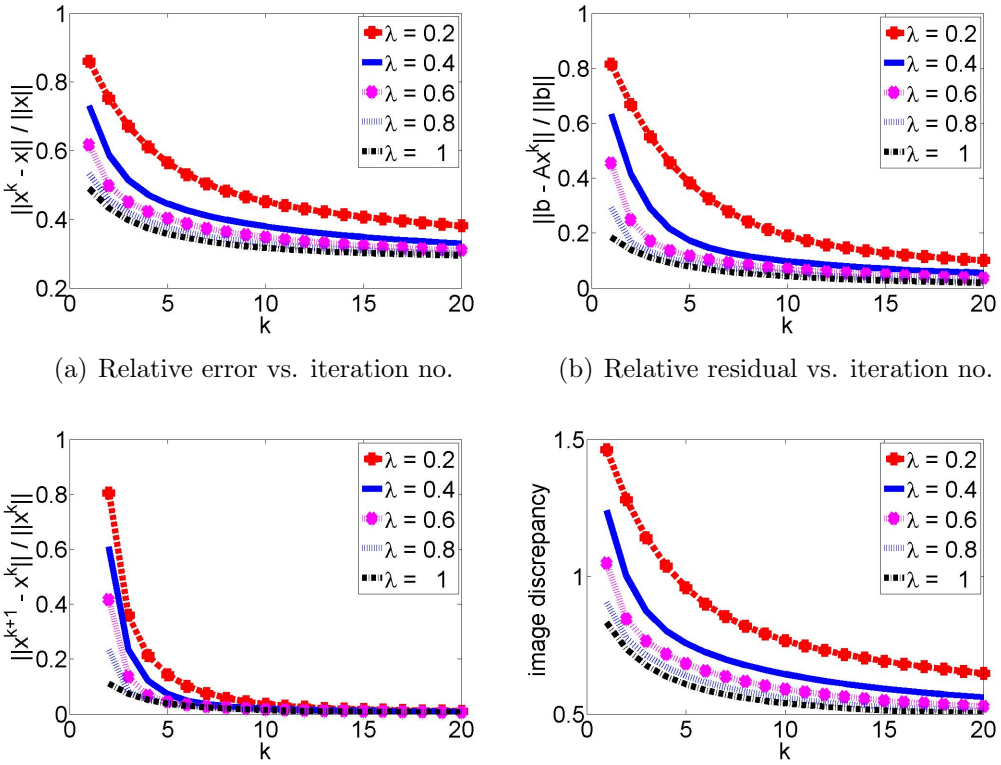

(a) Relative error vs. iteration no.

(b) Relative residual vs. iteration no.

(c) Relative solution difference vs. iteration no.

(d) Image discrepancy vs. iteration no.

Figure B.42: SART method applied to MRI Knee Phantom for a 512×512 image and $\lambda = 0.2, 0.4, .., 1$.

In the last iteration,

	min relative error	min relative residual	min relative solution difference	min discrepancy
λ	1	1	1	1

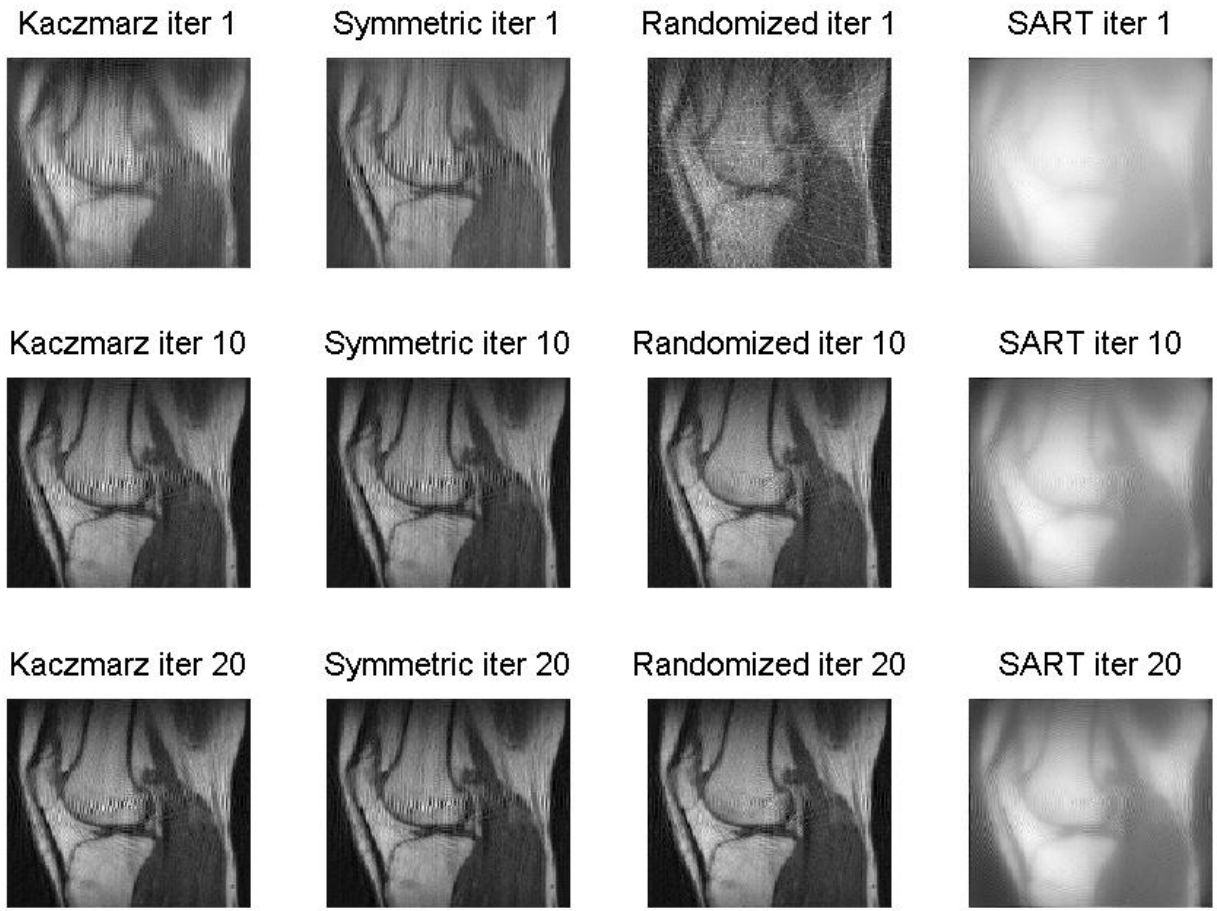

Figure B.43: Reconstruction of the 128×128 MRI Knee Phantom using Kaczmarz, Symmetric Kaczmarz, Randomized Kaczmarz and SART ($\lambda = 0.4$).

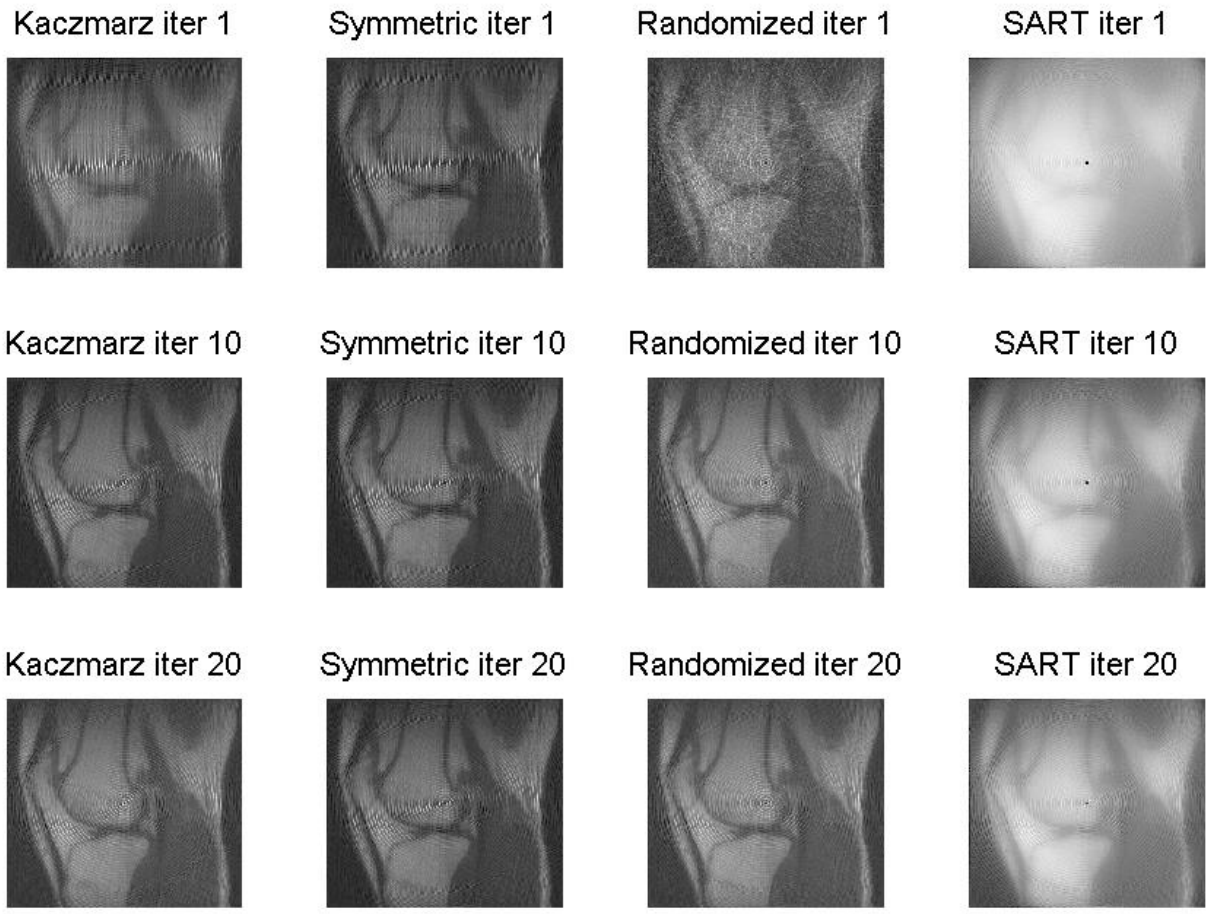

Figure B.44: Reconstruction of the 256×256 MRI Knee Phantom using Kaczmarz, Symmetric Kaczmarz, Randomized Kaczmarz and SART ($\lambda = 0.4$).

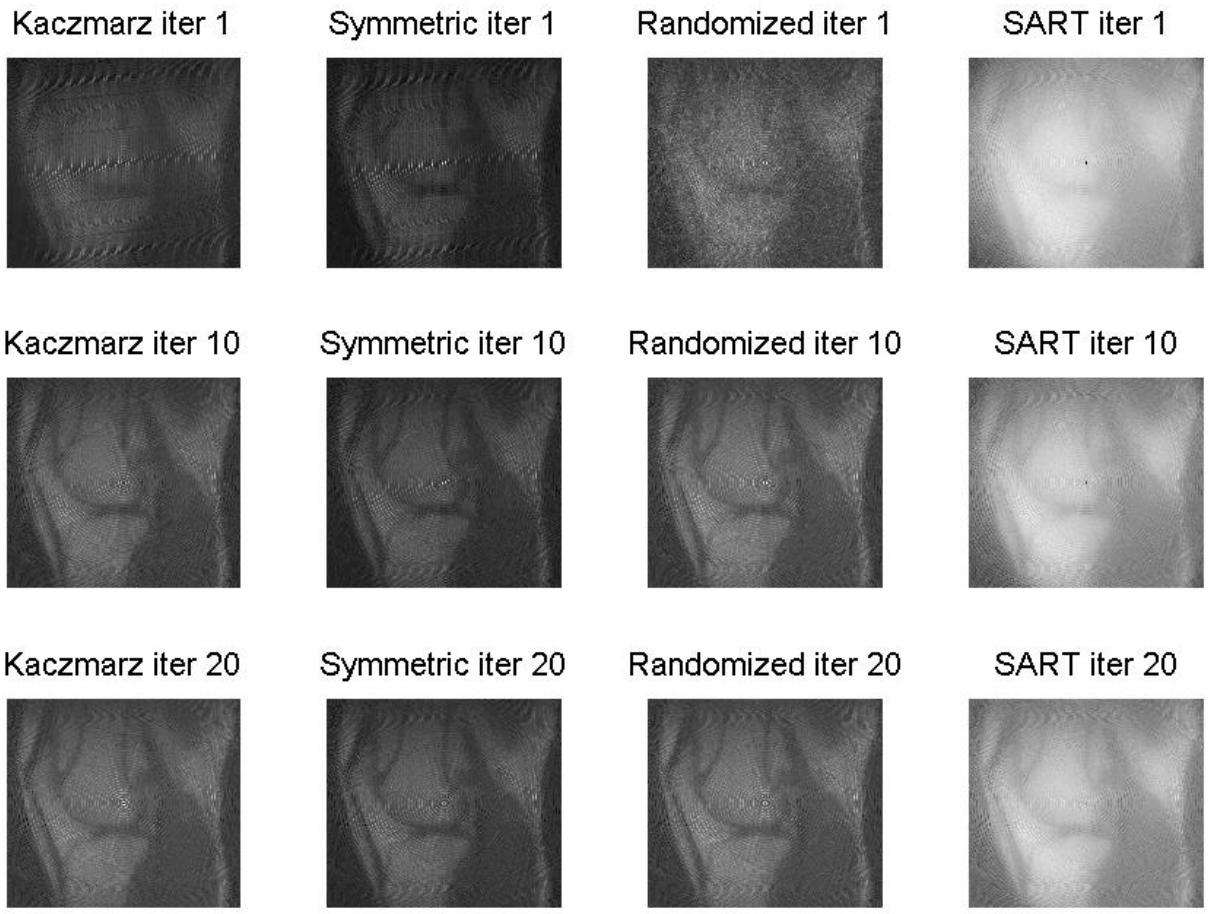

Figure B.45: Reconstruction of the 512×512 MRI Knee Phantom using Kaczmarz, Symmetric Kaczmarz, Randomized Kaczmarz and SART ($\lambda = 0.4$).

size	method	worst λ	max discrepancy	best λ	min discrepancy	time/iter(s)
128	Kacz.	1	0.3009	0.2	0.2443	5.54
	Symm.	1	0.3566	0.2	0.2398	16.36
	Rand.	0.2	0.2145	1	0.1844	14.39
	SART	0.2	0.6136	1	0.3549	0.02
256	Kacz.	1	0.4929	0.2	0.4204	38.68
	Symm.	1	0.5401	0.2	0.4312	82.06
	Rand.	0.2	0.4100	1	0.4073	46.37
	SART	0.2	0.6286	1	0.4176	0.11
512	Kacz.	1	0.6107	0.2	0.5683	193.62
	Symm.	1	0.6471	0.2	0.5696	348.84
	Rand.	0.2	0.5688	1	0.5678	200.42
	SART	0.2	0.6478	1	0.5012	0.24

Table B.3: Experimental results of applying different methods to MRI Knee phantom using relaxation parameters of $\lambda = 0.2, 0.4, .., 1$ for 20 number of iterations.

The experimental results shown in Table B.3 are obtained from the Colsher's discrepancy measurement method [4] in such a way that, after applying different ART methods to different phantom sizes, for $\lambda = 0.2, 0.4, .., 1$, the minimum and the maximum discrepancies, which indicate the best and the worst relaxation parameters, are found in iteration number 20.

As it can be seen, the results for the overdetermined system corresponding to 128×128 MRI Knee phantom are different from the results achieved for two underdetermined systems corresponding to 256×256 and 512×512 MRI Knee phantom image sizes. It is obvious that the results for both underdetermined systems follow the same pattern for their best and worst relaxation parameters, for various image reconstruction techniques.

Knee, Kaczmrarz, 128×128 **image,** $\lambda = 1, 1.2, .., 1.8$

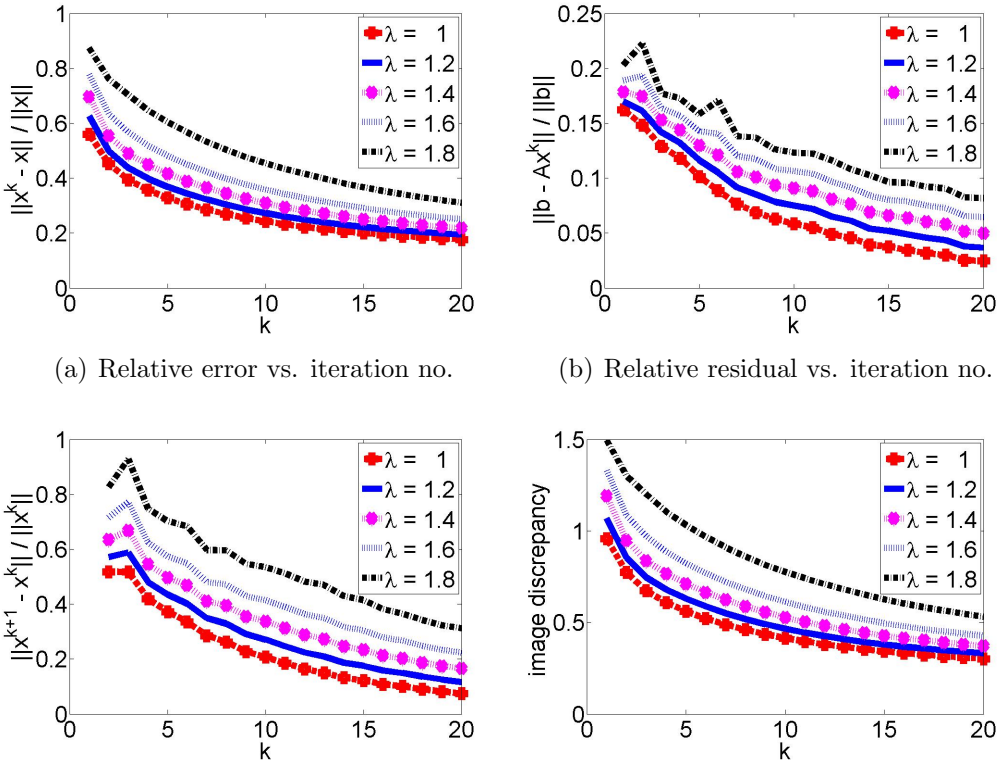

(a) Relative error vs. iteration no.

(b) Relative residual vs. iteration no.

(c) Relative solution difference vs. iteration no.

(d) Image discrepancy vs. iteration no.

Figure B.46: ART(Kaczmrarz's method) applied to MRI Knee Phantom for a 128×128 image and $\lambda = 1, 1.2, .., 1.8$.

In the last iteration,

	min relative error	min relative residual	min relative solution difference	min discrepancy
λ	1	1	1	1

Knee, Symmetric Kaczmrarz, 128×128 **image,** $\lambda = 1, 1.2, .., 1.8$

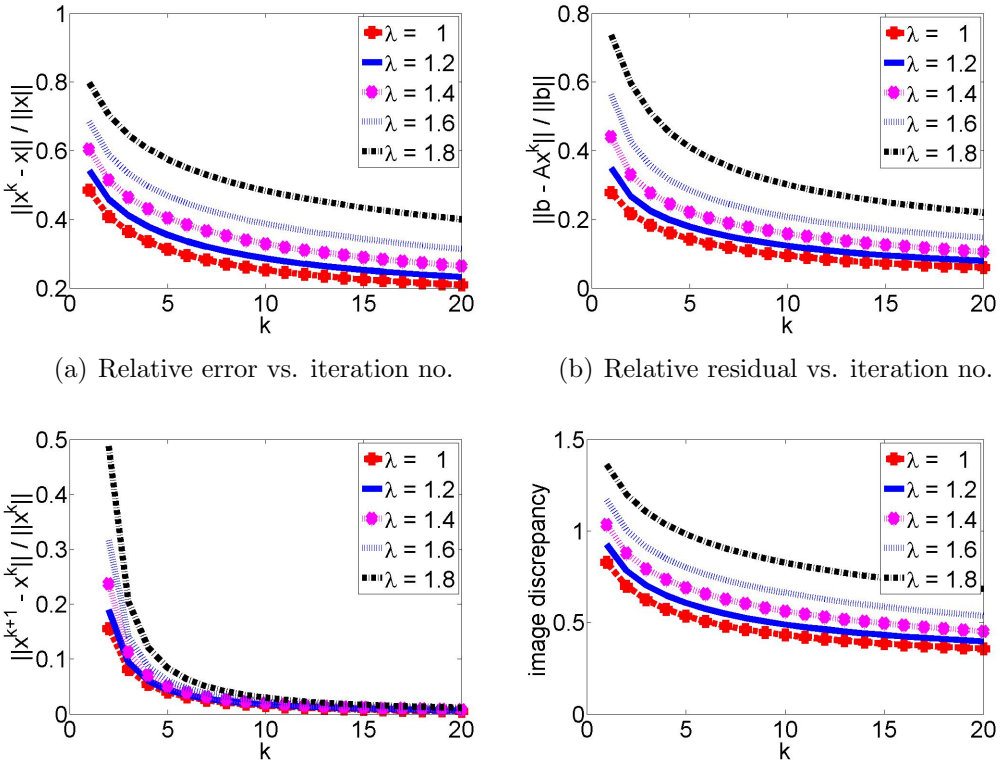

(a) Relative error vs. iteration no.

(b) Relative residual vs. iteration no.

(c) Relative solution difference vs. iteration no.

(d) Image discrepancy vs. iteration no.

Figure B.47: Symmetric Kaczmarz's method applied to MRI Knee Phantom for a 128×128 image and $\lambda = 1, 1.2, .., 1.8$.

In the last iteration,

	min relative error	min relative residual	min relative solution difference	min discrepancy
λ	1	1	1	1

Knee, Randomized Kaczmrarz, 128×128 **image,** $\lambda = 1, 1.2, .., 1.8$

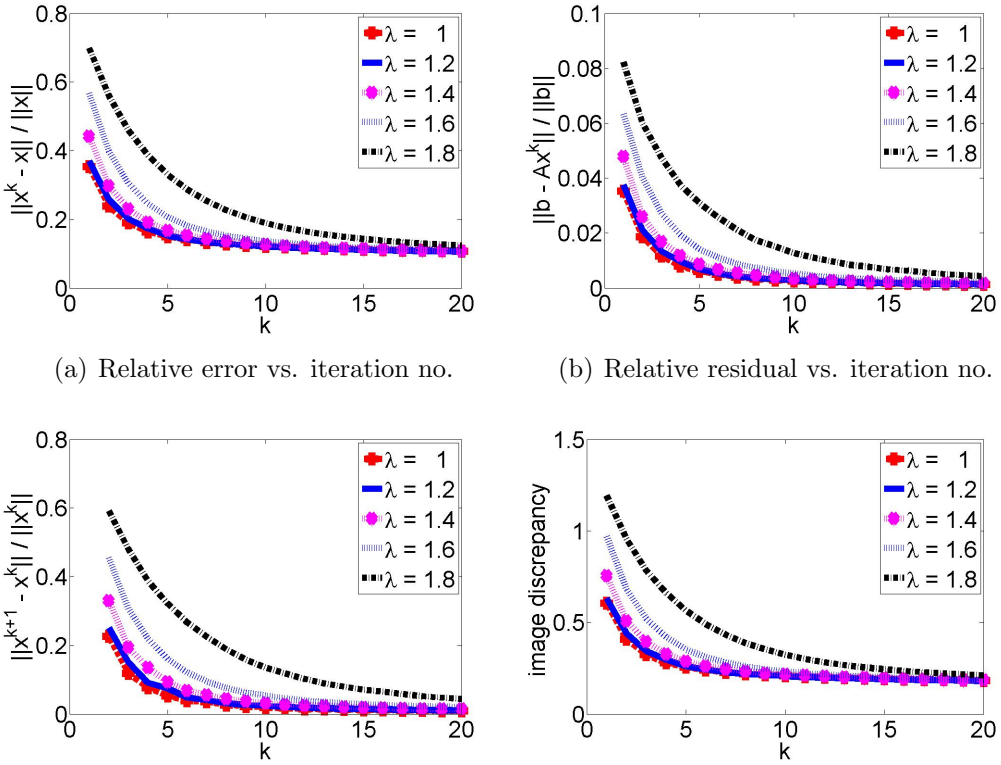

(a) Relative error vs. iteration no.

(b) Relative residual vs. iteration no.

(c) Relative solution difference vs. iteration no.

(d) Image discrepancy vs. iteration no.

Figure B.48: Randomized Kaczmarz's method applied to MRI Knee Phantom for a 128×128 image and $\lambda = 1, 1.2, .., 1.8$.

In the last iteration,

	min relative error	min relative residual	min relative solution difference	min discrepancy
λ	1	1	1	1.2

Knee, SART, 128×128 **image,** $\lambda = 1, 1.2, .., 1.8$

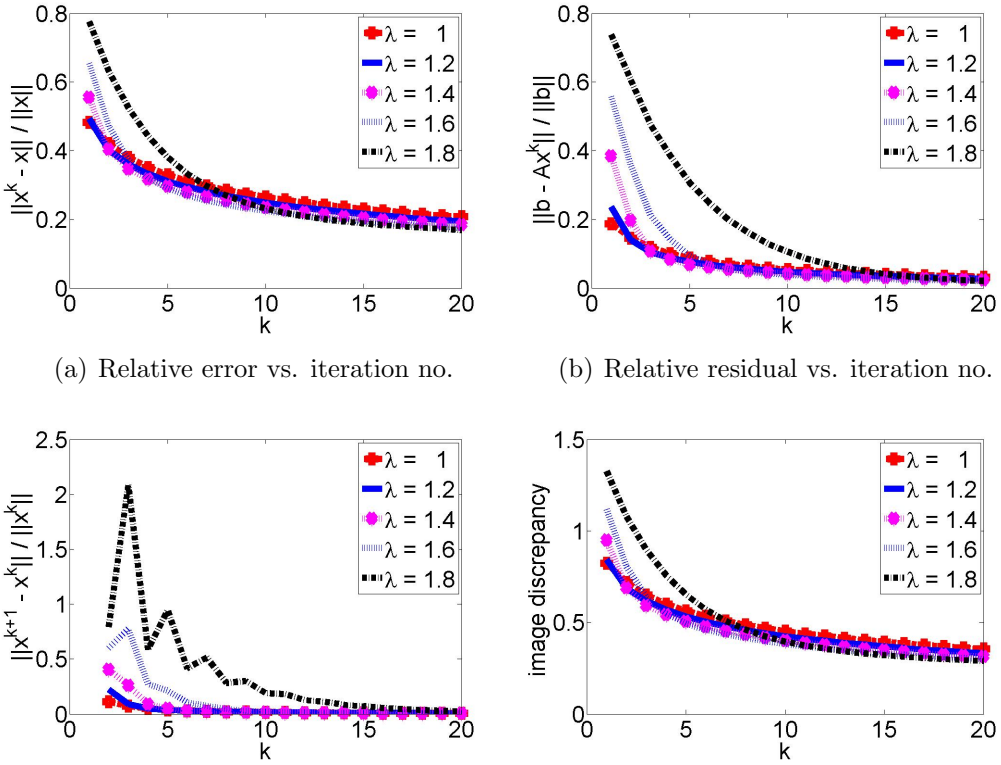

(a) Relative error vs. iteration no.

(b) Relative residual vs. iteration no.

(c) Relative solution difference vs. iteration no.

(d) Image discrepancy vs. iteration no.

Figure B.49: SART method applied to MRI Knee Phantom for a 128×128 image and $\lambda = 1, 1.2, .., 1.8$.

In the last iteration,

	min relative error	min relative residual	min relative solution difference	min discrepancy
λ	1.8	1.8	1.8	1.8

Knee, Kaczmrarz, 256×256 **image,** $\lambda = 1, 1.2, .., 1.8$

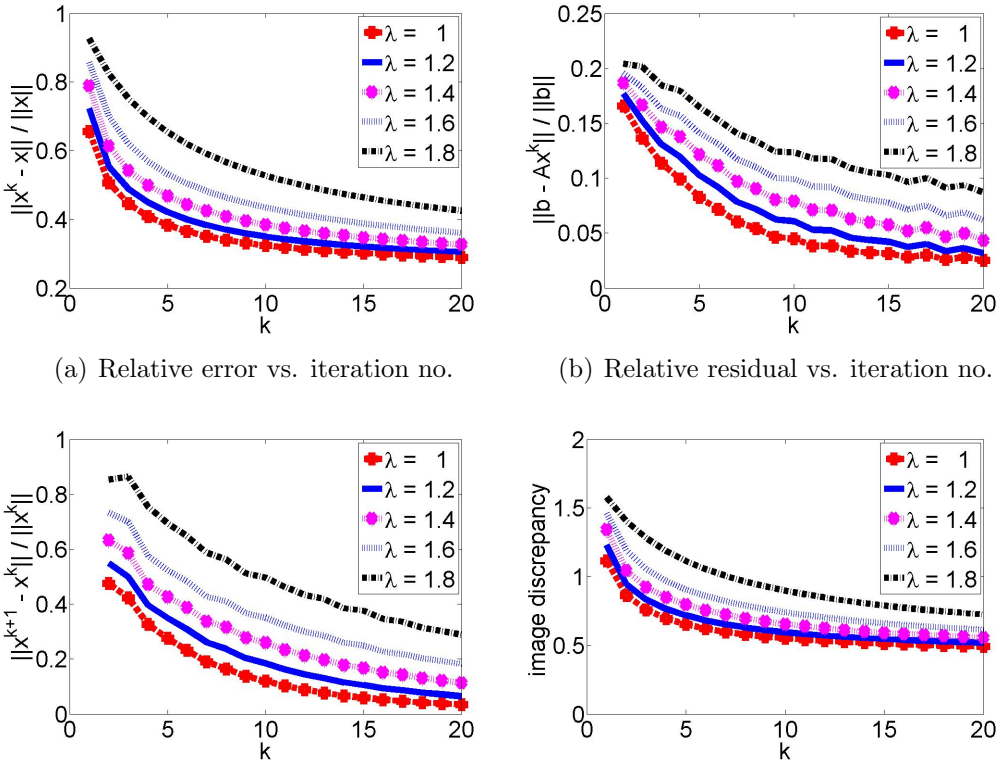

(a) Relative error vs. iteration no.

(b) Relative residual vs. iteration no.

(c) Relative solution difference vs. iteration no.

(d) Image discrepancy vs. iteration no.

Figure B.50: ART(Kaczmrarz's method) applied to MRI Knee Phantom for a 256×256 image and $\lambda = 1, 1.2, .., 1.8$.

In the last iteration,

	min relative error	min relative residual	min relative solution difference	min discrepancy
λ	1	1	1	1

Knee, Symmetric Kaczmarz, 256×256 **image,** $\lambda = 1, 1.2, .., 1.8$

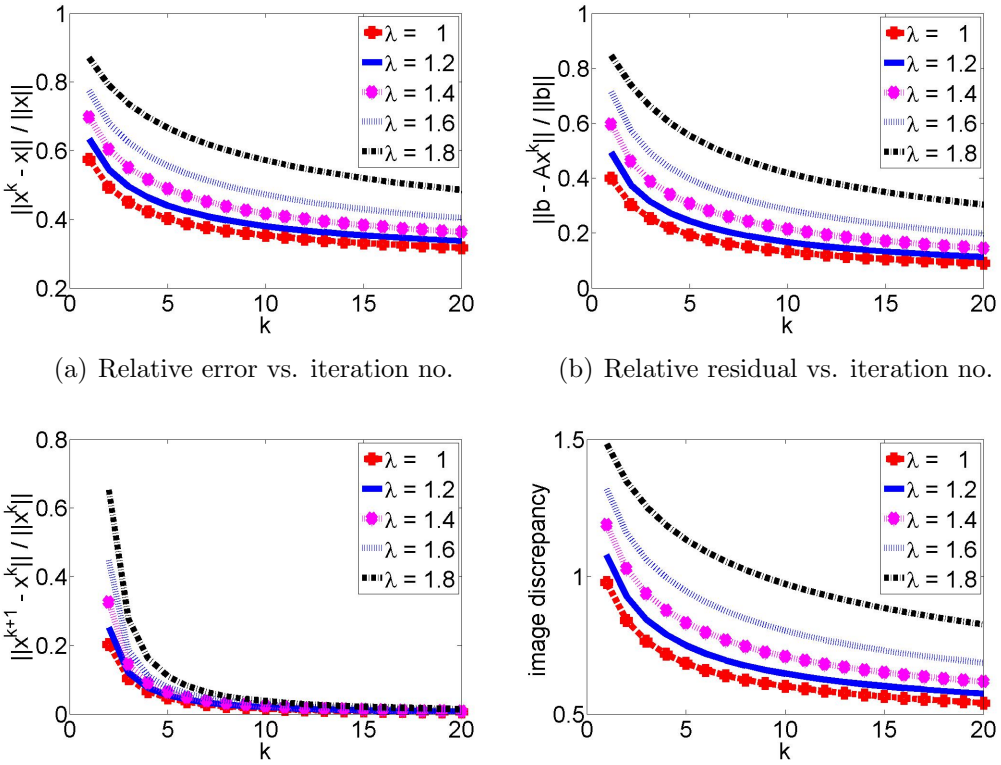

(a) Relative error vs. iteration no.

(b) Relative residual vs. iteration no.

(c) Relative solution difference vs. iteration no.

(d) Image discrepancy vs. iteration no.

Figure B.51: Symmetric Kaczmarz's method applied to MRI Knee Phantom for a 256×256 image and $\lambda = 1, 1.2, .., 1.8$.

In the last iteration,

	min relative error	min relative residual	min relative solution difference	min discrepancy
λ	1	1	1	1

Knee, Randomized Kaczmarz, 256×256 **image,** $\lambda = 1, 1.2, .., 1.8$

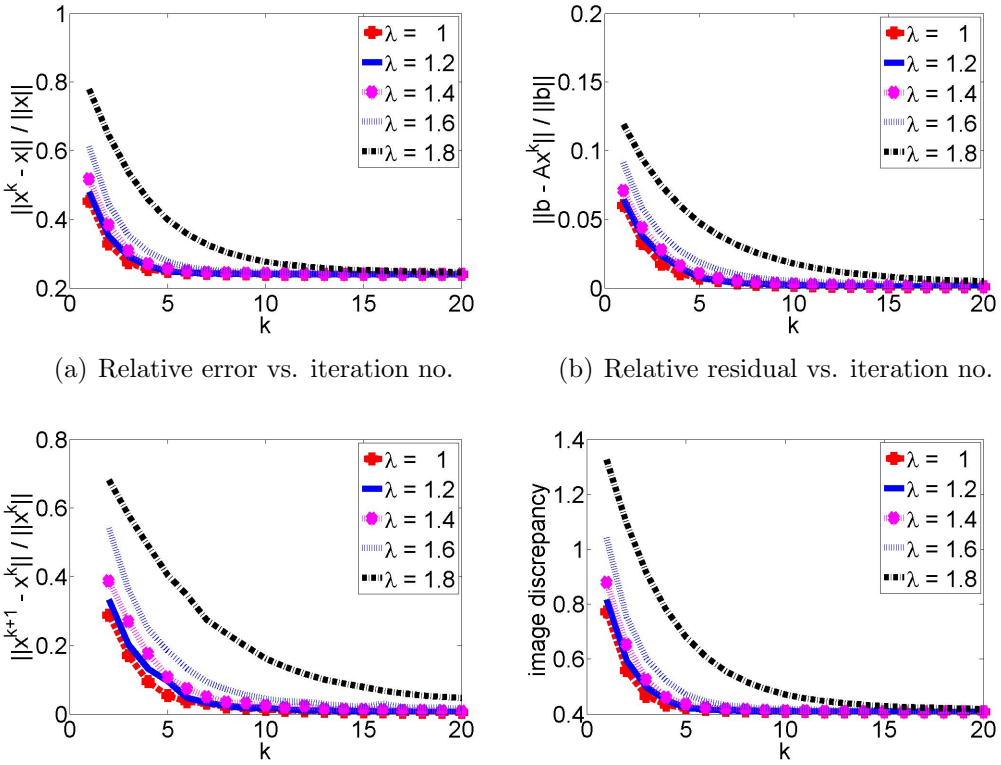

(a) Relative error vs. iteration no.

(b) Relative residual vs. iteration no.

(c) Relative solution difference vs. iteration no.

(d) Image discrepancy vs. iteration no.

Figure B.52: Randomized Kaczmarz's method applied to MRI Knee Phantom for a 256×256 image and $\lambda = 1, 1.2, .., 1.8$.

In the last iteration,

	min relative error	min relative residual	min relative solution difference	min discrepancy
λ	1	1	1	1

Knee, SART, 256×256 **image,** $\lambda = 1, 1.2, .., 1.8$

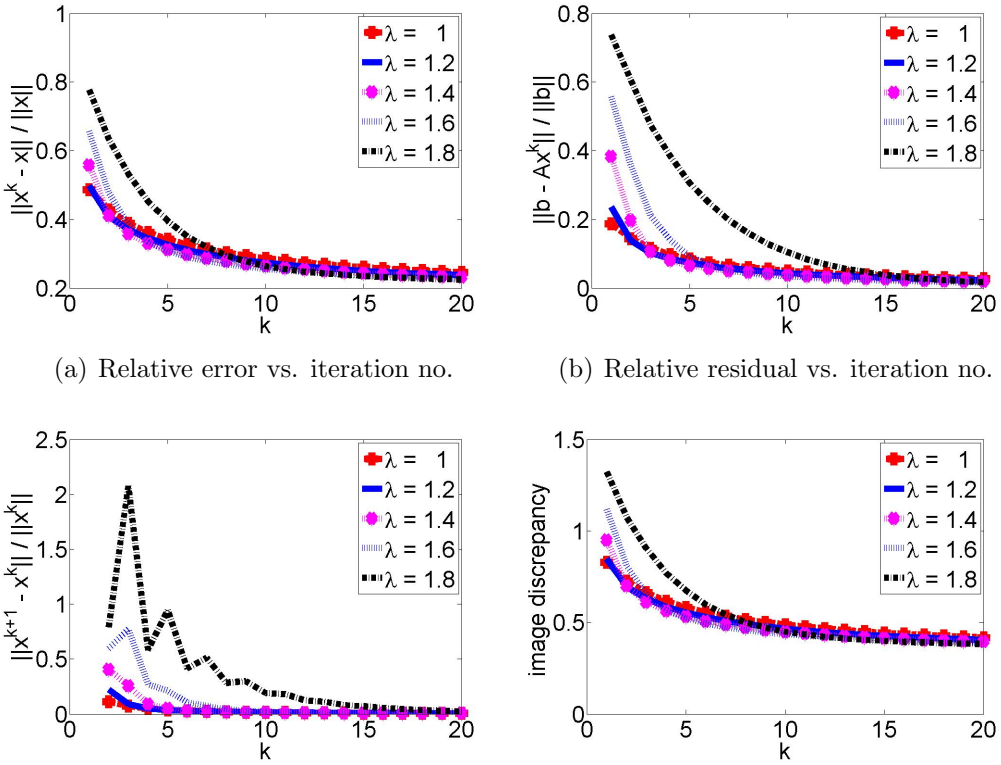

(a) Relative error vs. iteration no.

(b) Relative residual vs. iteration no.

(c) Relative solution difference vs. iteration no.

(d) Image discrepancy vs. iteration no.

Figure B.53: SART method applied to MRI Knee Phantom for a 256×256 image and $\lambda = 1, 1.2, .., 1.8$.

In the last iteration,

	min relative error	min relative residual	min relative solution difference	min discrepancy
λ	1.8	1.8	1.8	1.8

Knee, Kaczmrarz, 512×512 **image,** $\lambda = 1, 1.2, .., 1.8$

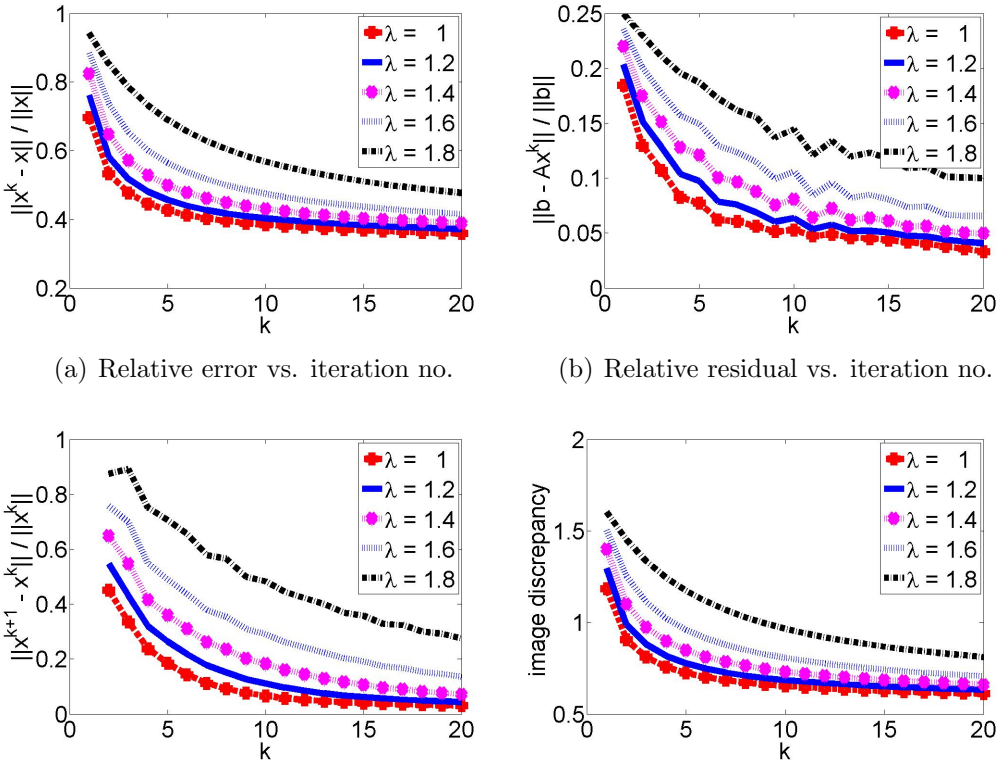

(a) Relative error vs. iteration no.

(b) Relative residual vs. iteration no.

(c) Relative solution difference vs. iteration no.

(d) Image discrepancy vs. iteration no.

Figure B.54: ART(Kaczmrarz's method) applied to MRI Knee Phantom for a 512×512 image and $\lambda = 1, 1.2, .., 1.8$.

In the last iteration,

	min relative error	min relative residual	min relative solution difference	min discrepancy
λ	1	1	1	1

Knee, Symmetric Kaczmrarz, 512×512 **image,** $\lambda = 1, 1.2, .., 1.8$

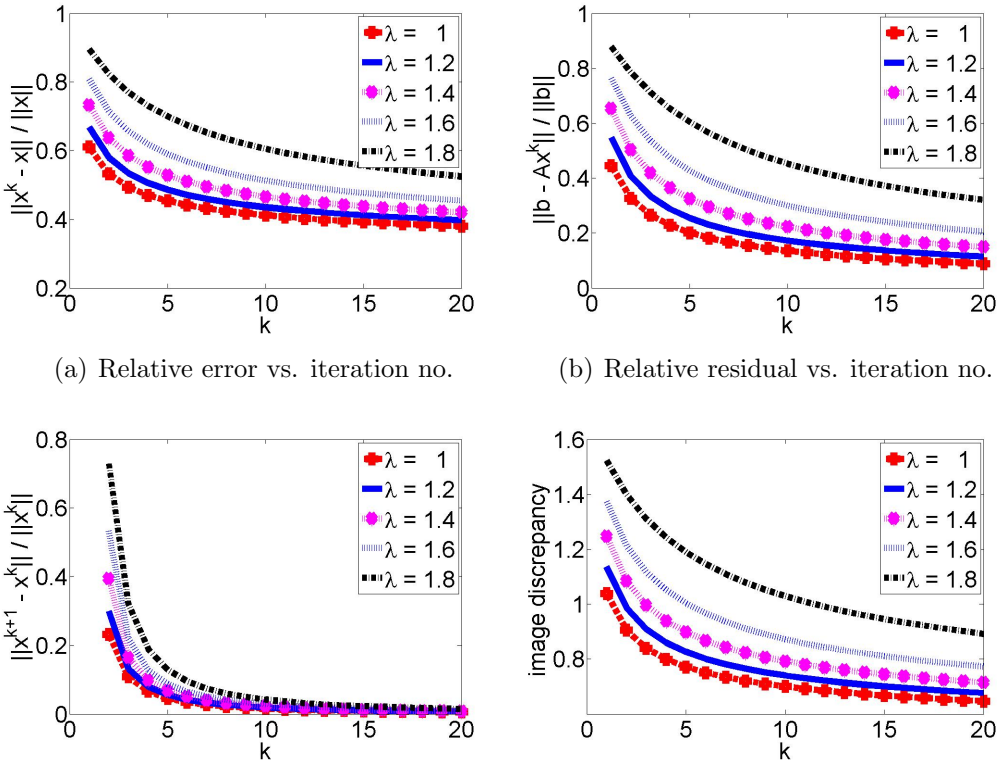

(a) Relative error vs. iteration no.

(b) Relative residual vs. iteration no.

(c) Relative solution difference vs. iteration no.

(d) Image discrepancy vs. iteration no.

Figure B.55: Symmetric Kaczmarz's method applied to MRI Knee Phantom for a 512×512 image and $\lambda = 1, 1.2, .., 1.8$.

In the last iteration,

	min relative error	min relative residual	min relative solution difference	min discrepancy
λ	1	1	1	1

Knee, Randomized Kaczmrarz, 512×512 **image,** $\lambda = 1, 1.2, .., 1.8$

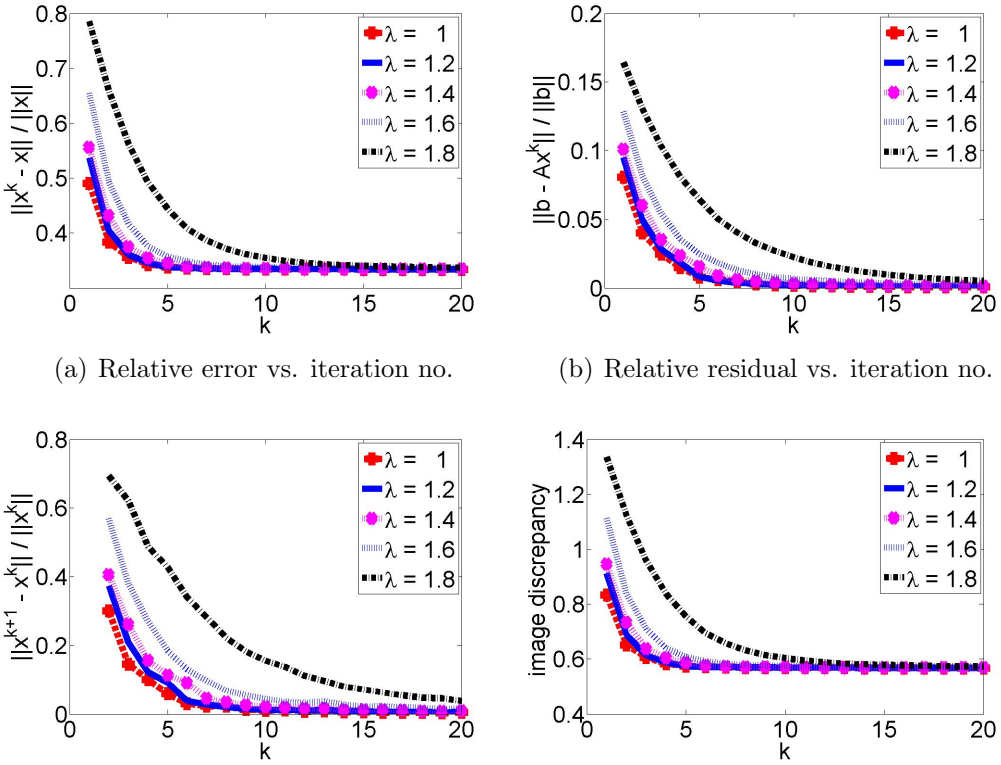

(a) Relative error vs. iteration no.

(b) Relative residual vs. iteration no.

(c) Relative solution difference vs. iteration no.

(d) Image discrepancy vs. iteration no.

Figure B.56: Randomized Kaczmarz's method applied to MRI Knee Phantom for a 512×512 image and $\lambda = 1, 1.2, .., 1.8$.

In the last iteration,

	min relative error	min relative residual	min relative solution difference	min discrepancy
λ	1	1	1	1

Knee, SART, 512×512 **image,** $\lambda = 1, 1.2, .., 1.8$

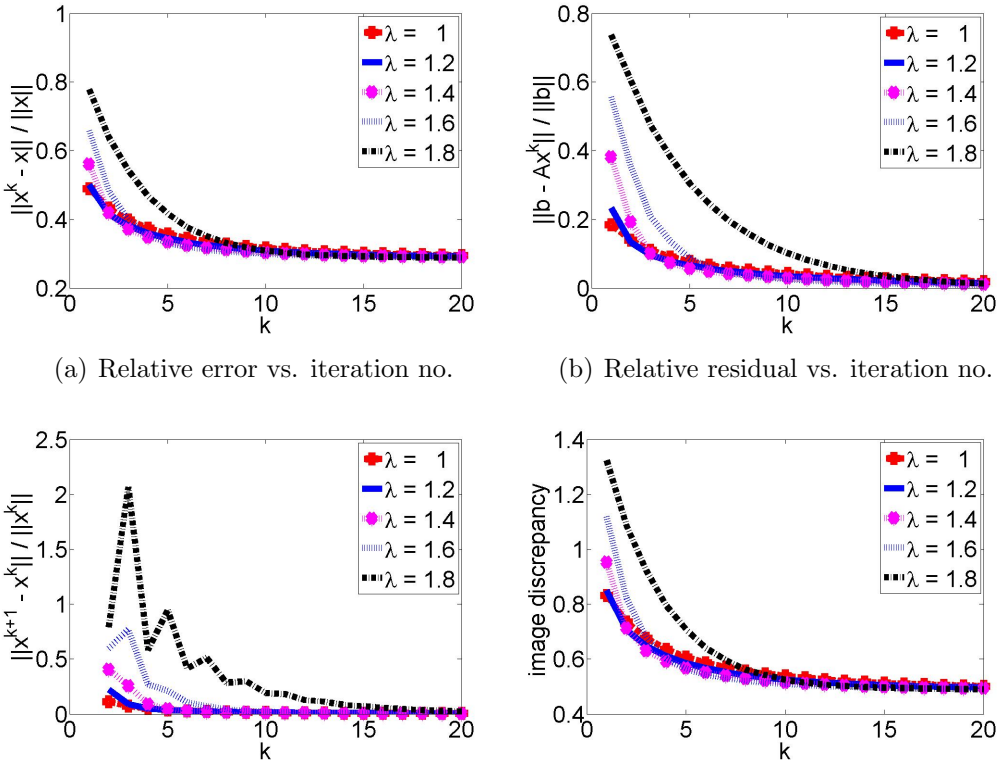

(a) Relative error vs. iteration no.

(b) Relative residual vs. iteration no.

(c) Relative solution difference vs. iteration no.

(d) Image discrepancy vs. iteration no.

Figure B.57: SART method applied to MRI Knee Phantom for a 512×512 image and $\lambda = 1, 1.2, .., 1.8$.

In the last iteration,

	min relative error	min relative residual	min relative solution difference	min discrepancy
λ	1.8	1.8	1.8	1.8

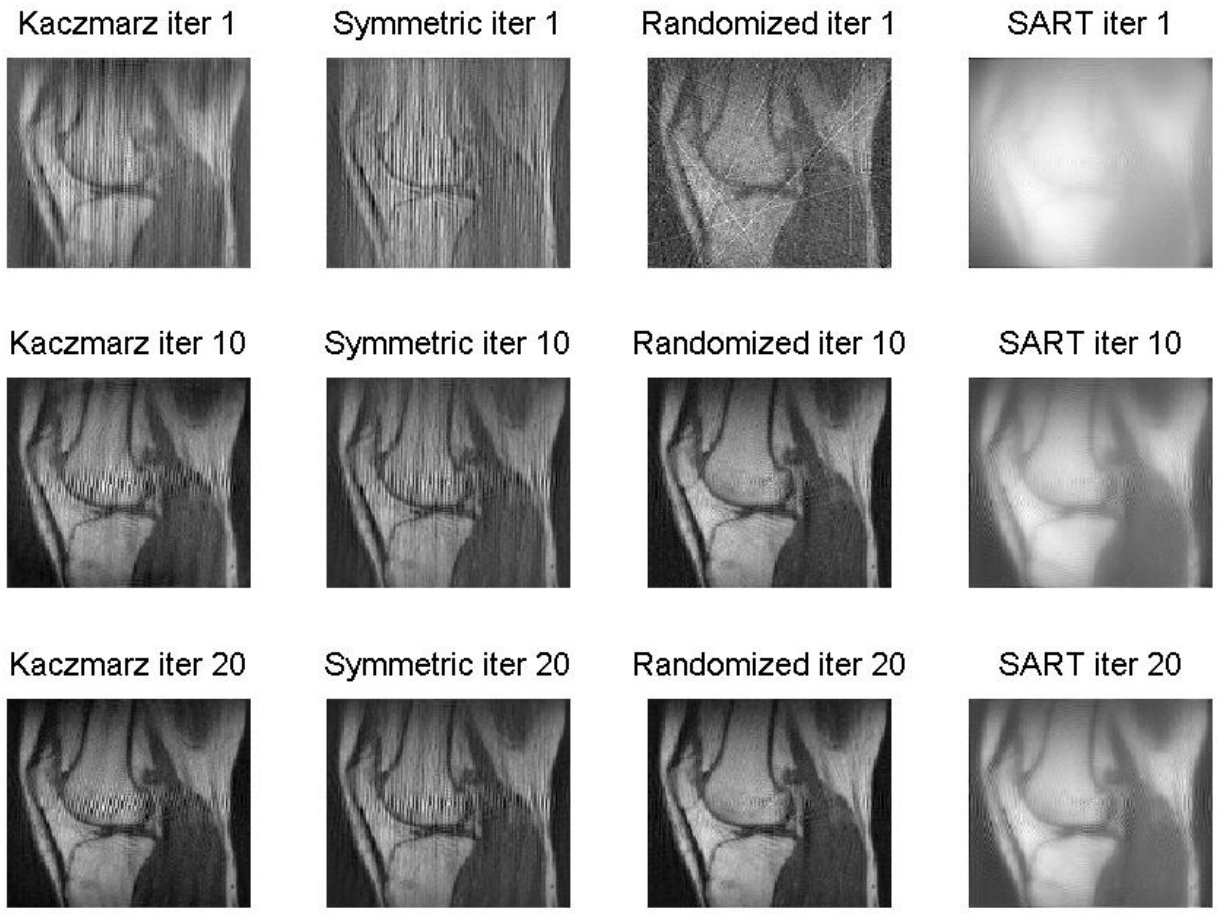

Figure B.58: Reconstruction of the 128×128 MRI Knee Phantom using Kaczmarz, Symmetric Kaczmarz, Randomized Kaczmarz and SART ($\lambda = 1.2$).

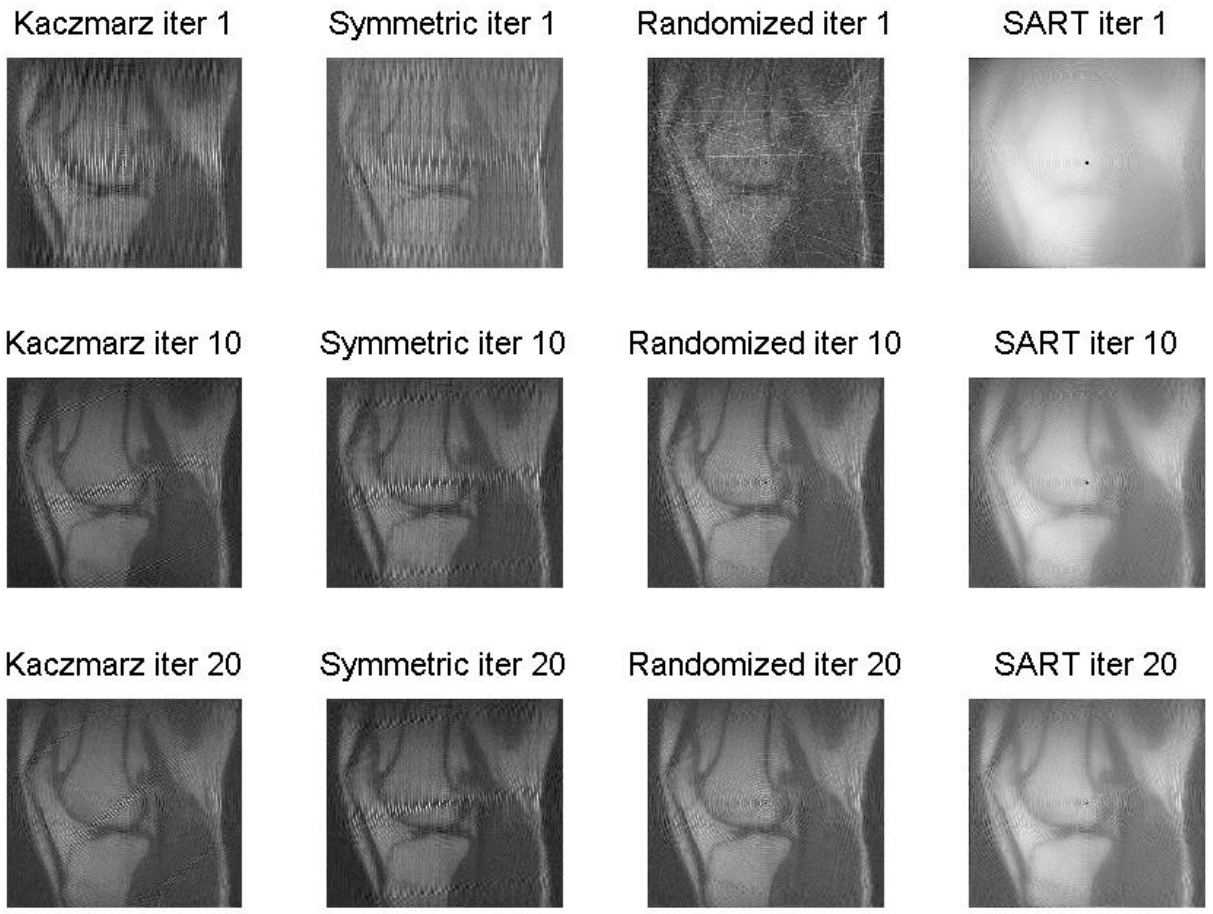

Figure B.59: Reconstruction of the 256×256 MRI Knee Phantom using Kaczmarz, Symmetric Kaczmarz, Randomized Kaczmarz and SART ($\lambda = 1.2$).

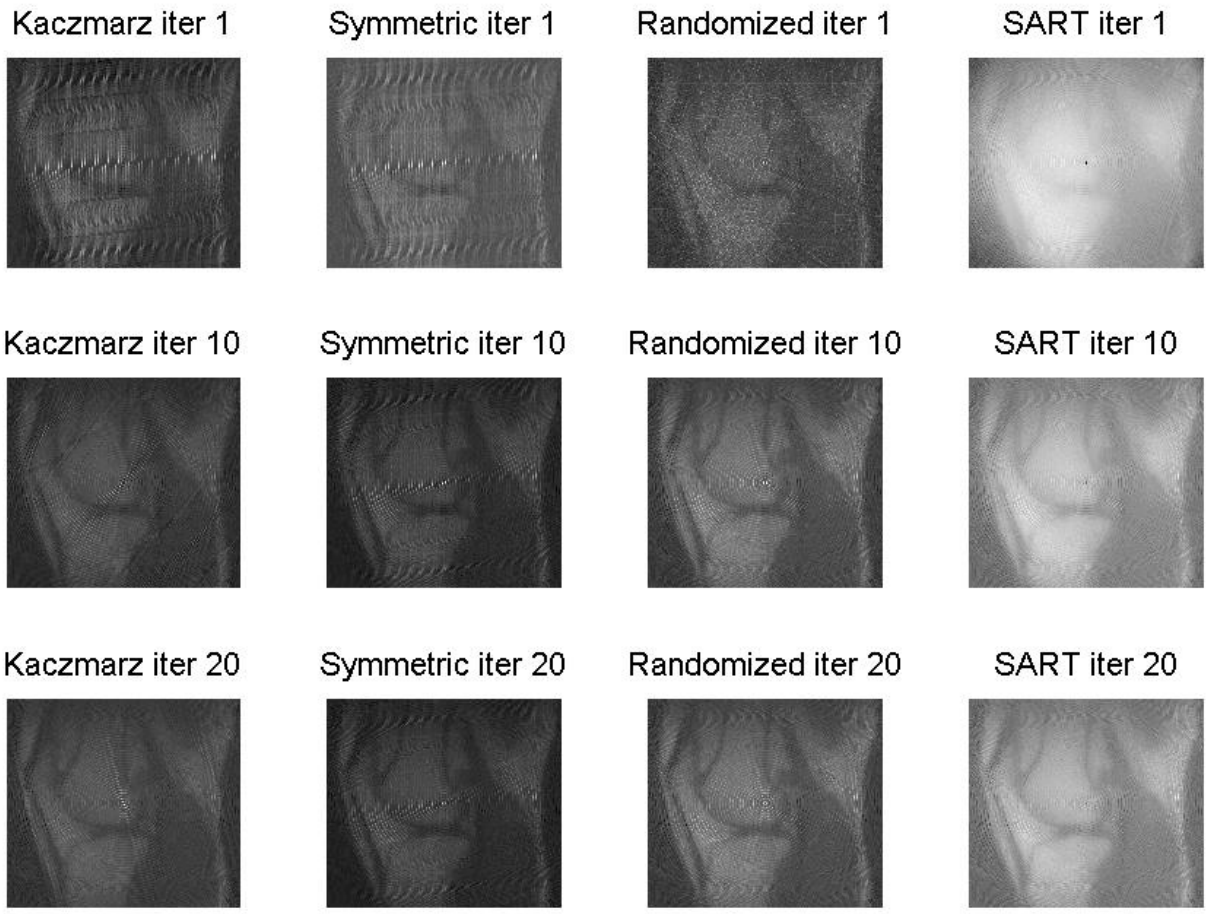

Figure B.60: Reconstruction of the 512×512 MRI Knee Phantom using Kaczmarz, Symmetric Kaczmarz, Randomized Kaczmarz and SART ($\lambda = 1.2$).

size	method	worst λ	max discrepancy	best λ	min discrepancy	time/iter(s)
128	Kacz.	1.8	0.5319	1	0.3009	14.11
	Symm.	1.8	0.6838	1	0.3566	15.30
	Rand.	1.8	0.2110	1.2	0.1813	9.89
	SART	1	0.3549	1.8	0.2884	0.02
256	Kacz.	1.8	0.7239	1	0.4929	31.65
	Symm.	1.8	0.8264	1	0.5401	73.77
	Rand.	1.8	0.4174	1	0.4073	68.33
	SART	1	0.4176	1.8	0.3822	0.09
512	Kacz.	1.8	0.8111	1	0.6107	214.95
	Symm.	1.8	0.8923	1	0.6471	388.61
	Rand.	1.8	0.5726	1.2	0.5678	228.28
	SART	1	0.5012	1.8	0.4902	0.32

Table B.4: Experimental results of applying different methods to MRI Knee phantom using relaxation parameters of $\lambda = 1, 1.2, .., 1.8$ for 20 number of iterations.

The experimental results shown in Table B.4 are obtained from the Colsher's discrepancy measurement method [4] in such a way that, after applying different ART methods to different phantom sizes, for $\lambda = 1, 1.2, .., 1.8$, the minimum and the maximum discrepancies, which indicate the best and the worst relaxation parameters, are found in iteration number 20.

As it can be seen, the results for the overdetermined system corresponding to 128×128 MRI Knee phantom are different from the results achieved for two underdetermined systems corresponding to 256×256 and 512×512 Knee phantom image sizes. It is obvious that the results for both underdetermined systems follow the same pattern for their best and worst relaxation parameters, for various image reconstruction techniques.

Bibliography

[1] A. H. Andersen and A. C. Kak, *Simultaneous algebraic reconstruction technique (sart): A superior implementation of the art algorithm*, Ultrason. Imag., pp. vol. 6, pp. 8194, 1984.

[2] A. Bjorck and T. Elfving, *Accelerated projection methods for computiong pseudoinverse solutions of systems of linear equations*, BIT, pp. Vol. 19 issue 2(1979), p. 145–163.

[3] Bracewell, *R.n. strip integration in radio astronomy*, Aust. J. Phys, pp. 9, 198, 1956.

[4] J. Colsher, *Iterative three-dimensional image reconstruction from tomographic projections*, Computing Graphic Image Processing, pp. 6, 513–537 (1977).

[5] T. Elfving and T. Nikazad, *Stopping rules for landweber type iteration*, Inverse problems, pp. 23 (2007), No. 4, 1417–1432.

[6] T. Elfving, T. Nikazad, and P. C. Hansen, *Semi-convergence and relaxation parameters for a class of sirt algorithms*, submitted to ETNA.

[7] G.Feeman, *The Mathematics of Medical Imaging*, Springer, New York, 2010.

[8] R. Gordon, R. Bender, and G. T. Herman, *Algebraic reconstruction techniques (art) for three-dimensional electron microscopy and x-ray photography*, J. Theor. Biol., pp. 29:471–481, 1970.

[9] U. Hamarik and U. Tautenbaum, *On the monotone error rule for parameter choice in iterative and continuous regularization methods*, BIT, pp. 41 (2001),10291038.

[10] P. C. Hansen and M. Saxild-Hansen, *Air tools - a matlab package of algebraic iterative reconstruction techniques*, IMM-Technical Report, 2010, DTU Informatics, p. Version 1.0 for Matlab 7.8.

[11] K. M. Hanson, *On the optimality of the filtered backprojection algorithm*, Journal of Computer Assisted Tomography, p. 1980.

[12] G. Herman, *Image Reconstruction from Projections-The Fundamentals of Computerized Tomography*, Academic Press, 1980.

[13] G. Herman and L. Meyer, *Algebraic reconstruction tehniques can be made computentionally efficient*, IEEE Transactions on Medical Imaging, pp. 12 (3) (1993) 600–609.

[14] G. T. Herman, *Fundamentals of computerized tomography: Image reconstruction from projection*, 2nd edition, Springer, 2009.

[15] M. Jiang and G. Wang, *Convergence of the simultaneous algebraic reconstruction technique (sart)*, IEEE TRANSACTIONS ON IMAGE PROCESSING, pp. VOL. 12, NO. 8, AUGUST 2003.

[16] S. Kaczmarz, *Angenherte auflsung von systemen linearer gleichungen*, Bulletin International de l'Acadmie Polonaise des Sciences et des Lettres. Classe des Sciences Mathmatiques et Naturelles. Srie A, Sciences Mathmatiques, pp. vol. 35, pp. 355357, 1937.

[17] C. F. V. Loan, *Introduction to Scientic Computing: A Matrix-Vector Approach using MATLAB*, Prentice Hall, 1997.

[18] J. Mesquita, *Choosing the art relaxation parameter for clear-PEM 2D image reconstruction*, Computer Methods And Programs In Biomedicine, Elsevier Irland, pp. Pages 183–190.

[19] V. Morozov, *On the solution of functional equations by the method of regularization*, Sovjet Math. Dokl., pp. 7 (1966), 414417.

[20] J. Radon, *ber die bestimmung von funktionen durch ihre integralwerte lngs gewisser mannigfaltigkeiten", berichte ber die verhandlungen der schsische akademie der wissenschaften*, Reports on the proceedings of the Saxony Academy of Science, pp. (69): 262277, 1917.

[21] R. Seeley, *An Intoruction to fourier Series and Integrals*, W. A. Benjamin, Inc., New York, 1966.

[22] L. Shepp and B. Logan, *The fourier reconstruction of a head section*, IEEE Trans-actions on Nuclear Science, pp. vol. NS–21, pp. 21–43, 1974.

[23] T. Strohmer and R. Vershynin, *A randomized kaczmarz algorithm for linear systems with exponential convergence*, Journal of Fourier Analysis and Applications, pp. vol. 15, pp. 262278, 2009.

[24] V. Volterra, *Leons sur les fonctions de linges*, Gauthier-Villars, p. Paris 1913.